TN 68 TRANSPORT PACKAGING

APPENDIX 2.10.5

TABLE OF CONTENTS

LIST OF TABLES

LIST OF FIGURES

APPENDIX 2.10.5

STRUCTURAL ANALYSIS OF THE TN-68 BASKET

2.10.5.1 Introduction

This appendix presents the structural analysis of the TN-68 fuel support basket. The basket is a welded assembly of stainless steel boxes and designed to accommodate 68 fuel assemblies. The fuel compartment stainless steel box sections are attached together locally by fusion welds to 304 stainless steel plates sandwiched between the stainless steel walls of adjacent box sections. The basket contains 68 compartments for proper spacing and support of the fuel assemblies.

The basket structure is open at each end and therefore, longitudinal fuel assembly loads are applied directly on the cask body and not on the fuel basket structure. The fuel assemblies are laterally supported in the stainless steel structural boxes, and the basket is laterally supported by the rails and the cask inner shell.

The deformations and stresses induced in the basket structure due to the applied lateral loads are determined using the ANSYS computer program[1]. The most severe loadings for which the basket are evaluated are the 30 foot hypothetical side drop and end drop accidents. The basket is also evaluated for a 1 foot side drop and end drop loads under the normal conditions. The g loads and drop orientations used for the basket structural analysis are described in Appendix 2.10.8. The dynamic load factor is calculated in Appendix 2.10.6. The inertial loads of the fuel assemblies are applied as equivalent densities on the stainless steel boxes. Quasistatic stress analyses are performed with applied loads in equilibrium with the reactions at the periphery of the basket. The calculated stresses in the basket structure are compared with the stress limits to demonstrate that the established design criteria are met.

2.10.5.1.1 Geometry

The details of the TN-68 basket are shown on TN Drawing Nos. 972-71-5, and -6. As described above, the basket structure consists of an assembly of stainless steel boxes or cells joined by fusion welds and separated by stainless steel and poison plates. The stainless box, stainless steel plate and poison plate between fuel compartments is effectively a sandwich panel. The panel consists of one 5/16 in. thick 304 stainless steel plate and one 5/16 in. thick poison plate sandwiched between two 3/16 in. thick 304 stainless boxes. The 304 stainless steel members are the primary structural components. The poison plates provide the heat conduction path from the fuel assemblies to the cask cavity wall, and also provide criticality control.

A representative basket wall panel between fuel compartments is shown in Figure 2.10.5-1. The panel plates are welded together at discrete locations (1 fusion weld every 12. 2 inches) along their length. The adjacent fuel compartment stainless steel walls are fusion welded to both adjacent box sections. This method of construction forms a very strong honeycomb-like structure of boxes. The nominal open dimension of each fuel compartment cell or box is 6.0 in. x 6.0 in. The pitch of the cells is approximately 6.69 in. The overall basket length including

hold down ring, (164 in. + 13.25 in.) 177.25 in., is less than the cask cavity length to allow for loading the fuel assemblies, thermal expansion and tolerance stackup.

Structural rails oriented parallel to the axis of the cask are attached to the periphery of the basket to establish and maintain basket orientation, to prevent twisting of the basket assembly, and to support the edges of those plates adjacent to the rails, which would otherwise be free to slide tangentially around the cask cavity wall under lateral inertial loadings.

The basket hold down ring is set between the top of the basket assembly and inside surface of the lid assembly. The hold down ring is used to prevent the basket assembly from sliding freely in the axial direction during the normal transport condition.

2.10.5.1.2 Weight

A value of 705 lb. is assumed for the weight of each fuel assembly including fuel channels. Under lateral inertial loading each assembly is assumed to be uniformly supported across the width and along the length of the basket wall. The inertia of the basket structure (weight of the basket x G load) is also included in the analysis.

2.10.5.1.3 Temperature

Thermal analyses are performed to obtain the temperature distributions in the basket for various conditions. These analyses are presented in Chapter 3. The effects of axial and radial thermal expansion of the basket are evaluated in Section 2.10.5.3.4.

2.10.5.2 Basket Finite Element Model Development (For Side Impact Analysis)

The basket model is an extremely large and complex ANSYS model. Because of the number of plates in the basket and the size of the basket, certain modeling approximations are necessary. The basket structure construction is repetitive symmetry (1 fusion weld every 12.2 inches along the length). It is practical to model only a single transverse slice (12.2 inches length) using a three-dimensional finite element model. The elements used in the model to represent the plates are Shell 63 quadrilateral shell elements and the rails are modeled by Solid 45 3D structural solid elements. For conservatism, the poison plates are not assumed to carry the structural load (except through the thickness support) and are not included in the model, but their weight (inertial load) is included in the stress calculation.

The fuel compartment corners and basket periphery are carefully modeled to define each plate connection. The connections between stainless steel boxes, stainless boxes and poison plates, stainless steel boxes and aluminum rails are made by node couplings. The nodes at the locations of fusion welds are coupled in all degrees of freedom (the fusion welds rigidly connect the stainless steel boxes and stainless steel plates together at these nodes). The nodes of various plates are coupled together in the out of plane direction so that they will bend in unison under surface pressure or other lateral loading and to simulate the through thickness support provided by the poison plates. Figures 2.10.5-1 and 3 show the typical basket panel ANSYS finite element model simulation. The component assembly model computer plot is shown on Figure 2.10.5-4 and the individual component computer plots are shown on Figures 2.10.5-5 to 2.10.5-7.

2.10.5.3 Basket Under Normal Condition Loads

2.10.5.3.1 Description

The poison plates in the TN-68 basket are heat conductors and provide the necessary criticality control. The 304 stainless steel members are the primary structural components.

The poison plate strength is neglected under normal and accident condition loadings (except for through thickness load transfer capability). This analysis approach produces conservatively high calculated values of primary stresses in the stainless steel components. The primary stress analysis of the basket under the normal condition loads is described below.

2.10.5.3.2 Basket Analysis Under 1 Foot Side Drop Load

Finite Element Model

The ANSYS finite element model described in Section 2.10.5.2 is used to perform the structural analysis of the basket.

Loading

The basket is analyzed for 0°, 30°, and 45° lateral loads to bound the possible maximum stress cases. The lateral load orientation angles are defined in Figures 2.10.5-8, 2.10.5-9, and 2.10.5-10.

All analysis is based on 1g acceleration. The loading due to poison plates and fuel assembly weight are applied as equivalent densities. The poison plate weight is distributed on all four sides of stainless steel boxes, and the fuel assembly weights are distributed on the top panel of the SST-ALUM-SST sandwich for the 0° lateral load orientation and proportionally distributed on the top & side panels for the 30° and 45° lateral load orientations.

Boundary Conditions

The boundary condition at each point of contact between the basket and cask body cavity depends on the direction of the applied inertial load. As the basket is forced in a particular lateral direction, it separates from the cask wall on one side and reacts against the wall on the other side. At the locations where the basket loses contact with the wall, no restraint or support is provided in the model. For vertical inertial loading on a horizontal cask and basket, contact is lost between the basket and cask wall at the top half of the structure. The load distributions and boundary conditions are shown on Figures 2.10.5-8 through 2.10-5-10.

Material Properties

The material properties of the 304 stainless steel plates are taken from ASME[2] Code, Section II, Part D. The material properties of the aluminum alloy (6061-T6) are also taken from the ASME Code. These properties are listed with specific reference in Chapter 2. Chapter 3 shows the

temperature distribution at various locations of the basket and rails. The maximum calculated temperatures for the various sections of the basket and rails are also summarized in Chapter 3. Based on this thermal analysis, the maximum basket plate temperature is less than 470°F and the maximum rail temperature is less than 320°F. The structural analysis of the basket and rails conservatively assumes a uniform temperature of 500°F for basket and 350°F for the rails.

Analysis and Stress Results

Analyses using the basket system model are performed for the 0°, 30°, and 45° lateral load orientations relative to the basket plates as indicated in Figures 2.10.5-8 through 2.10.5-10. In all cases, the analyses for the individual loads are performed using the linear elastic method so that ratios can be used to obtain stress results for specified loads. Detailed stress, displacements, and forces in the finite element model are available in ANSYS output files. These results were postprocessed. The nodal stress intensities and deformed geometry for 0°, 30°, and 45° load cases are plotted in Figures 2.10.5-11 through 2.10.5-25. The stress intensities shown in figures are calculated based on an average fuel assembly weight of 690 lb. Since the analysis is linearly elastic, the results are ratioed for stresses due to a maximum fuel assembly weight of 705 lbs and are summarized in Tables 2.10.5-1 to 2.10.5-4. These maximum stresses are evaluated in Section 2.10.5.3.6 to verify that the design criteria are met.

Stresses at Stainless Steel Fusion Welds

ANSYS computer code is used to calculate the shear stresses at the fusion welds. Two drop orientations are analyzed. Small finite element models for these analyses were constructed with the following modifications using the finite element model described in Section 2.10.5.2.

- Figure 2.10.5-29 shows the full basket model and the locations where the small models will be extracted and modified for fusion weld shear stresses calculations.
- Removed all aluminum rail elements (SOLID45). Also removed all the shell elements, except one center vertical row of elements as shown in Figures 2.10.5-29 and 2.10.5-29A for 0° side impact orientation and one 45° row of elements as shown in Figures 2.10.5-29 and 2.10.5-29B for 45° side impact orientation. All the boundary conditions and couplings at the unused nodes were removed.
- Symmetry boundary conditions were applied at the cut surfaces.
- Removed the couplings at the fusion welds and replaced them with Elastic Pipe Element (PIPE16) of 0.5" outer dia. and 0.25 " thickness. The diameter of pipe elements for the 0° side impact model at the symmetry boundaries was reduced to 0.3536" (thickness = 0.1768) for 1/2 section area.
- All material properties, real constants and couplings of the reduced models are the same as described in Section 2.10.5.2. The element and node numbers are, however, compressed in the small models.

The calculated average shear stresses for 0° and 45° side impact orientations are listed in the following table for 1G side drop load. These stresses are evaluated in Section 2.10.5.3.6 to verify that the design criteria are met.

Drop Orientation	Shear Stresses (ksi)
0°	0.04
45°	0.07

2.10.5.3.3 Basket Analysis Under 1 Foot End Drop Vertical Load

Under vertical loads, the fuel assemblies and basket are forced against the bottom of the cask. It is important to note that, for any vertical or near vertical loading, the fuel assemblies react directly against the bottom of the cask cavity and not through the basket structure as in lateral loading.

1 Foot End Drop Vertical Load - 304 Stainless Steel

The analysis of the basket subjected to the 1 foot end drop vertical load for the panels with poison plate is shown in Figure 2.10.5-26. A full length of compartment wall (164 in. long) with a span length of 6.375 in. is evaluated for compressive loading. The analysis is based on 1g acceleration using the linear elastic method so that ratios can be used to obtain stress results for specified loads. A maximum compressive force of (1 × 163) 163 lbs. occurs at the bottom of the wall. Stresses are conservatively calculated by assuming all of the load is taken by the 304 stainless steel. Therefore

σ = Total Compressive Load/Cross Section of 304SS = 163 lbs/2.39 in.^{2} = 68.2 psi

There are cutouts in 4 locations at the bottom of the basket for lifting. In addition there are drain slots (1.0" wide × 0.5" high) at the bottom of the basket. For these locations, an analysis of the vertical g loadings has been evaluated for each box section.

Total weight of one box section (164" long) = 163 lbs × 4 = 652 lbs

Total area = (2.39 in.^{2} × 4) × (17.3/25.5) = 6.49 in.^{2}

σ = Total Compressive Load/Cross Section of 304SS = (652) lbs/6.49 in.^{2} = 100 psi

These maximum stresses are evaluated in Section 2.10.5.3.6 to verify that the design criteria are met.

1 Foot End Drop Vertical Load - Stainless Steel Fusion Weld

Under the vertical load, each fusion weld is designed to support a panel including one 0.3125" thick × 10.4" high × 6.1875" span poison plate and one 0.3125" thick × 1.75" high × 6.1875" span stainless steel, therefore, the total weight of this panel is:

$W = (0.3125" \times 10.4" \times 6.1875") \times 0.1\ lb/in.^3 + (0.3125" \times 1.75" \times 6.1875") \times 0.29\ lb/in.^3 = 3\ lbs$

Under 1 g vertical load, the shear stress, $\tau = W/A = 3 / [\pi (0.5)^2/4] = 15.3$ psi

This maximum stress is evaluated in Section 2.10.5.3.6 to verify that the design criteria are met.

1 Foot End Drop Vertical Load - Aluminum Rails

Under vertical load, each rail is designed to support its own weight. The weight and areas of the rail are:

	Area (in.^{2})	Weight (164" long),lbs
Small Rail (Figure 2.10.5-28)	8.78	145
Large Rail (Figure 2.10.5-27)	16.34	270

Therefore, the maximum compressive stress under 1 g vertical load is:

$\sigma_1 = 145 \times 1/8.78 = 16.5$ psi
$\sigma_2 = 270 \times 1/16.34 = 16.5$ ksi

These maximum stresses are evaluated in Section 2.10.5.3.6 to verify that the design criteria are met.

1 Foot End Drop Vertical Load – Hold Down Ring

Under vertical load, the basket hold down ring is designed to support its own weight, weight of basket and basket rails. The weight and areas of the rail are:

Weight of Basket and Rails = 25.9 kips
Weight of Basket Hold Down Ring = 1.4 kips

Cross Area of Basket Hold Down Ring = 344.4 in^2

Therefore, the maximum compressive stress under 1g vertical load is:

$\sigma = (25.9 + 1.4) \times 1000/344.4 = 79.3$ psi

This maximum stress is evaluated in Section 2.10.5.3.6 to verify that the design criteria are met.

2.10.5.3.4 Basket Thermal Expansion Analysis

The thermal analysis of the basket is described in Chapter 3. The thermal analysis is performed to determine the basket temperatures for the condition with maximum solar heating, maximum decay heat from the cask contents, and 100°F daily average ambient air. The temperatures are used to evaluate the effects of axial and radial thermal expansion in the basket components. The following table summaries the thermal analysis results from Chapter 3, these results support the selection of cask body and basket components temperatures for thermal expansion analysis purposes.

Component	Max. Calculated Temperature °F	Selected Temperature for Thermal Expansion Analysis °F
Cask Body	< 270	250**
Basket Plate	< 470	500
Fuel Cladding	< 500	550

** Conservatively using lower temperature for thermal expansion analysis.

In order to prevent thermal stress, adequate clearance shall be provided between the poison plates and stainless steel plates, and between the basket outer diameter and cask cavity inside diameter, for free thermal expansion. To verify that adequate provision exists, the thermal expansions between different components are calculated as follows:

Thermal Expansion Between the Length of Fuel Assembly and Cask Cavity

The spent fuel assemblies are assumed to be at 550°F and cask shell temperature at 250°F. The length of the spent fuel assembly when hot is:

$$L_F = L_T + (L_Z \times \alpha_Z + L_S \times \alpha_S)\,\Delta T$$

Where for the design basis GE 7×7 (longest BWR fuel):

L_F = Hot length of BWR fuel assembly, in.

L_T = Total length of fuel assembly at room temperature = 176.16 in.

L_Z = Length of Zircaloy guide tube = 160.47 in.

α_Z = Zircaloy coefficient of thermal expansion = 3.73×10^{-6} in./in.°F at 550°F

L_S = Length of stainless steel per fuel assembly = 15.73 in.

α_S = Stainless steel coefficient of thermal expansion = 9.45×10^{-6} in./in.°F at 550°F

$\Delta T = 550^\circ F - 70^\circ F = 480^\circ F$

Therefore:

$L_F = 176.52$ in.

Allowing 1.0 inch for irradiation growth of the spent fuel assembly, the total assembly length including thermal expansion is 177.52 inches. The length of the cask cavity at room temperature is 178.0 inches. The minimum length of the cask cavity at 250°F is:

$L_{CH} = L_{CC} + L_{CC} \times \alpha_C \times \Delta T$

Where:

L_{CH} = Hot length of cask cavity, in.

L_{CC} = Minimum cask cavity length at room temperature = 178.0 in.

α_C = Carbon steel coefficient of thermal expansion = 6.27×10^{-6} in./in.°F at 250°F

$\Delta T = 250^\circ F - 70^\circ F = 180^\circ F$

Therefore:

$L_{CH} = 178.20$ in. > 177.52 in.

Thus, adequate clearance has been provided between the BWR spent fuel assemblies and the cask cavity length to permit free thermal expansion.

Thermal Expansion Between the O. D. of Basket and I. D. of Cask Cavity

The basket temperature is assumed to be at 500°F and cask shell temperature at 250°F. The maximum outside diameter of the basket when hot is:

$D_{BH} = D_{BC} + (D_{BC} \times \alpha_S)\ \Delta T$

Where:

D_{BH} = Hot outside diameter of basket, in.

D_{BC} = Maximum outside diameter of basket at room temperature = 69.24 in.

α_S = Stainless steel coefficient of thermal expansion = 9.37×10^{-6} in./in.°F at 500°F

$\Delta T = 500^\circ F - 70^\circ F = 430^\circ F$

Therefore:

$D_{BH} = 69.52$ in.

The minimum inside diameter of the cask cavity at room temperature is 69.50 inches. The minimum inside diameter of the cask cavity at 250°F is:

$D_{CH} = D_{CC} + (D_{CC} \times \alpha_c)\ \Delta T$

Where:

D_{CH} = Minimum inside diameter of cask when hot, in.

D_{CC} = Minimum inside diameter of cask cavity at room temperature = 69.5 in.

α_C = Carbon steel coefficient of thermal expansion = 6.27×10^{-6} in./in.°F at 250°F

$\Delta T = 250°\ F - 70°F = 180°F$

Therefore:

$D_{CH} = 69.58$ in. > 69.52 in.

Thus, adequate clearance has been provided between the outside diameter of the basket and the inside diameter of the cask cavity to permit free thermal expansion.

<u>Thermal Expansion Between the Length of Basket (including Basket hold-down Ring) and Cask Cavity</u>

The basket temperature is assumed to be at 500°F and cask shell temperature at 250°F. The length of the basket when hot is:

$L_{BH} = L_{BC} + (L_{BC} \times \alpha_S)\ \Delta T$

Where:

L_{BH} = Hot length of basket including basket hold-down ring, in.

L_{BC} = Total length of basket including hold-down ring at room temperature = 177.25 in.

α_S = Stainless steel coefficient of thermal expansion = 9.37×10^{-6} in./in.°F at 500°F

$\Delta T = 500°\ F - 70°F = 430°F$

Therefore:

$$L_{BH} = 177.96 \text{ in.} < 178.20 \text{ in.}$$

Thus, adequate clearance has been provided between the basket and the cask cavity length to permit free thermal expansion.

Thermal Expansion Between Basket Stainless Steel and Poison Plates (Radial Direction)

The basket temperature is assumed to be at 500°F and there are four (4) different lengths of basket plates in the radial direction, the thermal expansion calculations are based on nominal basket length. The differential thermal expansion between stainless steel and poison plates at these four different locations are:

$$\Delta_1 = 66.94 \times (13.82 - 9.37) \times 10^{-6} \times (500\text{-}70) = 0.128 \text{ in.}$$

$$\Delta_2 = 53.81 \times (13.82 - 9.37) \times 10^{-6} \times (500\text{-}70) = 0.103 \text{ in.}$$

$$\Delta_3 = 40.44 \times (13.82 - 9.37) \times 10^{-6} \times (500\text{-}70) = 0.077 \text{ in.}$$

$$\Delta_4 = 13.69 \times (13.82 - 9.37) \times 10^{-6} \times (500\text{-}70) = 0.026 \text{ in.}$$

Therefore, at these locations, minimum spaces of 0.15 in., 0.13 in., 0.1 in., and 0.05 in. are provided between stainless steel and poison plates (poison plate will be cut short) to allow free thermal expansion.

Thermal Expansion Between Basket Stainless Steel and Poison Plates (Axial Direction)

There are thirteen (13) poison plate sections (see Figure 2.10.5-2) along the axial direction, the nominal height of the poison plate is 10.4", therefore, the maximum differential thermal expansion between the poison and stainless steel plates at 500°F is:

$$\Delta = 10.4 \times (13.82 - 9.37) \times 10^{-6} \times (500\text{-}70) = 0.0199''$$

Therefore, a minimum clearance of 0.023" is provided to permit free thermal expansion.

Based on the above calculations, adequate clearances have been provided for thermal expansion. Thus no thermal stress will be induced in the baskets.

Thermal Expansion Under Fire Accident Condition

Under the fire accident condition (reference to Chapter 3), the basket temperature does not change appreciably while the cask temperature rises during the fire accident. The gaps between the outside diameter of the basket and inside diameter of the cask, the length of the basket and cask cavity, and the length of the fuel assemblies and cask cavity will slightly increase, therefore, no thermal stress will be induced in the basket.

The thermal expansions between the basket stainless steel plates and poison plates in the radial directions are recalculated as follows (the maximum basket temperature is 534°F, using temperature of 550°F for thermal expansion calculation):

$$\Delta_1 = 66.94 \times (13.97 - 9.45) \times 10^{-6} \times (550\text{-}70) = 0.145 \text{ in.}$$

$$\Delta_2 = 53.81 \times (13.97 - 9.45) \times 10^{-6} \times (550\text{-}70) = 0.117 \text{ in.}$$

$$\Delta_3 = 40.44 \times (13.97 - 9.45) \times 10^{-6} \times (550\text{-}70) = 0.088 \text{ in.}$$

$$\Delta_4 = 13.69 \times (13.97 - 9.45) \times 10^{-6} \times (550\text{-}70) = 0.03 \text{ in.}$$

Therefore, minimum spaces of 0.15 in., 0.13 in., 0.1 in., and 0.05 in. provided at these locations between stainless steel and poison plates are adequate.

The thermal expansions between the basket stainless steel plates and poison plates in the axial directions are recalculated as follows (based on maximum basket temperature of 550°F):

$$\Delta = 10.4 \times (13.97 - 9.45) \times 10^{-6} \times (550\text{-}70) = 0.02256''$$

Therefore, minimum clearance of 0.023" provided at this location between stainless steel and poison plates is adequate.

2.10.5.3.5 Design Criteria

The basis for the 304 stainless steel fuel compartment box section stress allowables is Section III, Subsection NG of the ASME[3]Code. The primary membrane stress intensity and primary membrane plus bending stress intensities are limited to S_m (S_m is the Code allowable stress intensity) and 1.5 S_m, respectively, at any location in the basket for Normal Service Conditions. The average shear stress is limited to $0.6S_m$.

The ASME Code provides a basic 3 S_m limit on primary plus secondary stress intensity for Level A (normal) conditions. That limit is specified to prevent ratcheting of a structure under cyclic loading and to provide controlled linear strain cycling in the structure so that a valid fatigue analysis can be performed. The Code also provides guidance in the application of plastic analyses which can be performed to demonstrate shakedown (absence of ratcheting) and to determine stresses for fatigue evaluation. Ratcheting and fatigue cannot occur in the basket since thermal cycling will not occur in this basket design. The numerical values of primary stress intensity limits are listed in the following table.

TN-68 Basket Structural Design Criteria for Normal Conditions

Numerical Values of Primary Stress Intensity Limits			
	304 SS at 500°F[1] (ksi)	SB 221, 6061-T6 Aluminum Rails at 350°F[2], (ksi)	ASME Reference
Membrane Stress Intensity P_m $(0.9 \times S_m)$	15.75 [3]	6.30	Subsection NG NG-3221.1
Membrane + Bending Stress Intensity $P_m + P_b$ $(1.5 \times 0.9 \times S_m)$	23.63[3]	9.45	Subsection NG NG-3221.2
Average Shear Stress at 500°F τ $(0.3 \times 0.6 \times S_m)$	3.15[4]		Subsection NG NG-3227.2b
Average Shear Stress at 400°F τ $(0.3 \times 0.6 \times S_m)$	3.37[4]		Subsection NG NG-3227.2b

Notes:

1. The Maximum basket temperature is less than 470°F (Chapter 3), allowable stress is conservatively using 500°F.
2. The Maximum rail temperature is less than 320°F (Chapter 3), allowable stress is conservatively using 350°F.
3. The allowables were reduced (× 0.9) to include the quality factor for full penetration based on progressive MT or PT examination (NG-5231)
4. The allowables were reduced (× 0.3) to include the quality factor for fusion weld based on visual examination (NG-5260)

2.10.5.3.6 Evaluation- Stress Due to Normal Condition Service

The following table summarizes the normal condition basket structural analysis:

Stress Summary of Normal Condition Structural Analysis

Loading	Stress Category	Max. Stress (ksi) (1G)	Allowable Stress (ksi)	Max. Allowable G load	Max. Calculated G Load Including DLF(2)	Reference Section/Table
304 Stainless Steel Plate						
End Drop	P_m	0.1	15.75	158	15	Sect. 2.10.5.3.3
Side drop	P_m	0.33	15.75	48	35	Table 2.10.5-1 (0° drop)
	$P_m + P_b$	0.59	23.63	40	35	Table 2.10-1 (0° drop)
Stainless Steel Fusion weld						
End Drop	τ	0.02	3.15	158	15	Sect. 2.10.5.3.3
Side Drop	τ	0.07	3.37(1)	48	35	Sect. 2.10.5.3.2
6061-T6 Aluminum Rail						
End Drop	P_m	0.02	6.30	315	15	Sect. 2.10.5.3.3
Side Drop	P_m	0.10	6.30	63	35	Table 2.10.5-2 (Location 1)
	$P_m + P_b$	0.15	9.45	63	35	Table 2.10.5-2 (Location 1)
304 Stainless Steel Basket Hold Down Ring						
End Drop	P_m	0.08	15.75	197	15	Sect. 2.10.5.3.3

Notes:

1. The maximum shear stresses due to lateral side drop load are occurred at peripheral of the basket. The basket temperatures at these panels are less than 400°F (≈ 380°F, see Figure 3.4-6 of Chapter 3), therefore, the allowable shear stress is calculated based on 400°F temperature.
2. DLF = Dynamic Load Factor

Based on the results of these analyses, the basket, rails, and hold down ring are structurally adequate up to 40G. This G load is higher than the calculated G load of 15G for 1 foot end drop and 35G for 1 foot side drop.

The basket is therefore structurally adequate and it will properly support and position the fuel assemblies under normal loading conditions.

2.10.5.4 Basket Under Accident Condition Loads - Stress Analysis

The basket structural analyses performed in Section 2.10.5.3 used linear elastic analyses with a 1 G unit load. The results of these elastic analyses can be ratioed up for the G loads in the accident load cases.

2.10.5.4.1 Design Criteria For Accident Loading Conditions

The stress criteria are taken from Section III, Appendix F of ASME[3] Code. The hypothetical impact accidents are evaluated as short duration Level D conditions. For elastic analysis, the primary membrane stress (P_m) is limited to the smaller of $2.4S_m$ or $0.7S_u$ and membrane plus bending stress intensities are limited to $1.5 \times P_m$. The average shear stress is limited to the smaller of $0.42\ S_u$ or $2 \times 0.6S_m$.

The fuel compartment walls, when subjected to compressive loadings, are also evaluated against ASME Code rules for component supports to ensure that buckling will not occur. The acceptance criteria (allowable buckling loads) are taken from ASME Code, Section III, Appendix F, paragraph F-1341.4, Plastic Instability Load. The allowable buckling load is equal to 70% of the calculated plastic instability load. The numerical values of Level D stress limits are listed in the following table.

TN-68 Basket Structural Design Criteria for Level D Conditions

Numerical Values of Primary Stress Intensity Limits			
	304 SS at 500°F (ksi)	SB 221, 6061-T6 Aluminum Rails at 350°F, (ksi)	ASME Reference
Membrane Stress Intensity P_m, (smaller of $2.4S_m$ or $0.7S_u$)	42.0	15.12	Appendix F F-1331.1a
Membrane + Bending Stress Intensity, $P_m + P_b$ ($1.5\ P_m$)	63.0	22.68	Appendix F F-1331.1c
Average Shear Stress (smaller of $0.42\ S_u$ or $2 \times 0.6S_m$)	21.0		Appendix F F-1331.1d or NG-3225
Average Shear Stress (smaller of $0.42\ S_u$ or $2 \times 0.6S_m$)	22.44**		Appendix F F-1331.1d or NG-3225

** based on 400°F.

2.10.5.4.2 Evaluation- Stress Due to Accident Loading Conditions

The following table summarizes the accident condition basket structural analysis:

Stress Summary of Accident Condition Structural Analysis

Loading	Stress Category	Max. Stress (ksi) (1G)	Allowable Stress (ksi)	Max. Allowable G load	Max. Calculated G Load Including DLF**	Reference Section/Table
304 Stainless Steel Plate						
End Drop	P_m	0.1	42.0	420	80	Sect. 2.10.5.3.3
Side drop	P_m	0.33	42.0	127	80	Table 2.10.5-1 (0° drop)
	$P_m + P_b$	0.59	63.0	107	80	Table 2.10.5-1 (0° drop)
Stainless Steel Fusion weld						
End Drop	τ	0.02	21.0	1050	80	Sect. 2.10.5.3.3
Side Drop	τ	0.07	22.44	321	80	Section 2.10.5.3.2
6061-T6 Aluminum Rail						
End Drop	P_m	0.017	15.12	889	80	Sect. 2.10.5.3.3
Side Drop	P_m	0.10	15.12	151	80	Table 2.10.5-2 (Location 1)
	$P_m + P_b$	0.15	22.68	151	80	Table 2.10.5-2 (Location 1)
304 Stainless Steel Basket Hold Down Ring						
End Drop	P_m	0.08	42.0	525	80	Sect. 2.10.5.3.3

** DLF = Dynamic Load Factor

Based on the results of these analyses, the basket, rails, and hold down ring are structurally adequate up to 107G (limited by stainless steel plate). This g load is higher than the analysed G load of 80G for 30 foot end drop and side drop.

The basket assembly is thereforestructurally adequate and it will properly support and position the fuel assemblies under accident loading conditions.

2.10.5.5 Basket Under Accident Condition Loads - Buckling analysis

2.10.5.5.1 Analysis of Basket to Determine the Buckling Loads

Additional analyses are performed in this section to evaluate the outer basket plate stability when the lateral inertial loading is applied at various angles relative to the plates. Analyses are performed for 0, 10, 20, 30, and 45 degree drop angles (Figure 2.10.5-30).

The basic structural element of the basket is considered to be a wall between fuel compartments which consists of 0.3125" thick stainless steel plate sandwiched between two 0.1875" thick stainless steel plates (the strength of poison plate is neglected from buckling load calculation, but its own weight is included). The overall dimensions of this outer basket wall are 6.1875" high and 12.17" wide (12.25" is used in the model, see Figures 2.10.5-31 and 2.10.5-32).

Finite Element Model

In order to calculate the buckling load, a three-dimensional ANSYS finite element model is constructed using a Shell 43 plastic large strain shell element. Shell 43 is well suited to model nonlinear, flat or warped, thin to moderately thick shell structures. The element has six degrees of freedom at each node: translations in the nodal x, y, and z directions and rotations about the nodal x, y, and z axes. The nodes at the locations of fusion welds are coupled for all degrees of freedom (the fusion welds rigidly connect the stainless steel boxes and stainless steel plates at these nodes). The nodes of various plates are coupled together in the out of plane direction so that they will bend in unison under surface pressure loading and to simulate the through thickness support provided by the poison plates. The finite element model is shown on Figure 2.10.5-33.

Geometric Nonlinearities

Since the structure experiences large deformations before buckling, the large displacement option of ANSYS is used for all the analyses. The deflections during each load step are used to continuously redefine the geometry of the structure, thus producing a revised stiffness matrix. Therefore, buckling can be analyzed with the large deflection option. If the rate of change in deflection (per iteration) is observed, an estimation of the stability of the structure can be made. In particular, if the change of displacement at any node is increasing, the loading is above critical and the structure will eventually buckle.

Material Nonlinearities

The basket is constructed from 304 stainless steel. A bilinear stress strain relationship is used to simulate the correct nonlinear material behavior. The following elastic and inelastic material properties are used in the analysis:

Mechanical Properties of SA-240 Type 304 SS

	400°F	500°F
Modulus of Elasticity (psi)	26.5×10^6	25.8×10^6
Yield Strength (psi)	20,700	19,400
Ultimate Strength (psi)	64,400	63,500
Tangent Modulus (psi)	109,463	110,457

Loadings

The loadings on the panel model (Figure 2.10.5-31, Location 1) were appropriately transferred from full size basket loadings. The loads used in 0, 10, 20, 30, and 45 degree drop analyses are summarized in the following table. Maximum loads of 200g were applied in each analysis. The automatic time stepping program option "Autots" was activated. This option lets the program decide the actual size of the load-substep for a converged solution. The program stops at the load substep when it fails to result in a converged solution. The last load step, with a converged solution, is the plastic instability load for the model. Figures 2.10.5-34 shows the loading conditions.

Summary of Loads for Different Drop Orientations Analysis
($F_y = F \cos\theta$, $P_x = P \sin\theta$)

Drop Orientation (Degree)	1G load (12.25" Length) (Weight including all SS & poison plates above the bottom panel, rails, and 9 fuel assemblies**)		200 G Load Computer Run	
	Axial Load F_y (lbs)	Trans. Load P_x (psi)	F_y (lbs)	P_x(psi)
0	675	0	135,000	0
10	665	0.148	133,000	29.6
20	634	0.29	126,800	58.0
30	585	0.425	117,000	85
45	477	0.601	95,400	120.2

** This assumption is very conservative for drop orientation other than 0 degree, for example, for 30 and 45 degree drops the bottom panel only supports 7 fuel assemblies instead of 9 fuel assemblies.

Boundary Conditions

The ANSYS finite element model conservatively assumes that both ends of column are hinged. The boundary conditions are shown on Figure 2.10.5-35. However, the stainless steel (0.3125" thick × 1.75" wide) and poison plates forming the panel extend beyond the panel and connect into other panels so that moments can be developed at the top and bottom panel edges. These reactive end moments will keep the ends from rotating during buckling. Reference to "Formulas for Stress and Strain" by Raymond Roark[5], Fourth Edition, Table XV indicates that:

Load Case No. (From Table XV of Roark)	Loading and Edge Condition	Formula for Critical Load (P)
2	End Load Both Ends Hinged	$P = (1)(\pi^2 EI/L^2)$
3	End Load Both Ends Fixed	$P = (4)(\pi^2 EI/L^2)$

Based on the formulas described above, the end conditions selected for the ANSYS model (both end hinged) are conservative and the calculated allowable compressive load has a large margin of safety.

ANSYS Finite Element Analysis Results

The plastic instability load and allowable buckling load for 0,10, 20, 30, and 45 degree orientation drops at 400°F and 500°F basket temperatures are summarized in the following tables. Based on the design criteria described in Section 2.10.5.4.1, the allowable buckling load is equal to 70% of the calculated plastic instability load. Displacement and nodal stress intensity plots for 0, 10, 20, 30, and 45 degree orientation drops (400°F) at the last converged load step are shown on Figures 2.10.5-36 through 2.10.5-40.

Plastic Instability Load and Allowable Buckling Load
(Figure 2.10.5-31, Location 1)

Drop Orientation (Degree)	Plastic Instability Load (G)		Allowable Buckling Load (0.7 × G)	
	400°F	500°F	400°F	500°F
0	174	162	122	113
10	160	151	112	106
20	154	146	108	102
30	152	145	106	101
45	164	155	115	109

Additional analysis is performed at location 2 (Figure 2.10.5-31) based on 30 degree drop orientation (lowest allowable buckling load) and basket temperature of 500°F and the result is listed in the following table.

Plastic Instability Load and Allowable Buckling Load
(Figure 2.10.5-31, Location 2)

Drop Orientation (Degree)	Plastic Instability Load, 500°F (G)	Allowable Buckling Load ($0.7 \times G$)
30	225	158

Result From Hand Calculation

As an order of magnitude check, the allowable buckling load based on 400°F temperature and 0 degree drop orientation is calculated below and compared to the ANSYS analysis results. As given in ASME[4] Code, Subsection NF, Paragraph NF-3322-1(c)(2)(a)(Level A Condition) and modified as per Appendix F, Paragraph F-1334 (Level D Condition), the compressive stress limit for the accident condition (Level D) when KL/r is less than 120 and $S_u > 1.2\ S_y$ is:

$F_a = 2 \times S_y\ [0.47 - (KL/r)/444]$

Where:

$K = 1$
$L = 6.1875"$
$S_y = 20{,}700$ psi (at 400°F)
$S_u = 64{,}400$ psi (at 400°F)
$I = b\ h^3/12 = 0.305$ in.^{4}
$A = 5.141$ in.^{2}
$r = (I/A)^{1/2} = 0.2436$ in.

$KL/r = 1 \times 6.1875/0.2436 = 25.4$

Substituting the values given above,

$F_a = 2 \times 20{,}700\ [0.47 - (25.4)/444] = 17{,}090$ psi

The maximum allowable force is $17090 \times 5.141 = 87{,}860$ lbs, therefore, the maximum allowable G load is:

$G = 87{,}860/675 = 130$

This value is reasonably close to the solution given by the ANSYS result (122 G).

Evaluation of the Stainless Steel Buckling Analysis

Based on the results of this analysis, it is concluded that the maximum allowable buckling load is 106g based on a stainless steel temperature of 400°F (Reference to Chapter 3, the maximum basket temperature at the outer basket panel is less than 380°F, therefore, using 400°F is conservative). This G load is higher than 80 G shown in the Appendix 2.10.8 cask impact analysis. The G load at the hottest part of the basket (less than 470°F) is located at the center of the basket (see Chapter 3), the ANSYS run at this location (Figure 2.10.5-31, location 2) based on 500°F temperature results in an allowable G load of 158. Therefore, the compressive and bending stresses developed in the stainless steel cannot cause the panel to buckle due to the accident load.

2.10.5.5.2 Analysis of the Aluminum Rails to Determine the Buckling Loads

The maximum membrane and bending stresses in the aluminum rails from the drop analyses at the most highly stressed location in the vertical member of the rail are listed below (1 G):

Location (Figure 2.10.5-27)	Maximum Membrane S.I. (ksi)	Maximum Bending S.I. (ksi)
2 (Table 2.10.5-2)	0.08	0.02**
3 (Table 2.10.5-2)	0.05	0.01**

** These bending stress intensities are obtained through linearization of the cross section using ANSYS postprocessor

Criteria to Ensure Stability Under Compressive Loading

As given in ASME[4] Code, Subsection NF, Paragraph NF-3322-1(c)(1)(a) and modified as per Appendix F, Paragraph F-1334, the compressive stress limit for the accident condition (Level D) when KL/r is less than C_c and $S_u \leq 1.2\ S_y$ is:

$$F_a = \frac{1.4\,[1 - (KL/r)^2/(2\,C_c^2)]\,S_y}{5/3 + [3\,(KL/r)/(8\,C_c)] - [(KL/r)^3/(8\,C_c^3)]}$$

Where:

$C_c = [(2\,\pi^2\,E)/S_y]^{1/2}$
$K = 1$
$L = 6.6"$ (location 2), $4.8"$ (Location 3)
$S_y = 20{,}000$ psi (at 350°F)
$S_u = 22{,}400$ psi (at 350°F)
$E = 9.0 \times 10^6$ (at 350°F)

$I = b\,h^3/12 = 1(0.75)^3/12 = 0.0351$ in.^{4}
$A = 1.0 \times 0.75\ 0.75$ in.^{2}
$r = (I/A)^{1/2} = 0.216$ in.

$KL/r = 1 \times 6.6/0.216 = 30.55$

$C_c = [(2\,\pi^2 \times 9.0 \times 10^6)/20{,}000]^{1/2} = 94.25$

$$F_a = \frac{1.4\,[1 - (30.55)^2/(2 \times 94.25^2)]\,(20000)}{5/3 + [3\,(30.55)/(8 \times 94.25)] - [(30.55)^3/(8 \times 94.25^3)]} = 14.87 \text{ ksi}$$

For L = 4.8 in.

$KL/r = 1 \times 4.8/0.216 = 22.22$

$C_c = [(2\,\pi^2 \times 9.0 \times 10^6)/20{,}000]^{1/2} = 94.25$

$$F_a = \frac{1.4\,[1 - (22.22)^2/(2 \times 94.25^2)]\,(20000)}{5/3 + [3\,(22.22)/(8 \times 94.25)] - [(22.22)^3/(8 \times 94.25^3)]} = 15.53 \text{ ksi}$$

Based on the above calculations, the allowable compressive stresses for the locations 2 & 3 are listed in the following table:

Location (Figure 2.10.5-27)	Allowable Compressive Stress (F_a, ksi)	Calculated Compressive Stress (1 G, ksi)
2	14.87	0.08
3	15.53	0.05

<u>Criteria To Prevent Failure Under Combined Loading (Compression + Bending)</u>

For combined axial compression and bending, equations 20 and 21 of Paragraph NF-3322.1 (e) (1) apply.

$$f_a / F_a + C_{mx}\,(f_b)/(1 - f_a/F_e)\,F_b \leq 1.0 \text{ ----------(1)}$$

and

$$f_a/(1.4)(0.6)\ S_y + f_b / F_b \leq 1.0 \text{ ----------(2)}$$

The allowable stresses for the above equations are determined as follows:

	Allowable Stress	ASME Code Reference
F_a	14.87 ksi (Location 2) 15.53 ksi (Location 3)	NF-3322-1(c)(1)(a)
F_b	0.66 S_y** =13.2 ksi	F-1334.5 (c)
C_{mx}	0.6	NF-3322.1 (e) (1) (b)
Note	The allowable stress F_a is multiplied by 1.4 as allowed by Paragraph F-1334 ($S_u \leq 1.2\ S_y$)	

** Conservatively use Level A allowable for Level D load calculations

The value of F_e is calculated by the formula below per Paragraph F-1334.5 (b):

$$F_e = \pi^2\ (E)/(1.3)\ (KL/r)^2$$

Where:

K is conservatively taken as 1
L is the free length of the member, 6.6 in. (Location 2), 4.8 in. (Location 3)
r is the radius of gyration, in.
E is the modulus of elasticity, 9.0×10^6 psi

This formula gives the following results for F_e:

Location	F_e (ksi)
2 (L = 6.6", r = 0.216 in.)	73.21
3 (L = 4.8", r = 0.216 in.)	138.39

The interaction equations were evaluated based on:

Location 2 (Assume 150 g)

$$f_a / F_a + C_{mx} (f_b)/(1 - f_a/F_e) F_b = 0.81 + 0.163 = 0.973 \leq 1$$

$$f_a/(1.4)(0.6) S_y + f_b / F_b = 0.714 + 0.227 = 0.94 \leq 1$$

Location 3 (Assume 150 g)

$$f_a / F_a + C_{mx} (f_b)/(1 - f_a/F_e) F_b = 0.483 + 0.144 = 0.63 \leq 1$$

$$f_a/(1.4)(0.6) S_y + f_b / F_b = 0.45 + 0.23 = 0.68 \leq 1$$

Evaluation of the Aluminum rail Buckling analysis

Based on the result of this analysis, it concluded that the maximum allowable buckling load for the aluminum rails is 150 G based on aluminum rail temperature of 350°F (Reference to Chapter 3, the maximum rail temperature is less than 320°F, therefore, using allowables based on 350°F temperature is conservative). This G load is much higher than the 80G load shown on Appendix 2.10.8 cask impact analysis. Therefore, the compressive and bending stresses developed in the aluminum rails due to the accident impact load cannot cause the rails to buckle.

2.10.5.5.3 Additional Evaluation Due to Fabrication Tolerances of Compartment Opening

The nominal open dimension of each fuel compartment cell or box is 6.0 in. × 6.0 in. However, due to fabrication tolerance the maximum compartment opening can go up to 6.08 in. The following section provides additional analysis to evaluate the basket stresses based on basket compartment opening of 6.10 in. × 6.10 in. (conservatively using larger dimension).

- Buckling Analysis

It is observed from Section 2.10.5.5.1 that the 30 degree side impact is the most critical and results in the lowest allowable buckling g load of 101 (based on 500°F). Since the change in the basket opening (from 6.0 in. to 6.10 in.) is minor, it is reasonably assumed that the 30 degree drop is also the most critical drop orientation for the basket with 6.10 in. opening.

The finite element model from Section 2.10.5.5.1 is modified to incorporate the 6.10 inch basket opening. ANSYS runs are made using the same material properties (at 500°F and 400°F), boundary conditions, loads, and procedures as described in Section 2.10.5.5.1. The results are listed in the following table.

Plastic Instability Load and Allowable Buckling Load
(Based on 6.10 in. Basket Opening)

Drop Orientation (Degree)	Plastic Instability Loads (G)		Allowable Buckling Loads (G)	
	400°F	500°F	400°F	500°F
30	151.9	142.5	106	100

- Primary Membrane Plus Bending Stress Intensity

From Table 2.10.5-1, the maximum membrane plus bending stress intensity is 0.59 ksi and occurred during a 0° side drop orientation. The bending stresses are the function of the load distribution and the span length. The loads and boundary conditions remain the same except that the span length is increased from 6.0 in. to 6.10 in. Therefore, the maximum stress intensity due to 1G load at 6.10 in. span is:

$$S.I. = 0.59 \times (6.10/6.0) = 0.60 \text{ ksi}$$

The maximum allowable g load for normal condition is:

$$G = 23.63/0.60 = 39$$

The maximum allowable g load for accident condition is:

$$G = 63/0.60 = 105$$

- Shear Stresses in Fusion Welds

The shear stress is a function of shear load and weld shear area. Since, both of these parameters are unchanged for this loading condition, therefore, the shear stress and allowable G load remain the same.

- Conclusion

Based on the above calculation, the allowable G loads are higher than 35G and 80G as shown on the Appendix 2.10.8 for the normal and accident cask impact analyses. Therefore, the basket will remain in place and maintain separation of the adjacent assemblies.

2.10.5.6 References

1. ANSYS Engineering Analysis System User's Manual, Rev. 5.2, Vol. 1 to 4, 1995.

2. ASME B&PV Code, Section II, Part D, 1995 including 1996 Addendum.

3. ASME B&PV Code, Section III Appendices and Subsection NG, 1995 including 1996 Addendum.

4. ASME B&PV Code, Section III, Subsection NF, 1995 including 1996 Addendum.

5. Roark, R. "Formulas for Stress and Strain" Fourth Edition.

Table 2.10.5-1
Summary of Basket Stress Analysis - Normal Condition
(1G Side Load)

Drop Orientation (Degree)	Component	Stress Category	Max. Stress (1G) (ksi)	Allowable Stress (ksi)	Reference Figures
0	S.S. Plate	P_m	0.22*	15.75	2.10.5-11
		$P_m + P_b$	0.59*	23.63	2.10.5-12
	S.S. Box	P_m	0.33*		2.10.5-13
		$P_m + P_b$	0.35*		2.10.5-14
	Fusion Weld	τ	0.04**	3.37	Section 2.10.5.3.2
30	S.S. Plate	P_m	0.19*		2.10.5-15
		$P_m + P_b$	0.44*		2.10.5-16
	S.S. Box	P_m	0.26*		2.10.5-17
		$P_m + P_b$	0.33*		2.10.5-18
45	S.S. Plate	P_m	0.16*		2.10.5-19
		$P_m + P_b$	0.37*		2.10.5-20
	S.S. Box	P_m	0.22*		2.10.5-21
		$P_m + P_b$	0.29*		2.10.5-22
	Fusion Weld	τ	0.07**		Section 2.10.5.3.2

* Maximum stress intensity
** Average shear stress

Table 2.10.5-2
Linearized Stress Intensities of Aluminum Rail - Normal Condition
(0° Side Load)

Location (Figures 2.10.5-27 & 28)	Stress Category	Max. S.I. 1G (ksi)	Allowable S.I. (ksi)
1	P_m	0.10	6.30 (S_m)
	$P_m + P_b$	0.15	9.45 ($1.5S_m$)
2	P_m	0.08	
	$P_m + P_b$	0.10	
3	P_m	0.05	
	$P_m + P_b$	0.05	
4	P_m	0.02	
	$P_m + P_b$	0.03	
5	P_m	0.02	
	$P_m + P_b$	0.02	

S. I. : Stress Intensity

Table 2.10.5-3
Linearized Stress Intensities of Aluminum Rail - Normal Condition
(30° Side Load)

Location (Figures 2.10.5-27 & 28)	Stress Category	Max. S.I. 1G (ksi)	Allowable S.I. (ksi)
1	P_m	0.07	6.30 (S_m)
	$P_m + P_b$	0.10	9.45 ($1.5S_m$)
2	P_m	0.07	
	$P_m + P_b$	0.08	
3	P_m	0.04	
	$P_m + P_b$	0.05	
4	P_m	0.02	
	$P_m + P_b$	0.03	
5	P_m	0.02	
	$P_m + P_b$	0.02	

Table 2.10.5-4
Linearized Stress Intensities of Aluminum Rail - Normal Condition
(45° Side Load)

Location (Figures 2.10.5-27 & 28)	Stress Category	Max. S.I. 1G (ksi)	Allowable S.I. (ksi)
1	P_m	0.06	6.30 (S_m)
	$P_m + P_b$	0.07	9.45 ($1.5S_m$)
2	P_m	0.06	
	$P_m + P_b$	0.06	
3	P_m	0.03	
	$P_m + P_b$	0.04	
4	P_m	0.02	
	$P_m + P_b$	0.02	
5	P_m	0.02	
	$P_m + P_b$	0.03	

Table 2.10.5-5
Summary of Basket Stress Analysis - Accident Condition
(Side Drop)

Drop Orientation (Degree)	Component	Stress Category	Max. Stress (1G) (ksi)	Allowable Stress (ksi)	Max. Allowable G Load
0	S.S. Plate	P_m	0.22*	42.0	191
		$P_m + P_b$	0.59*	63.0	107
	S.S. Box	P_m	0.33*		127
		$P_m + P_b$	0.35*		180
	Fusion Weld	τ	0.06**	22.44	374
30	S.S. Plate	P_m	0.19*		221
		$P_m + P_b$	0.44*		143
	S.S. Box	P_m	0.26*		162
		$P_m + P_b$	0.33*		191
45	S.S. Plate	P_m	0.16*		263
		$P_m + P_b$	0.37*		170
	S.S. Box	P_m	0.22*		191
		$P_m + P_b$	0.29*		217
	Fusion Weld	τ	0.07**	22.44	321

* Maximum stress intensity
** Average shear stress

Table 2.10.5-6
Linearized Stress Intensities of Aluminum Rail - Accident Condition
(0° Side Drop)

Location (Figures 2.10.5-27 & 28)	Stress Category	Max. S.I. 1g (ksi)	Allowable S.I. (ksi)	Max. Allowable G Loads
1	P_m	0.1	15.12	151
	$P_m + P_b$	0.15	22.68	151
2	P_m	0.08		189
	$P_m + P_b$	0.10		227
3	P_m	0.05		302
	$P_m + P_b$	0.05		454
4	P_m	0.02		756
	$P_m + P_b$	0.03		756
5	P_m	0.02		756
	$P_m + P_b$	0.02		1134

Table 2.10.5-7
Linearized Stress Intensities of Aluminum Rail - Accident Condition
(30° Side Drop)

Location (Figures 2.10.5-27 & 28)	Stress Category	Max. S.I. 1G (ksi)	Allowable S.I. (ksi)	Max. Allowable G Loads
1	P_m	0.07	15.12	216
	$P_m + P_b$	0.10	22.68	227
2	P_m	0.07		216
	$P_m + P_b$	0.08		284
3	P_m	0.04		378
	$P_m + P_b$	0.05		454
4	P_m	0.02		756
	$P_m + P_b$	0.03		756
5	P_m	0.02		756
	$P_m + P_b$	0.02		1134

Table 2.10.5-8
Linearized Stress Intensities of Aluminum Rail - Accident Condition
(45° Side Drop)

Location (Figures 2.10.5-27 & 28)	Stress Category	Max. S.I. 1G (ksi)	Allowable S.I. (ksi)	Max. Allowable G Loads
1	P_m	0.06	15.12	252
	$P_m + P_b$	0.07	22.68	324
2	P_m	0.06		252
	$P_m + P_b$	0.06		378
3	P_m	0.03		504
	$P_m + P_b$	0.04		567
4	P_m	0.02		756
	$P_m + P_b$	0.02		1134
5	P_m	0.02		756
	$P_m + P_b$	0.03		756

FIGURE WITHHELD UNDER 10 CFR 2.390

FIGURE WITHHELD UNDER 10 CFR 2.390

FIGURE WITHHELD UNDER 10 CFR 2.390

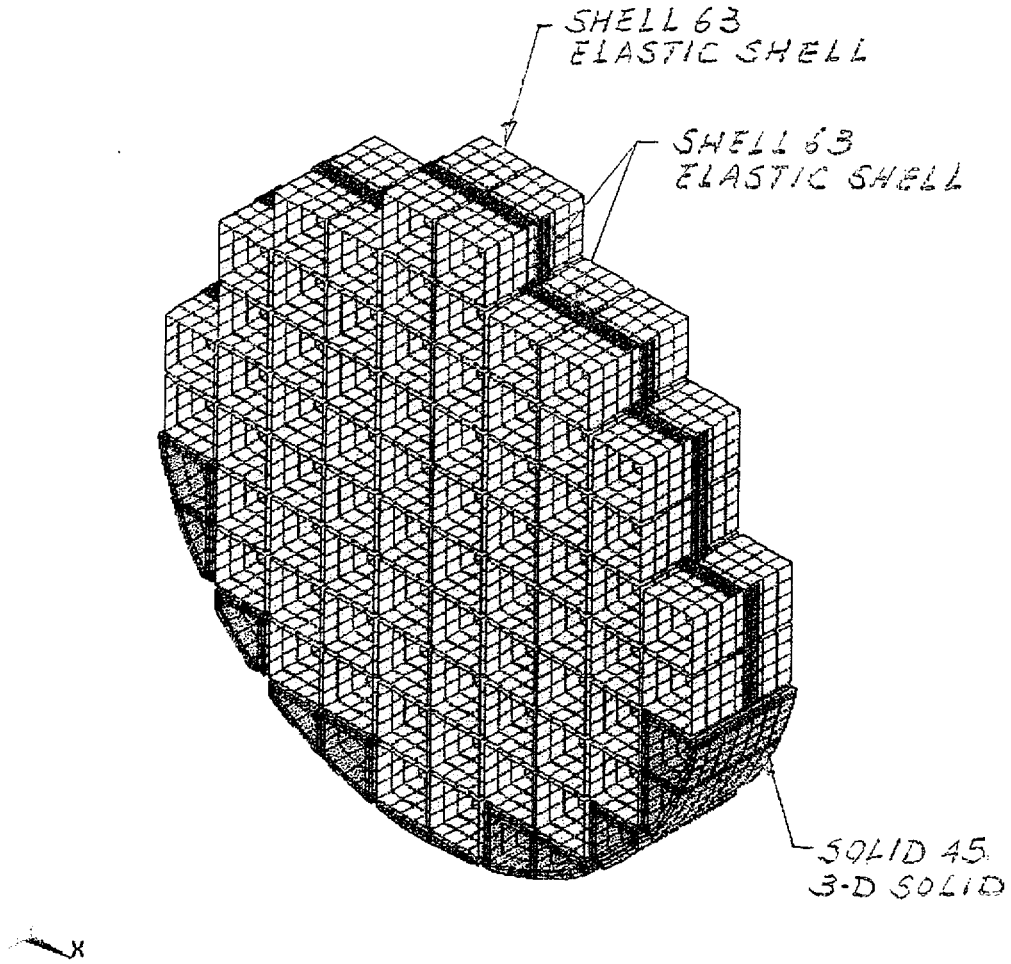

FIGURE 2.10.5-4
FINITE ELEMENT MODEL AND ELEMENT TYPES

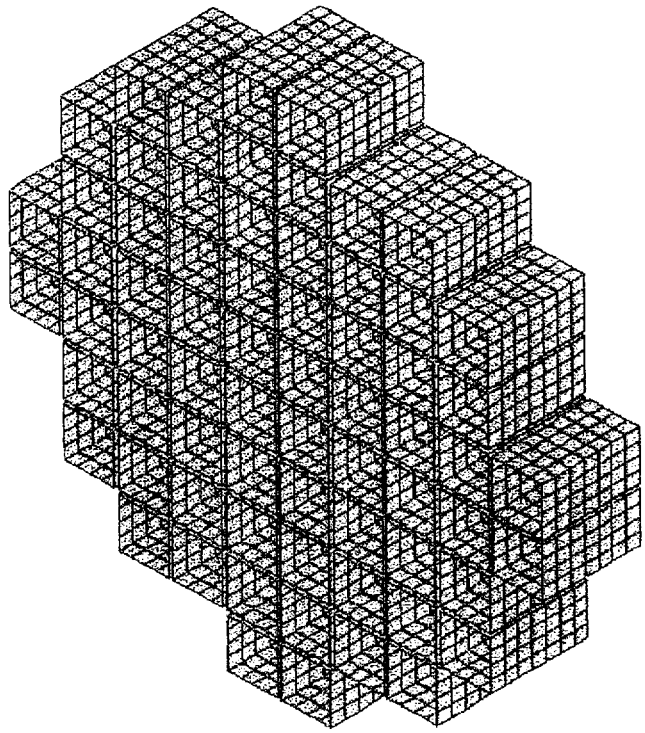

TN-68 Basket Finite Element Model - Stainless Steel Boxes

FIGURE 2.10.5-5
BASKET FINITE ELEMENT MODEL- STAINLESS STEEL BOXES

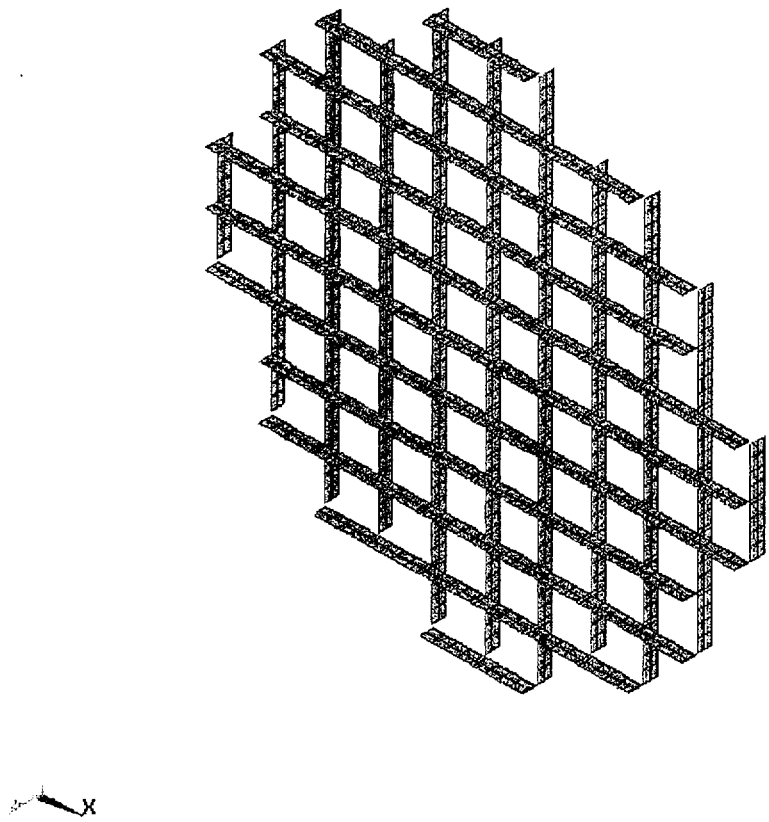

TN-68 Basket Finite Element Model - Stainless Steel Plates

FIGURE 2.10.5-6
BASKET FINITE ELEMENT MODEL- STAINLESS STEEL PLATES

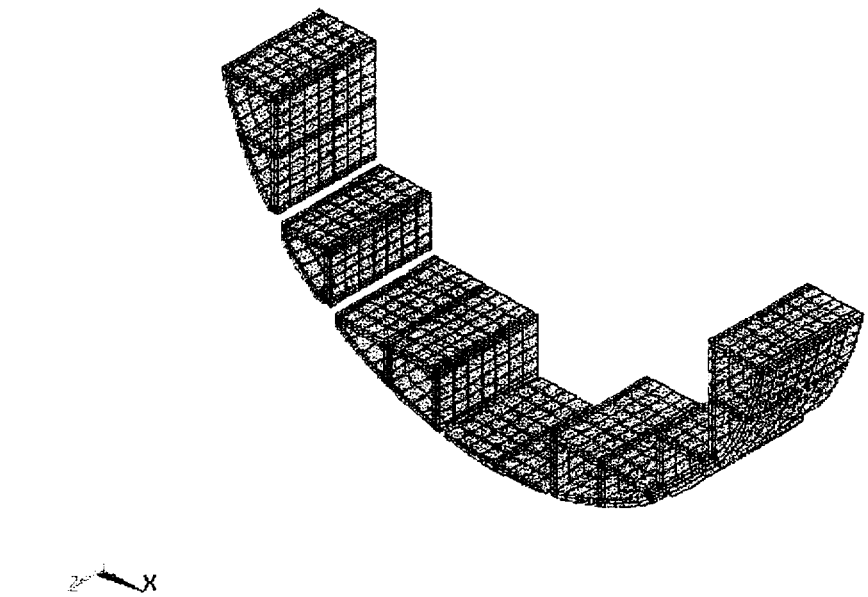

TN-68 Basket Finite Element Model - Aluminum Rails

FIGURE 2.10.5-7
BASKET FINITE ELEMENT
MODEL-ALUMINUM RAILS

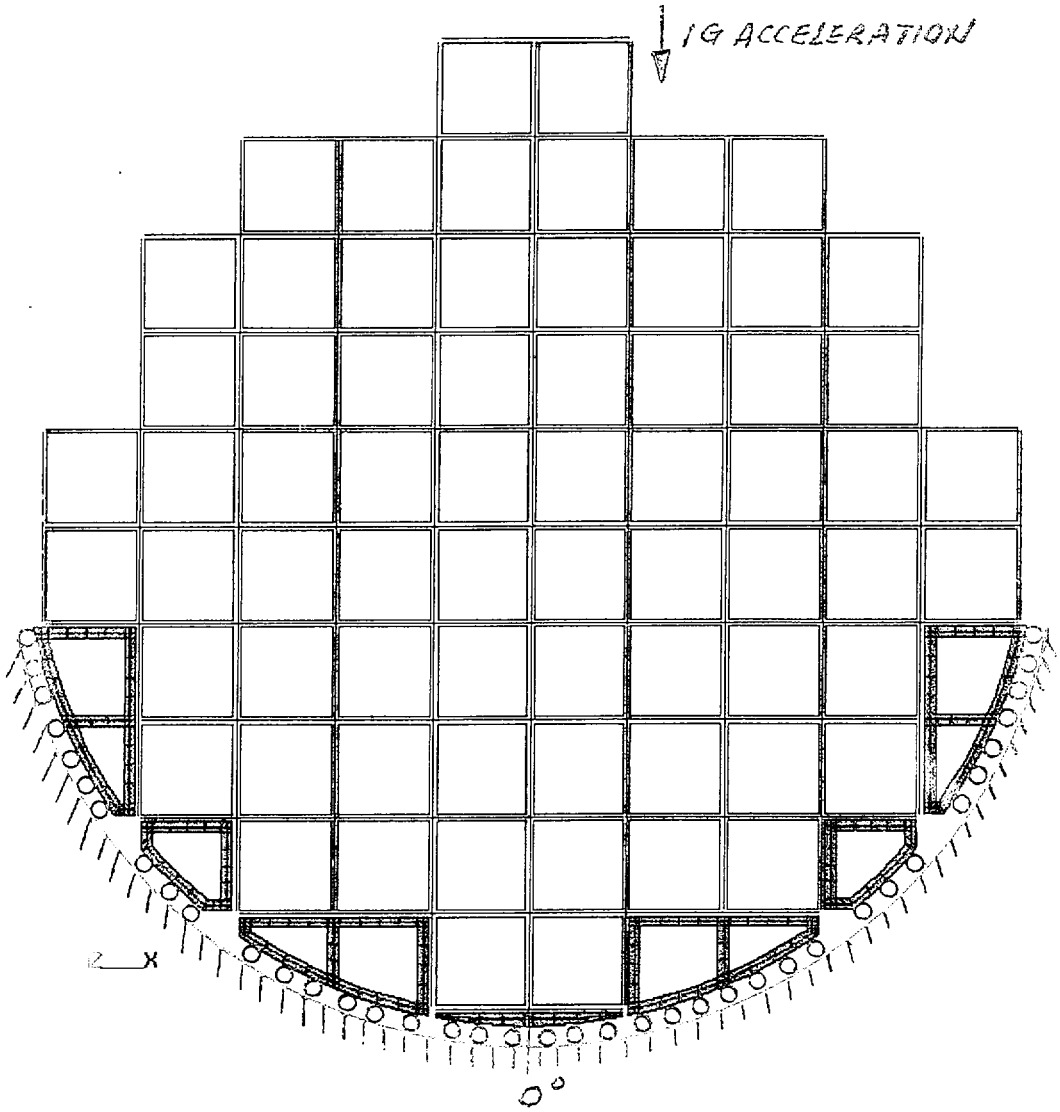

FIGURE 2.10.5-8
LOADING AND BOUNDARY
CONDITIONS-0° DROP

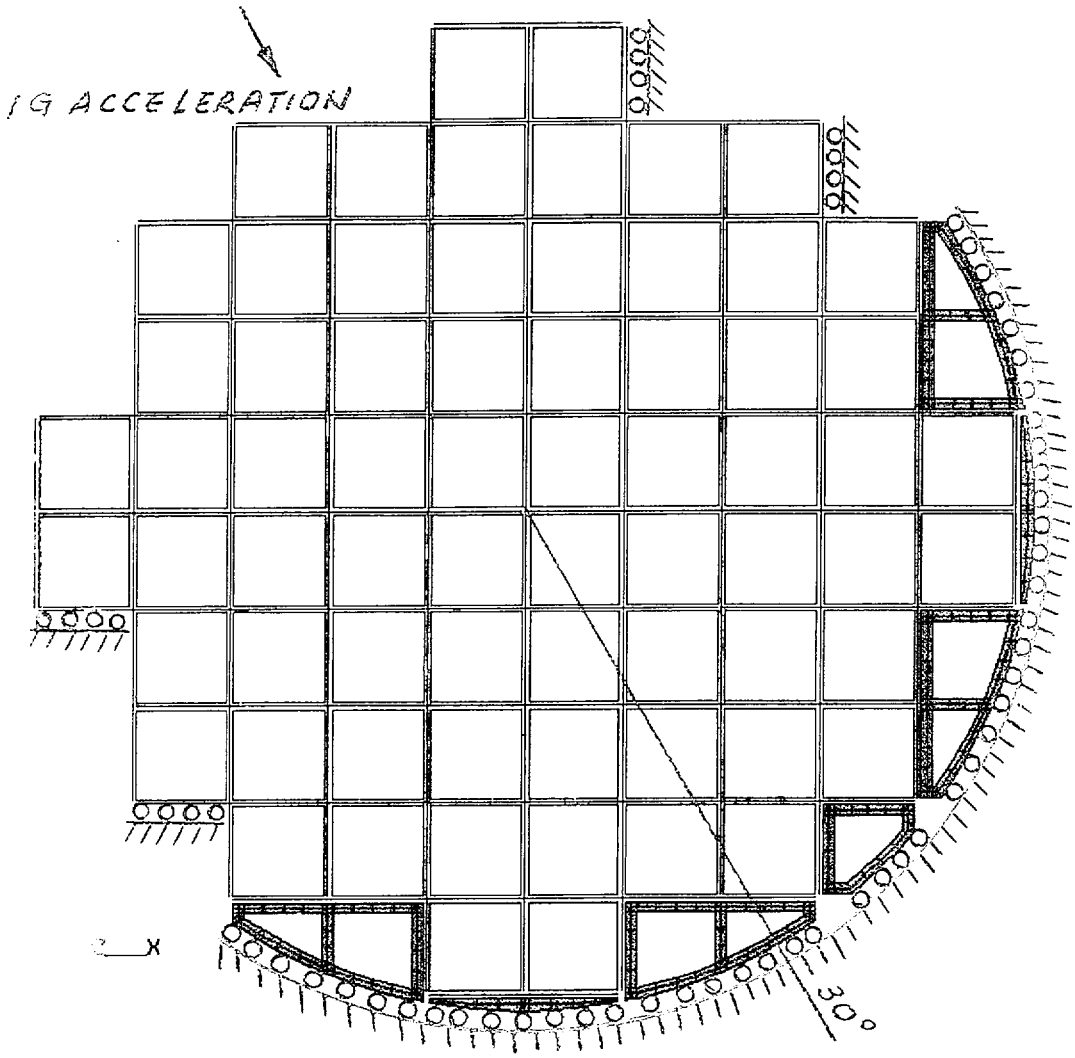

FIGURE 2.10.5-9
LOADING AND BOUNDARY
CONDITIONS-30° DROP

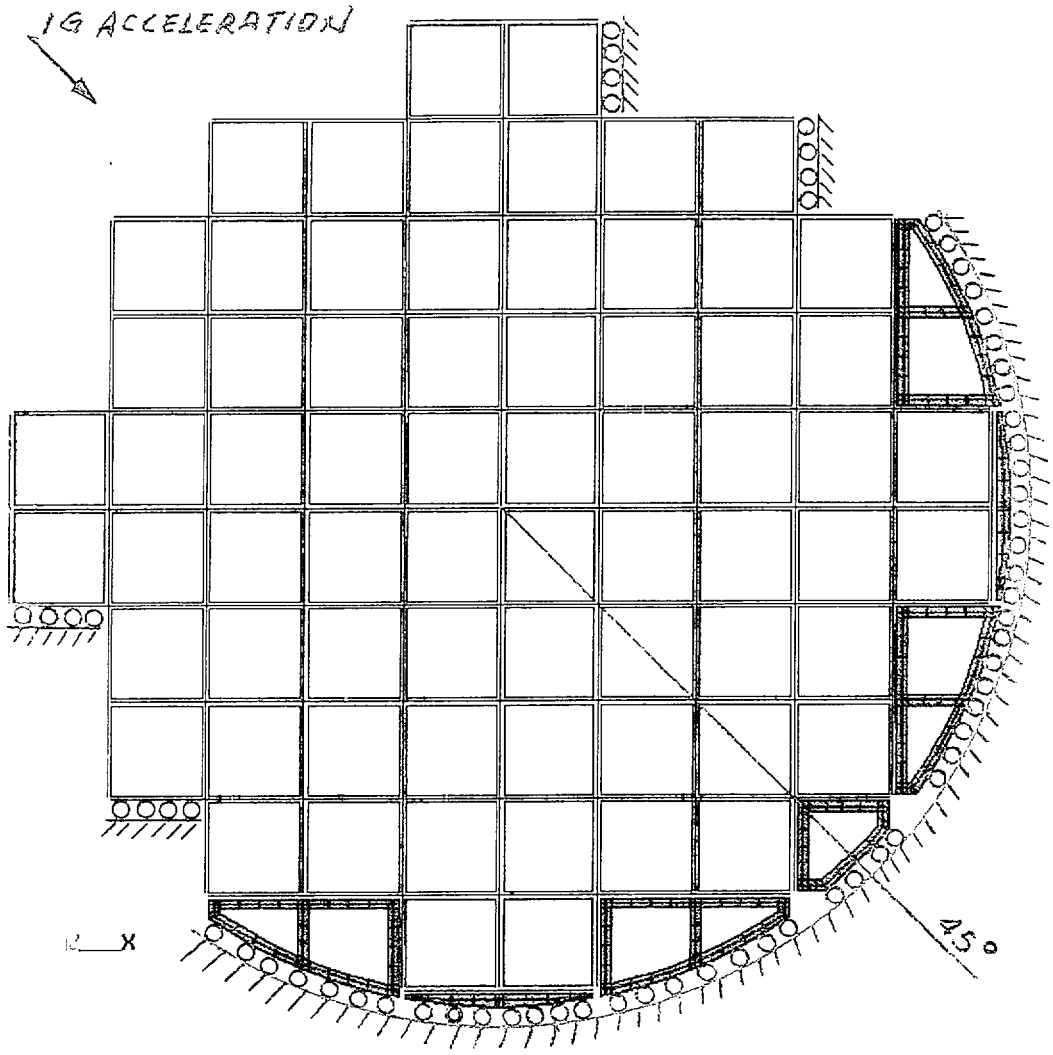

FIGURE 2.10.5-10
LOADING AND BOUNDARY
CONDITIONS-45° DROP

Figure 2.10.5-11
Membrane Stress Intensity (SS Plate)-0 Degree Drop

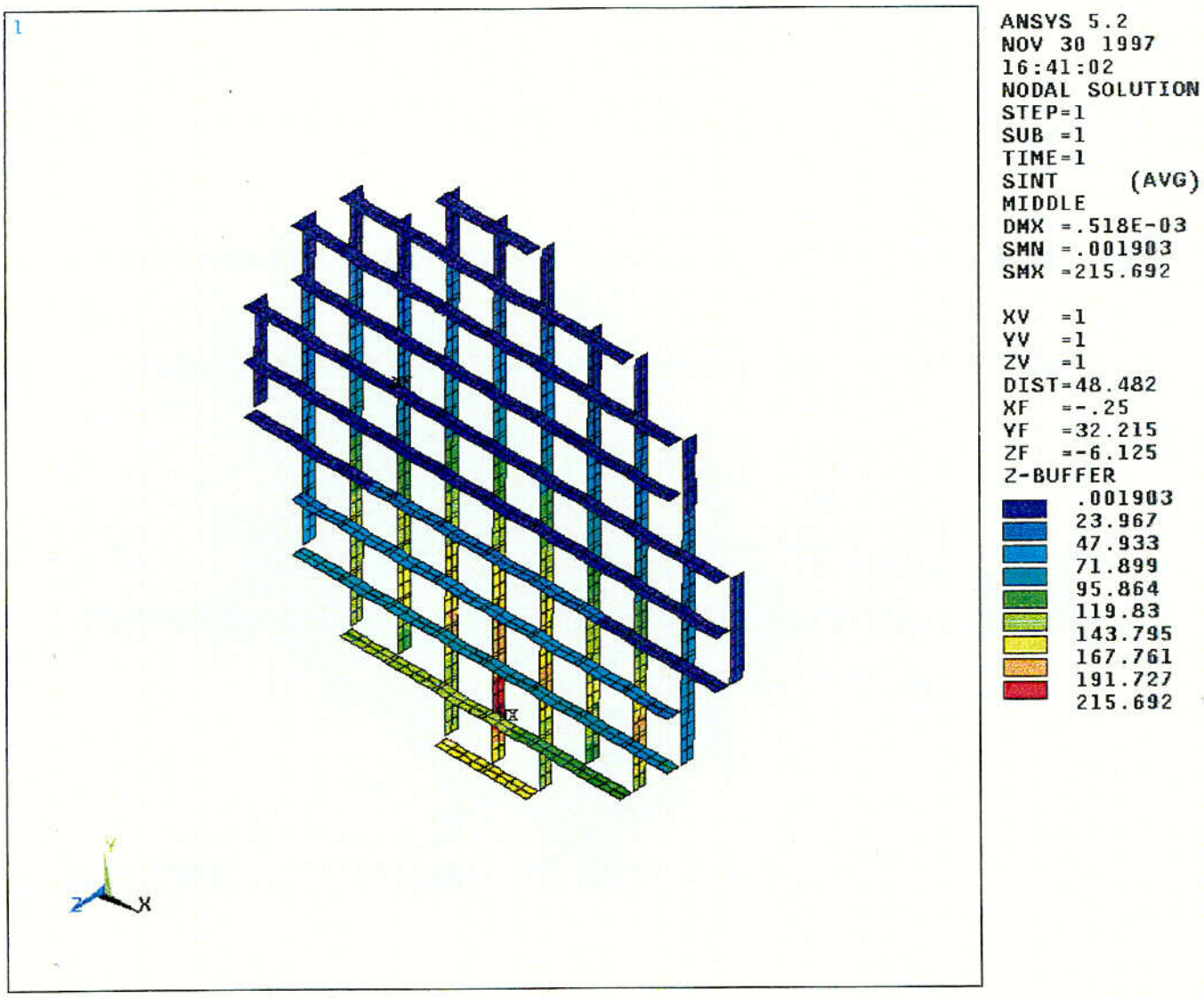

C-01

Figure 2.10.5-12
Membrane + Bending Stress Intensity (SS Plate)-0 degree Drop

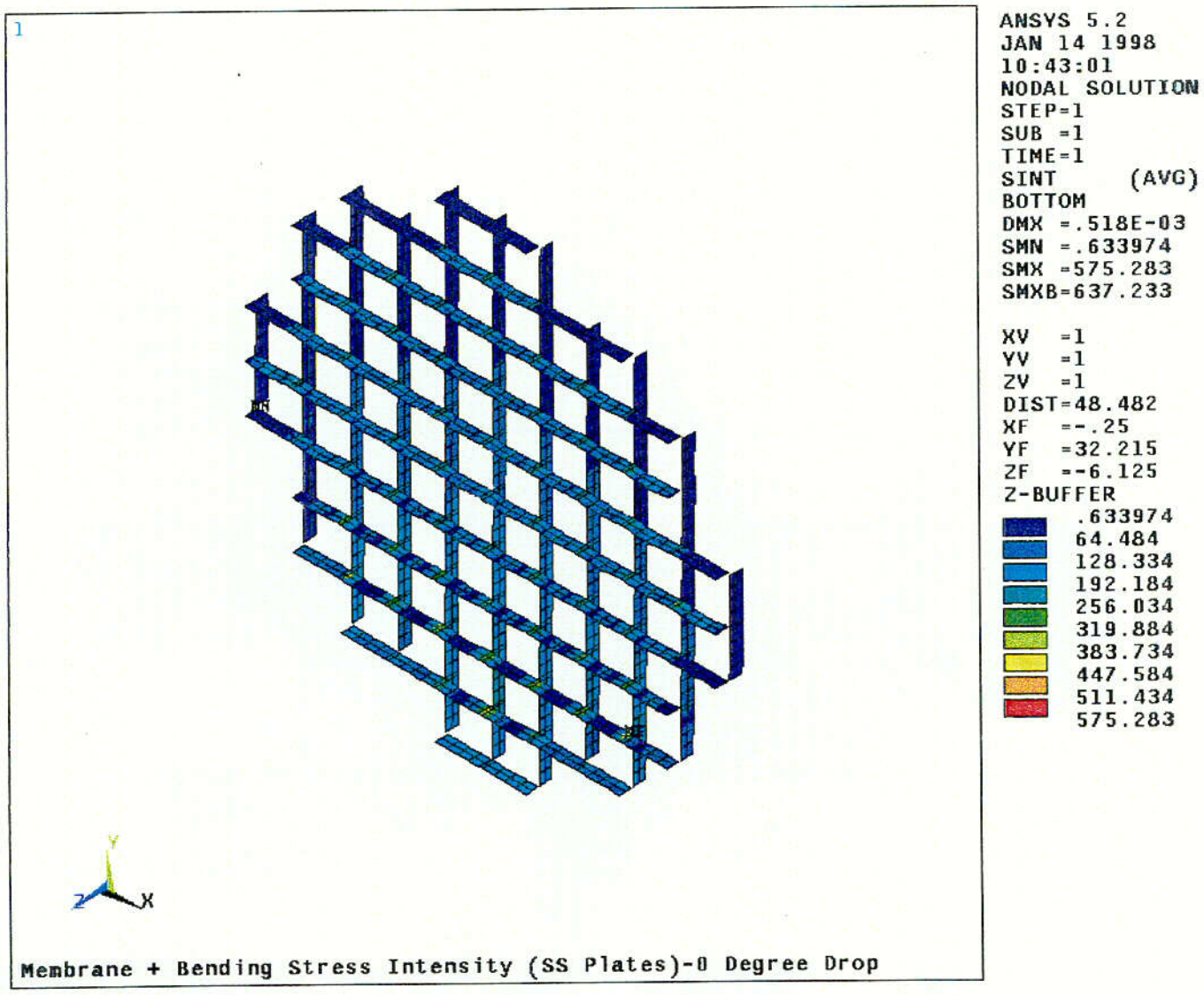

C-02

Figure 2.10.5-13
Membrane Stress Intensity (SS Box)-0 Degree Drop

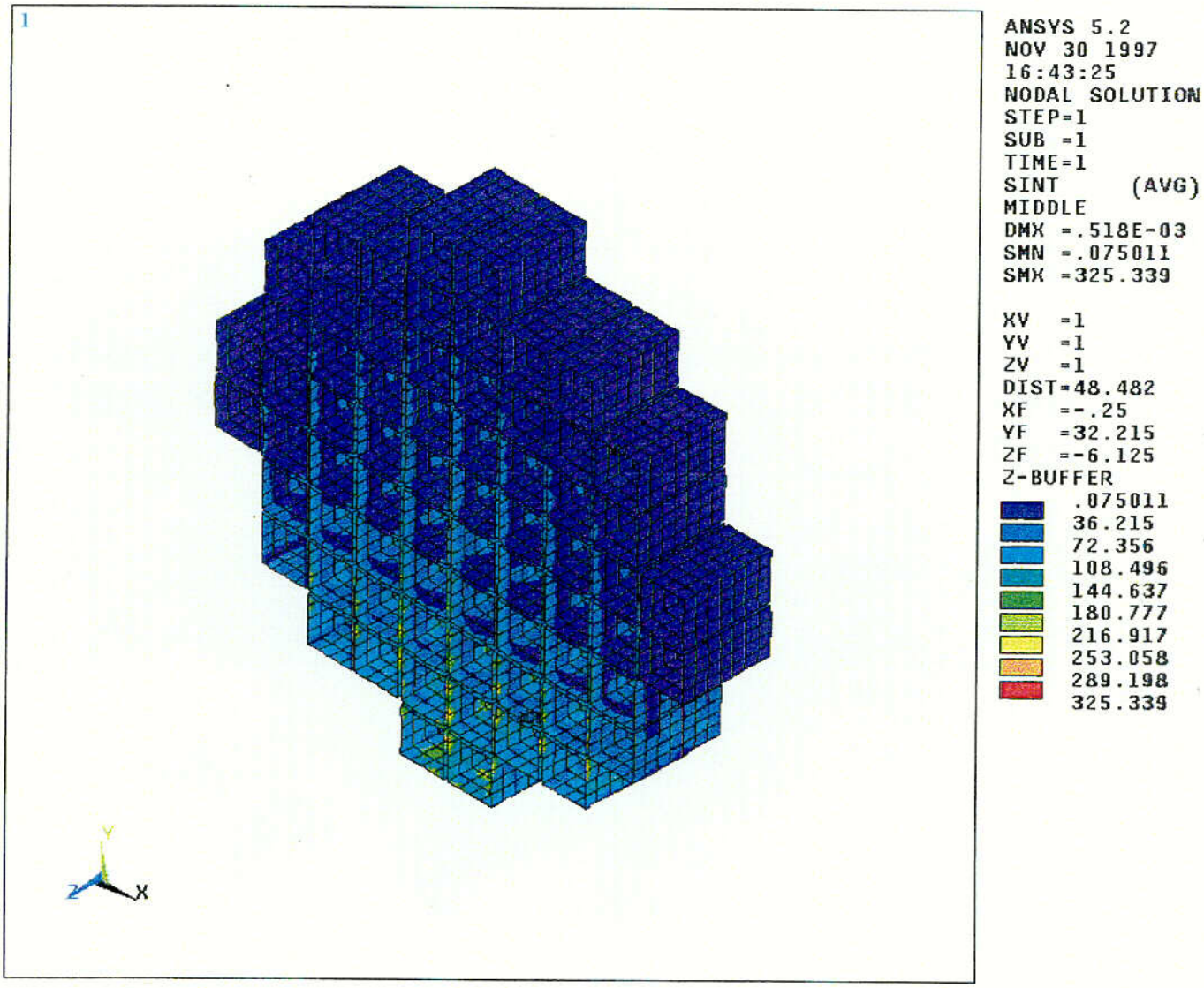

C-03

Figure 2.10.5-14
Membrane + Bending Stress Intensity (SS Box)-0 Degree Drop

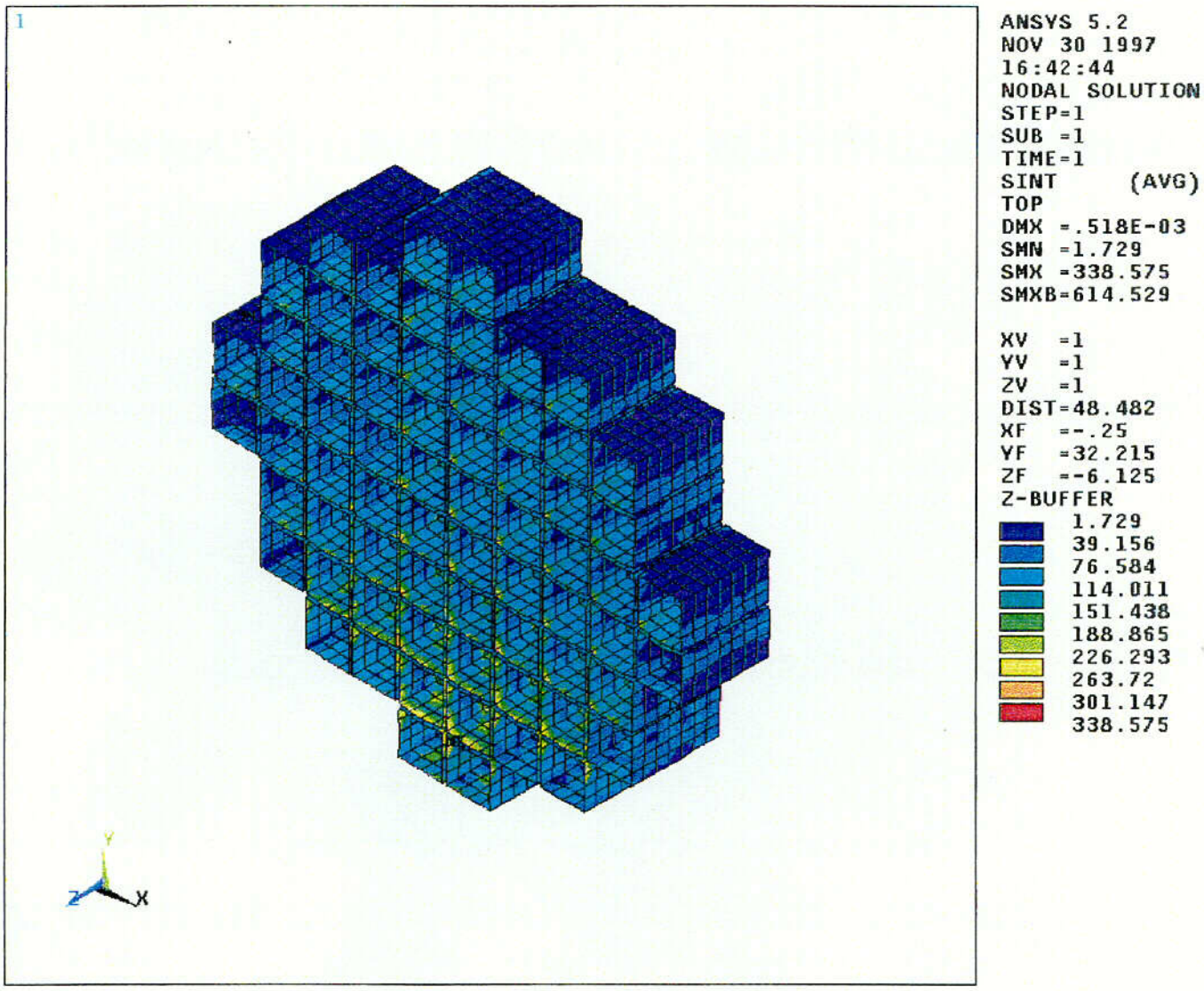

C-04

Figure 2.10.5-15
Membrane Stress Intensity (SS Plate)-30 Degree Drop

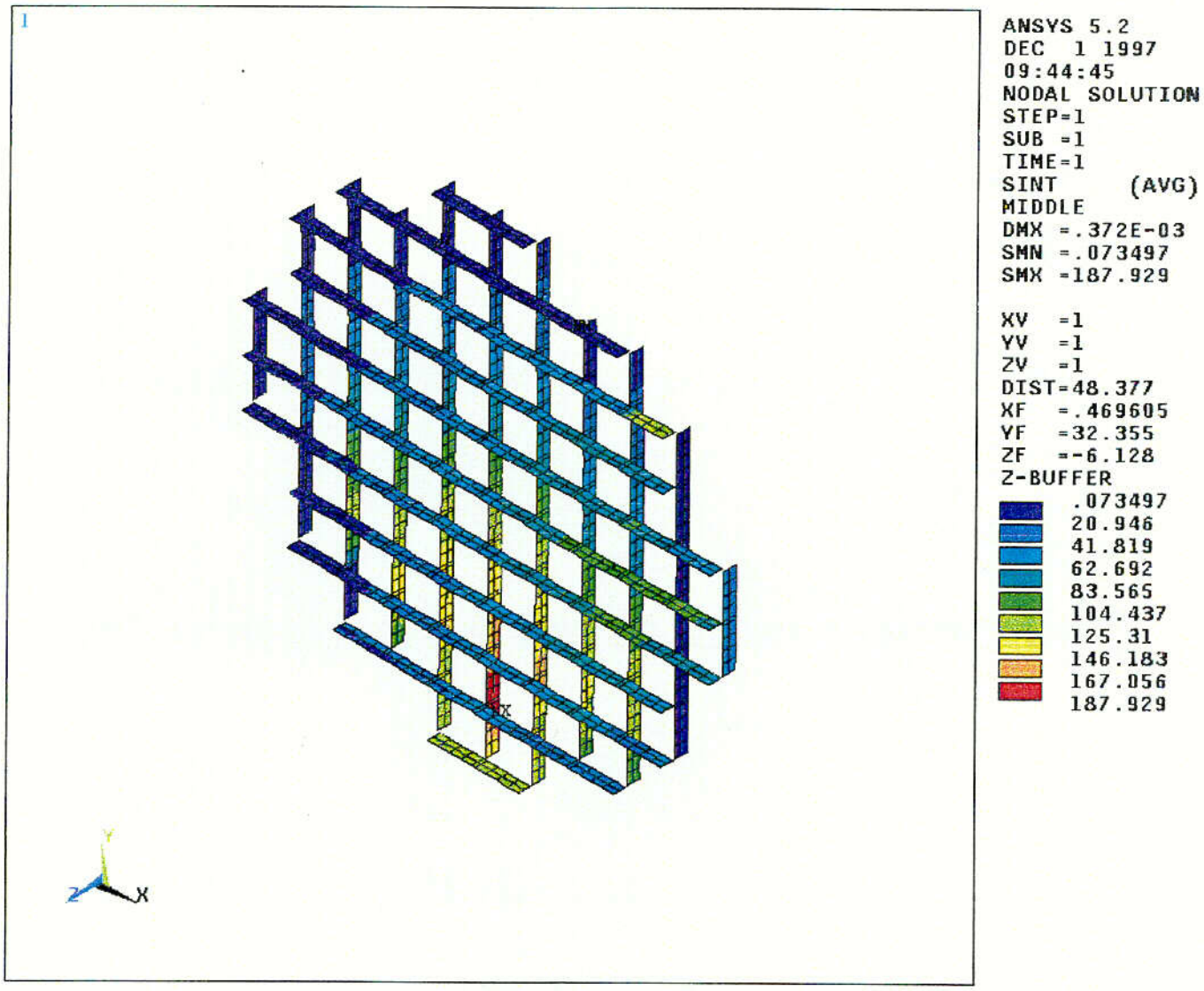

C-05

Figure 2.10.5-16
Membrane + Bending Stress Intensity (SS Plate)-30 degree Drop

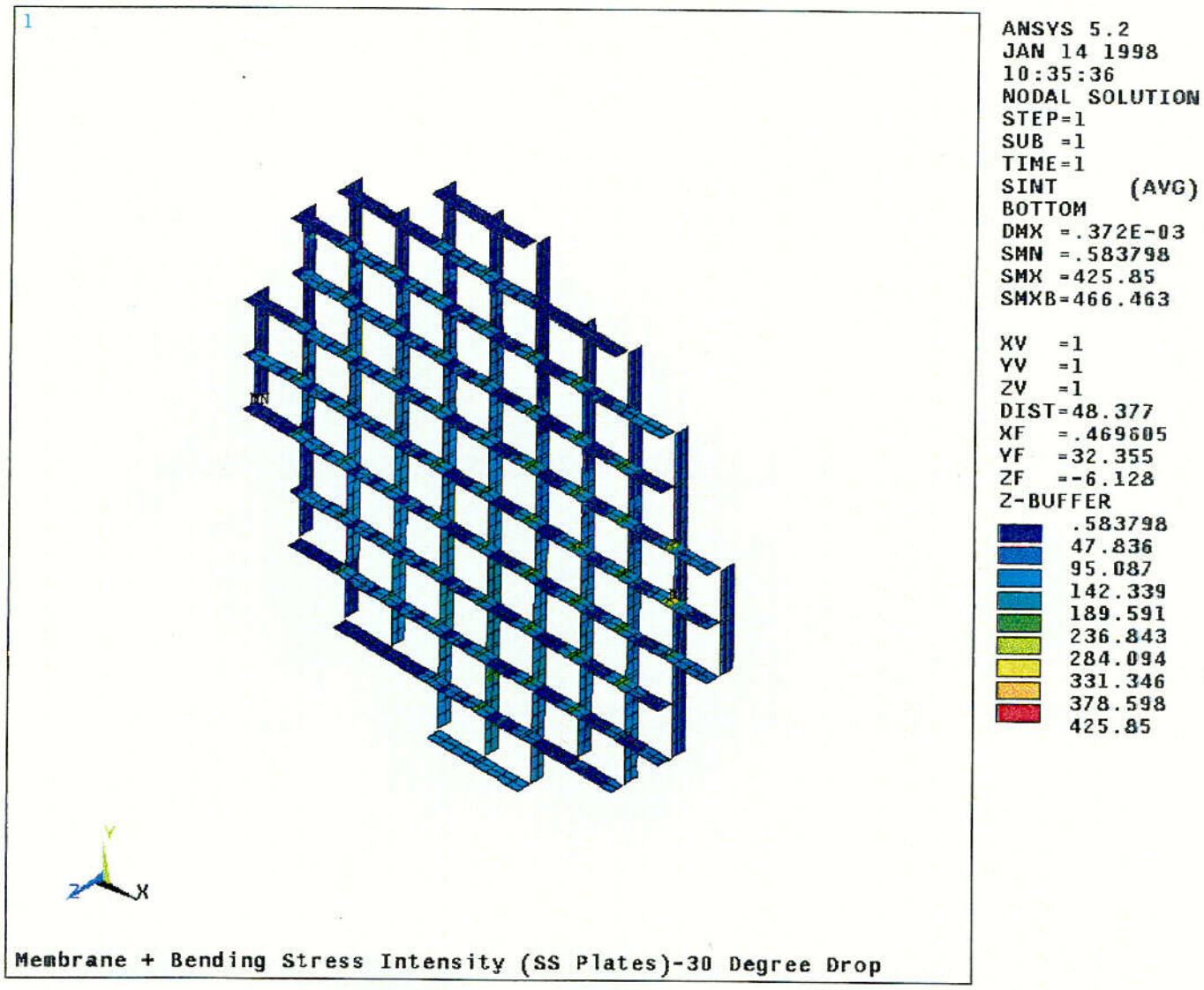

C-06

Figure 2.10.5-17
Membrane Stress Intensity (SS Box)-30 Degree Drop

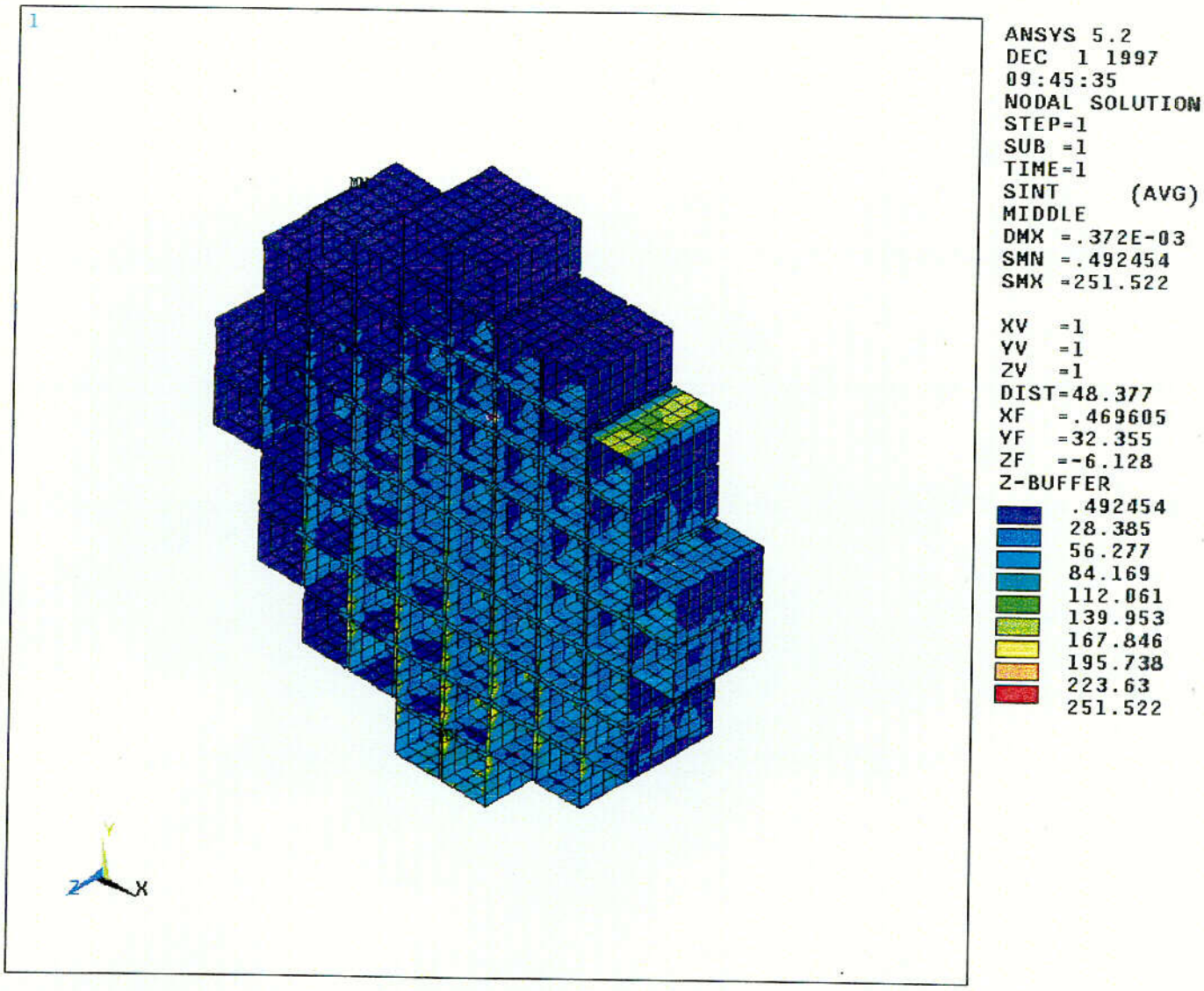

C-07

Figure 2.10.5-18
Membrane + Bending Stress Intensity (SS Box)-30 Degree Drop

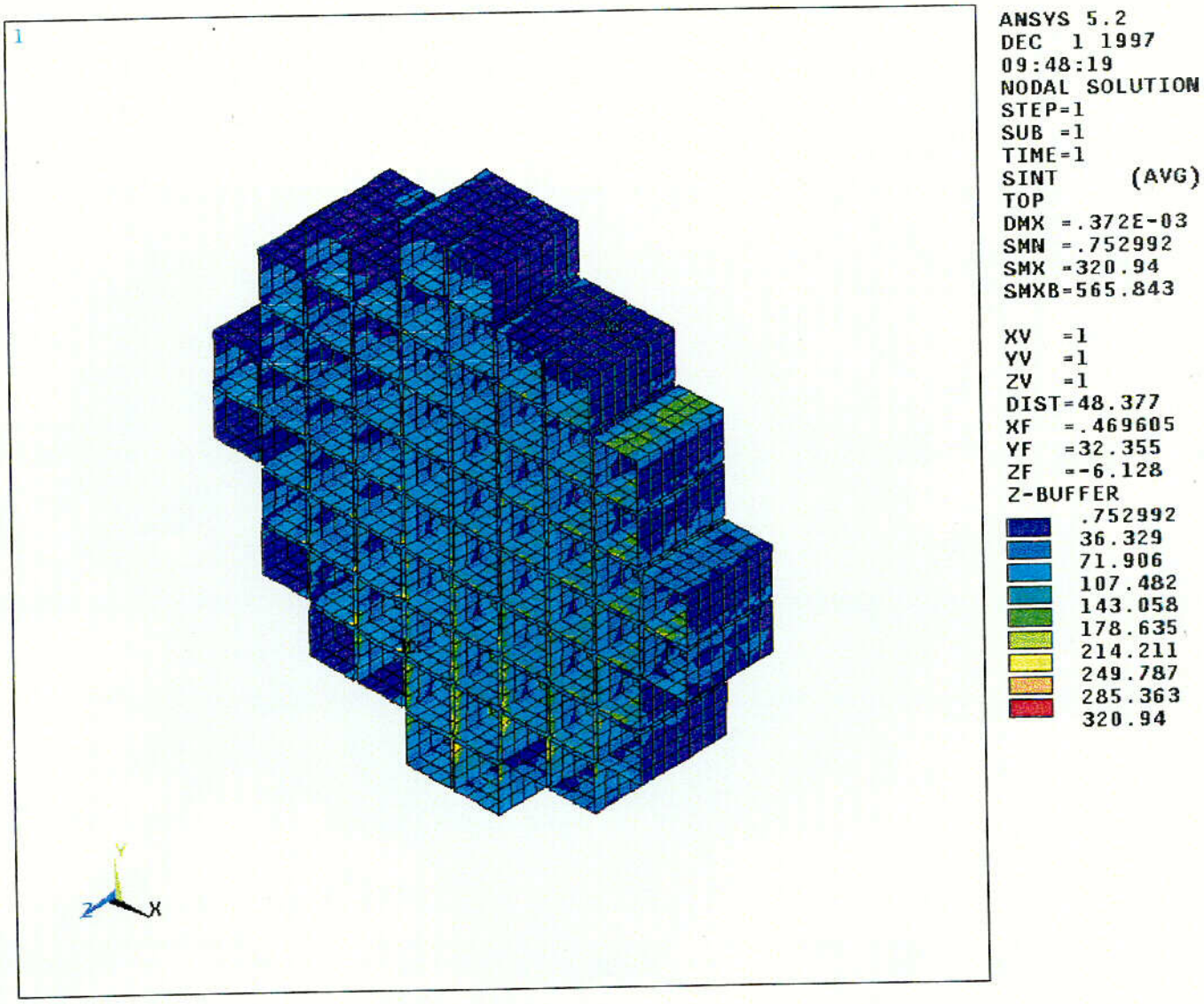

C-08

Figure 2.10.5-19
Membrane Stress Intensity (SS Plate)-45 Degree Drop

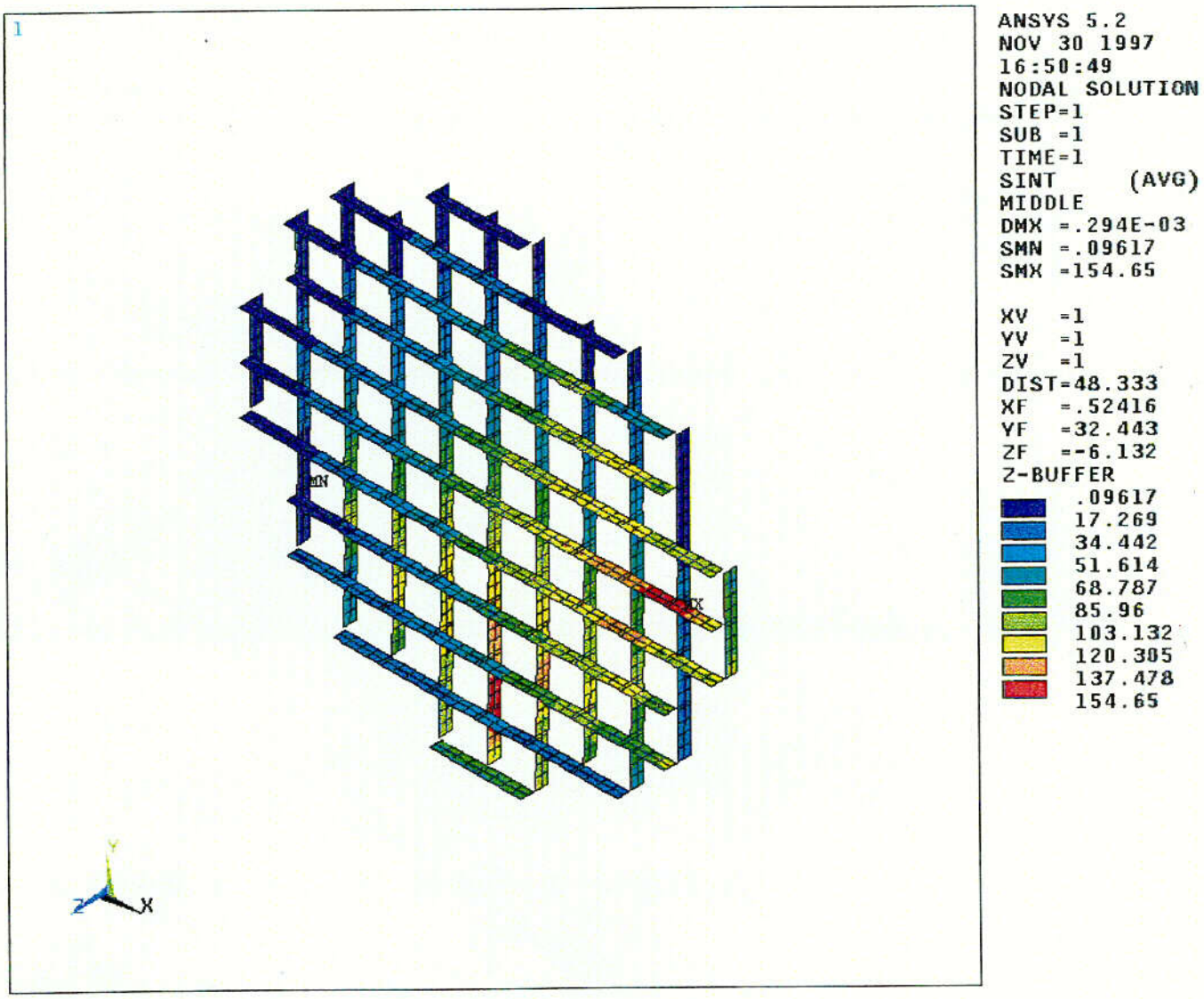

C-09

Figure 2.10.5-20
Membrane + Bending Stress Intensity (SS Plate)-45 Degree Drop

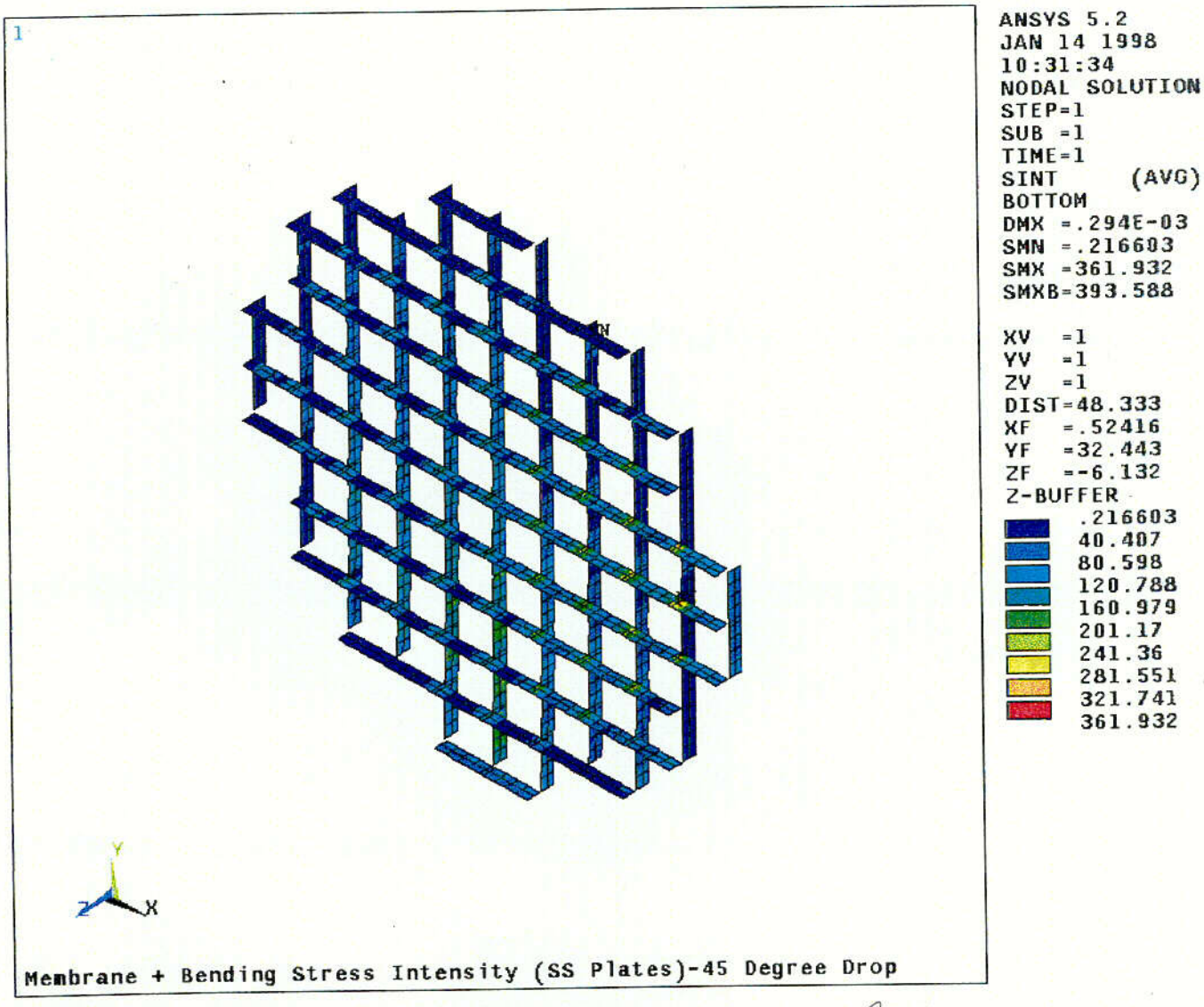

C-10

Figure 2.10.5-21
Membrane Stress Intensity (SS Box)-45 Degree Drop

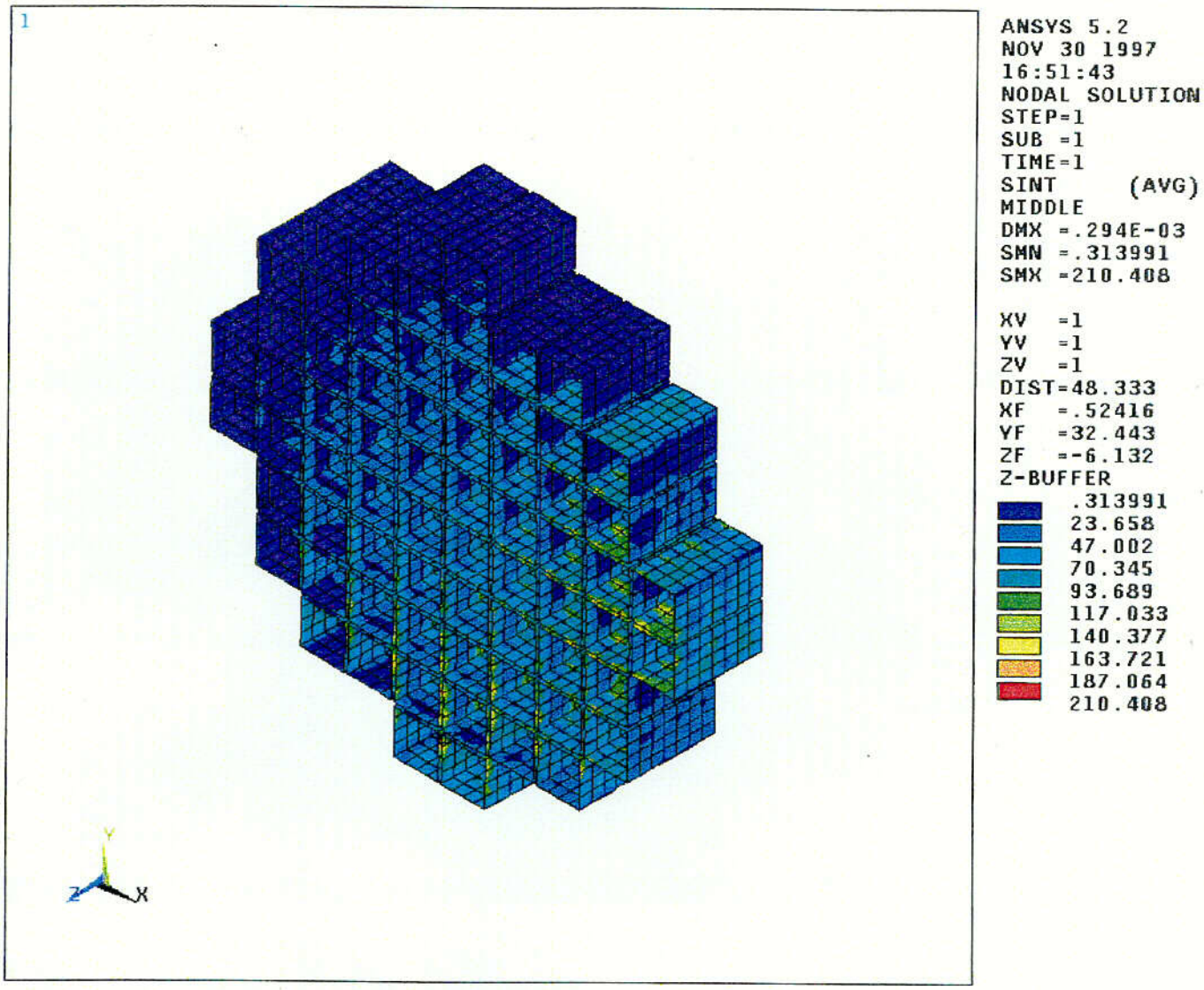

C-11

Figure 2.10.5-22
Membrane + Bending Stress Intensity (SS Box)-45 Degree Drop

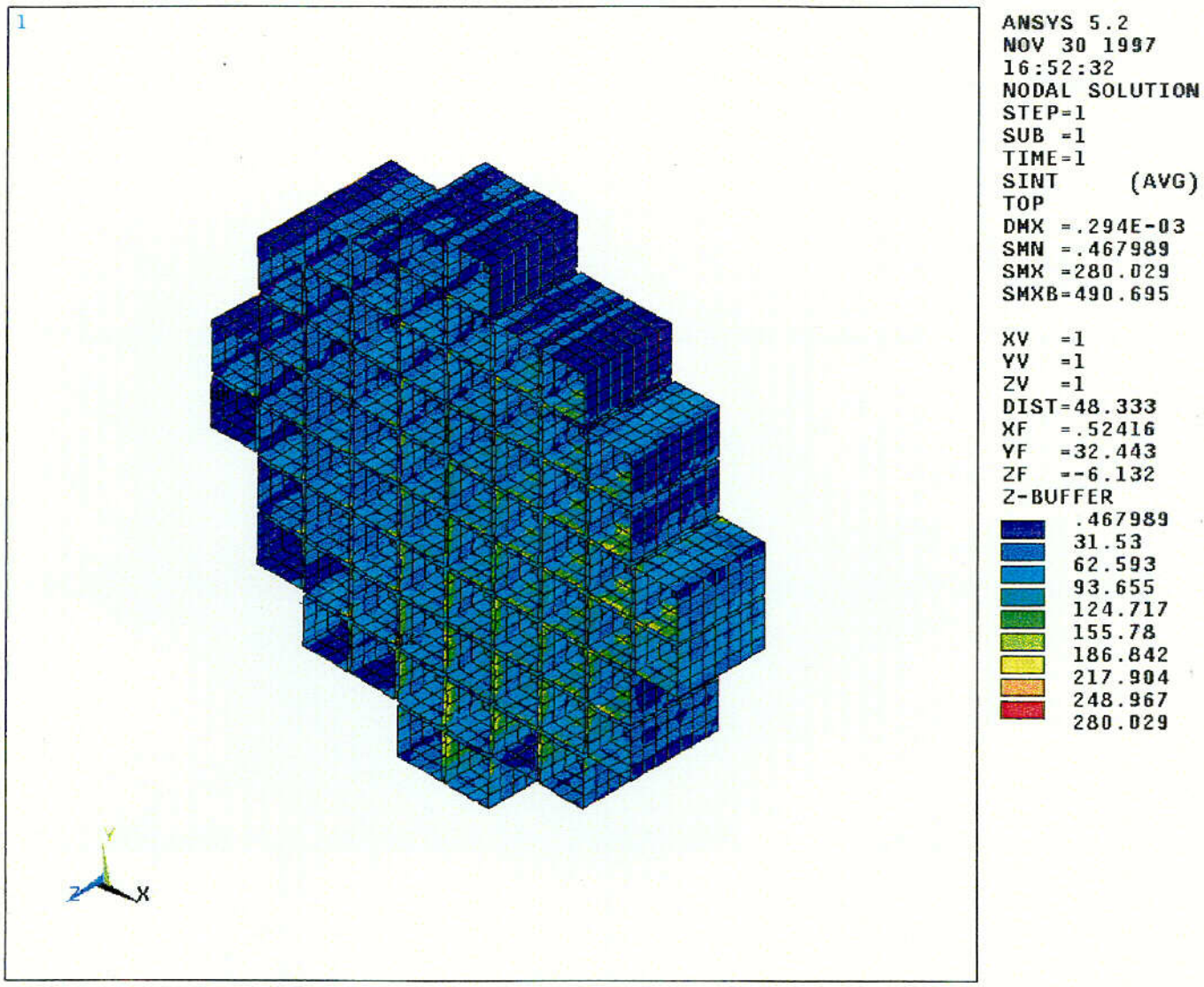

C-12

Figure 2.10.5-23
Nodal Stress Intensity (Aluminum Rails)-0 Degree Drop

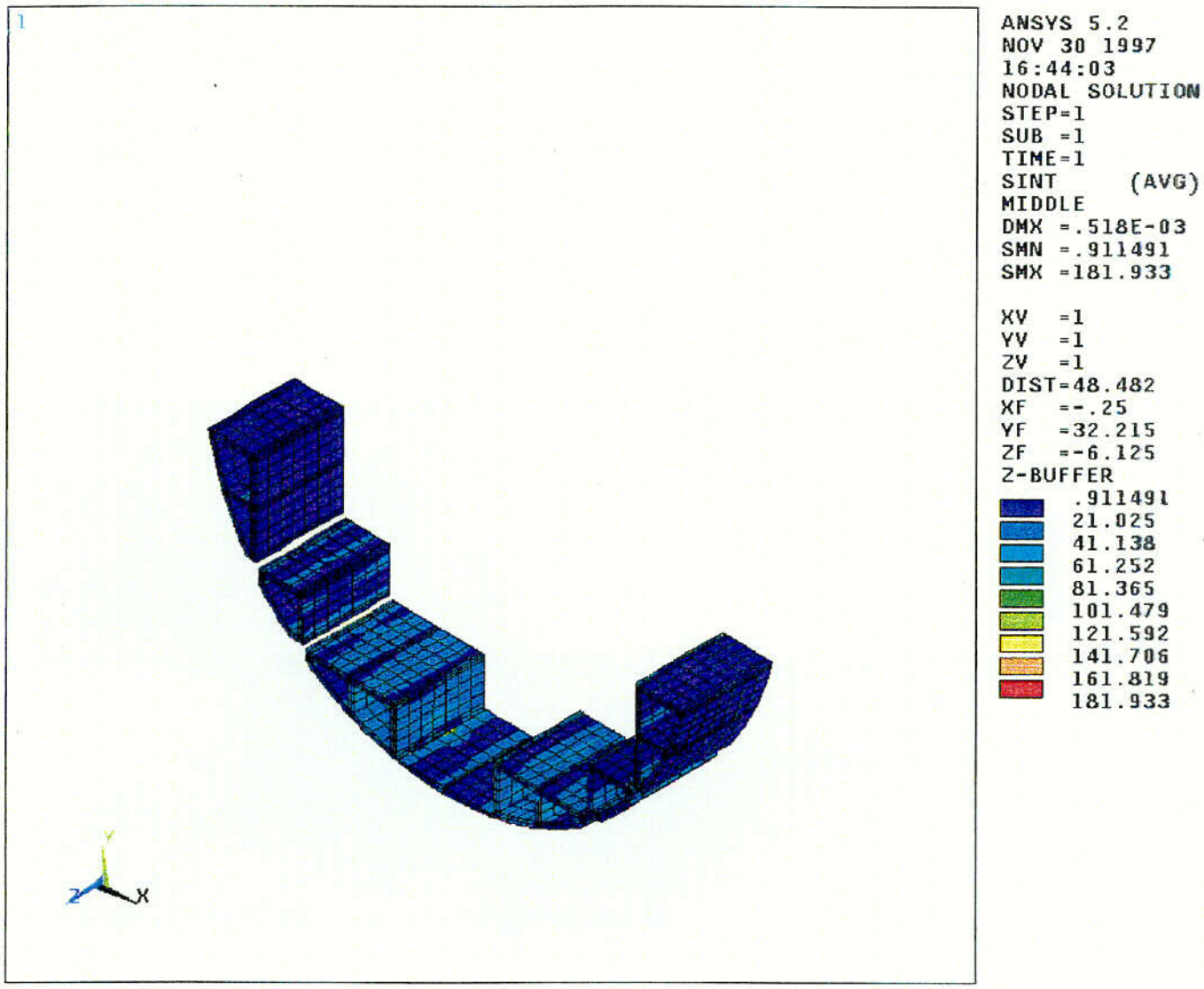

C-13

Figure 2.10.5-24
Nodal Stress Intensity (Aluminum Rails)-30 Degree Drop

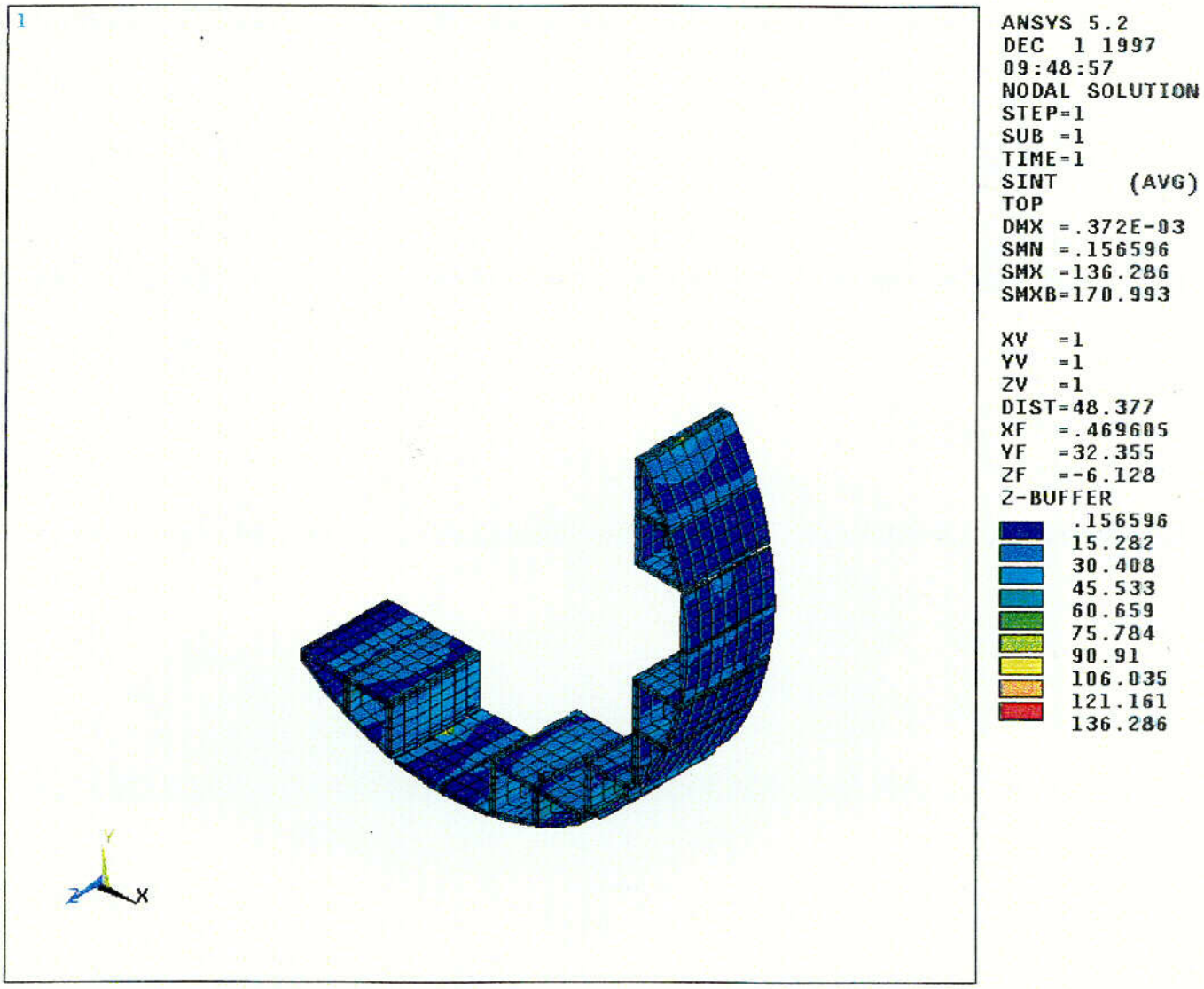

C-14

Figure 2.10.5-25
Nodal Stress Intensity (Aluminum Rails)-45 Degree Drop

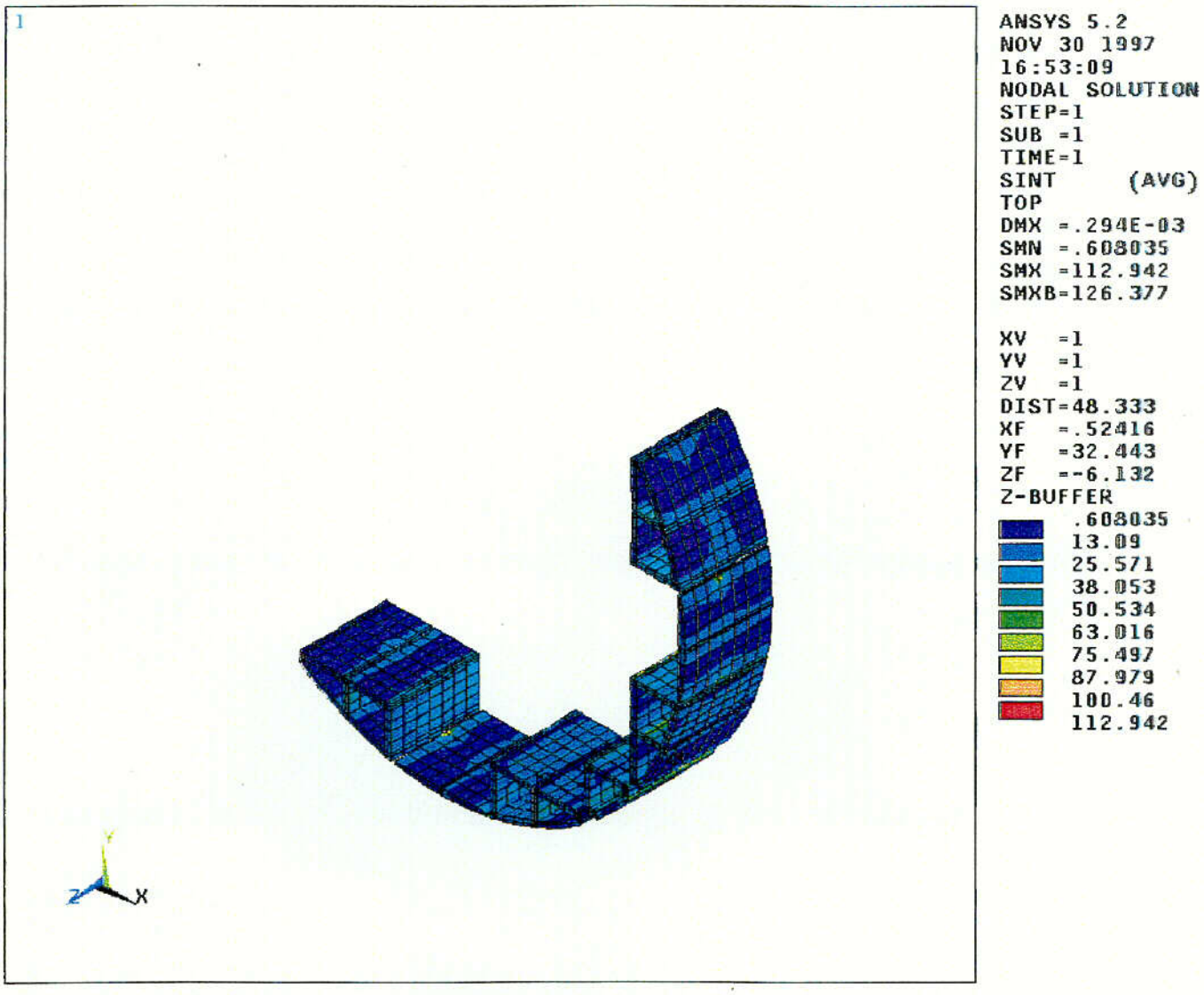

C-15

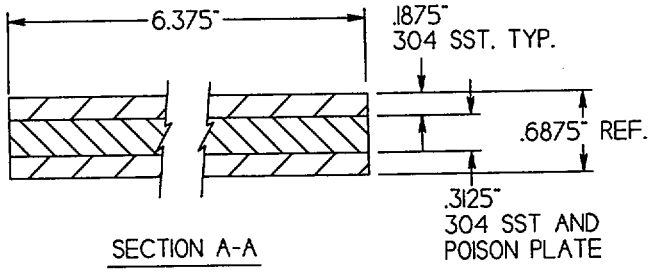

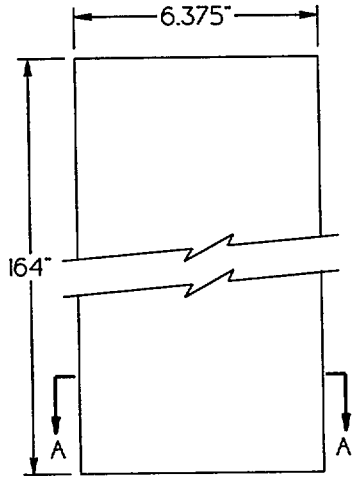

WEIGHT OF 3/16" SST:
2 x 6.375" x .1875" x 164" x .29 = 114 LBS.

WEIGHT OF POISON PLATE:
13 x 6.375" x .3125" x 10.4" x .1 = 27 LBS.

WEIGHT OF 5/16" SST:
13 x 6.375" x .3125" x 1.75" x .29 = 13 LBS.

WEIGHT OF 3/8" SST (BASKET HOLDDOWN):
1 x 6.375" x .375" x 13.25" x .29 = 9 LBS.

TOTAL WEIGHT (1G) = 114 + 27 + 13 + 9 = 163 LBS.

AREA OF 304 SST = 2 x 6.375" x .1875" = 2.39 IN.^{2}

COMPRESSIVE STRESS AT THE BOTTOM OF THE PANEL (1G)

$$\sigma = \frac{1 \times 163}{2.39} = 68.2 \text{(PSI)}$$

FIGURE 2.10.5-26
BASKET STRESS DUE TO
1G VERTICAL LOAD

REV. 0 4/99

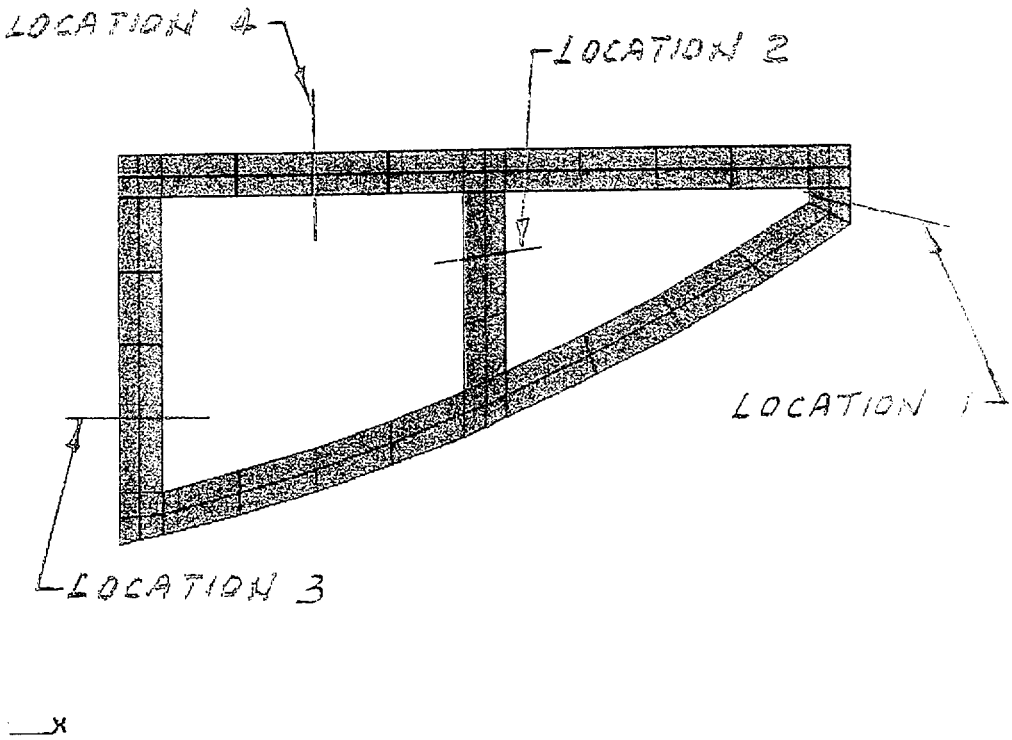

FIGURE 2.10.5-27
STRESS REPORT LOCATION
(BIG RAIL)

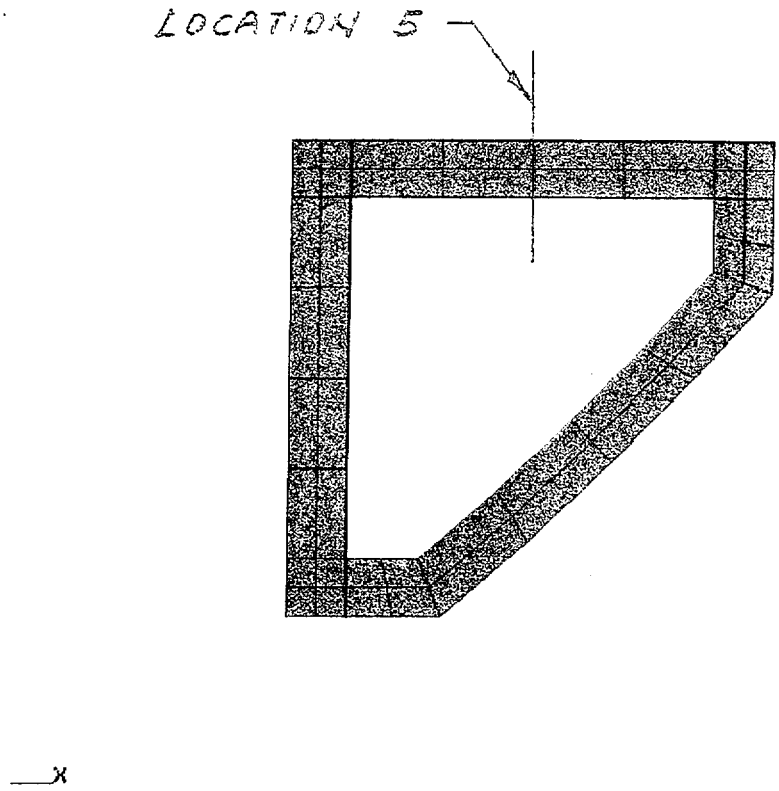

FIGURE 2.10.5-28
STRESS REPORT LOCATION
(SMALL RAIL)

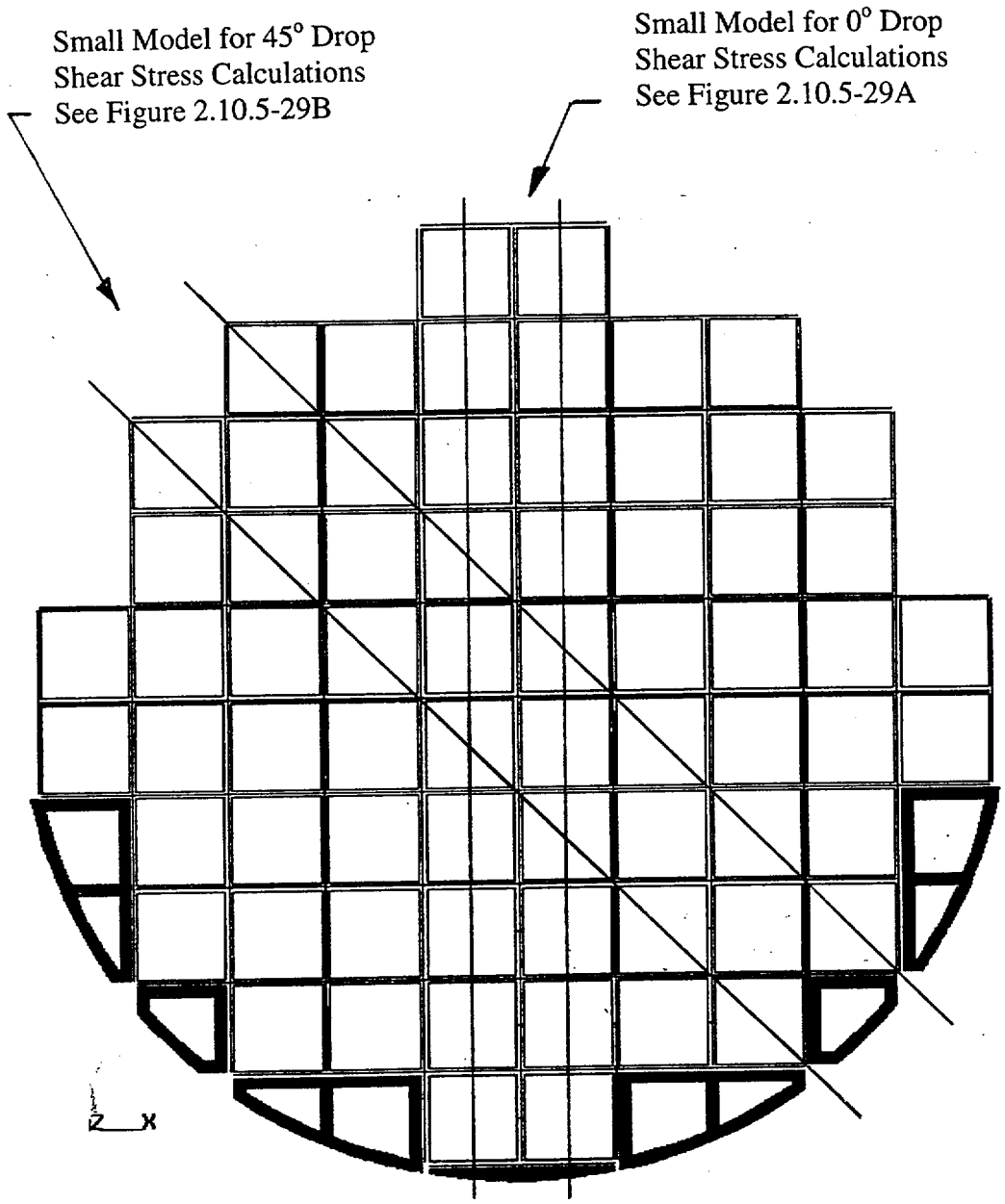

FIGURE 2.10.5-29
FULL BASKET MODEL

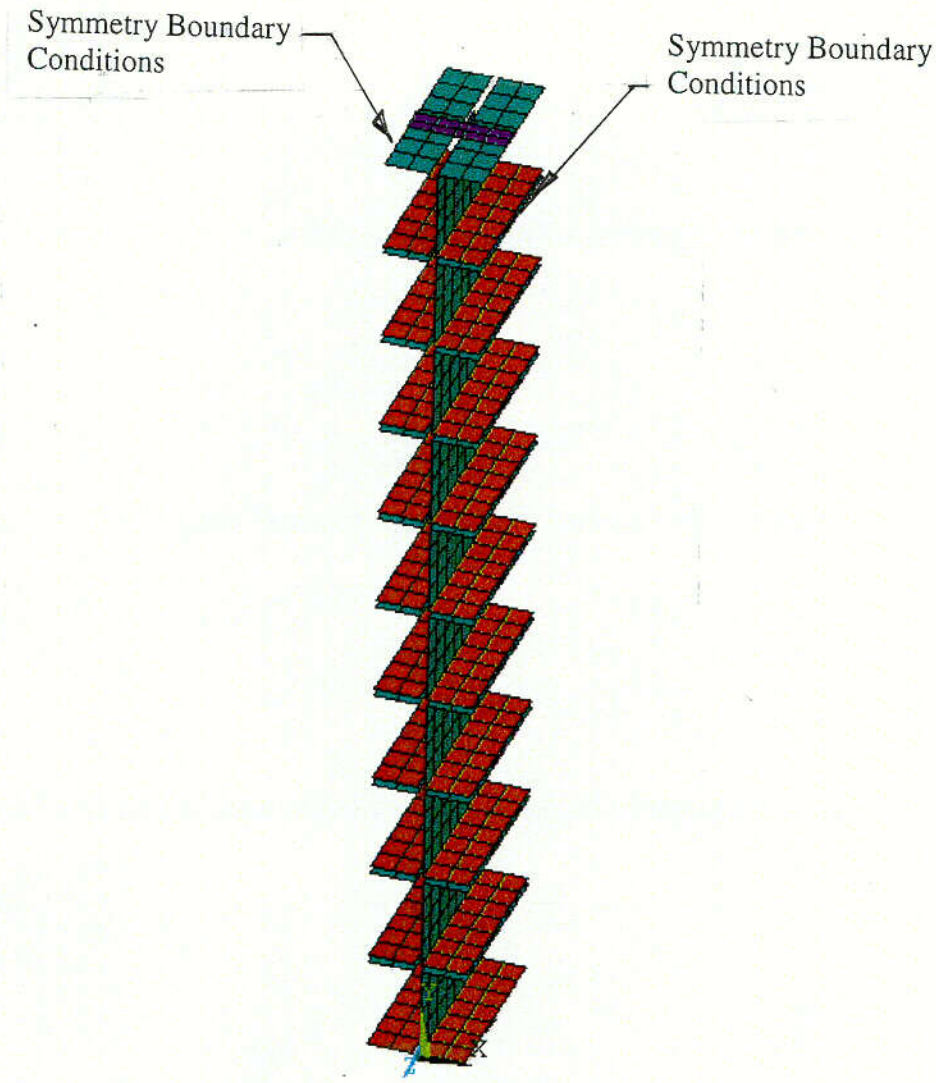

FIGURE 2.10.5-29A
BASKET MODEL FOR
SHEAR STRESS CALCULATION
(0° DROP)

REV. 0 4/99

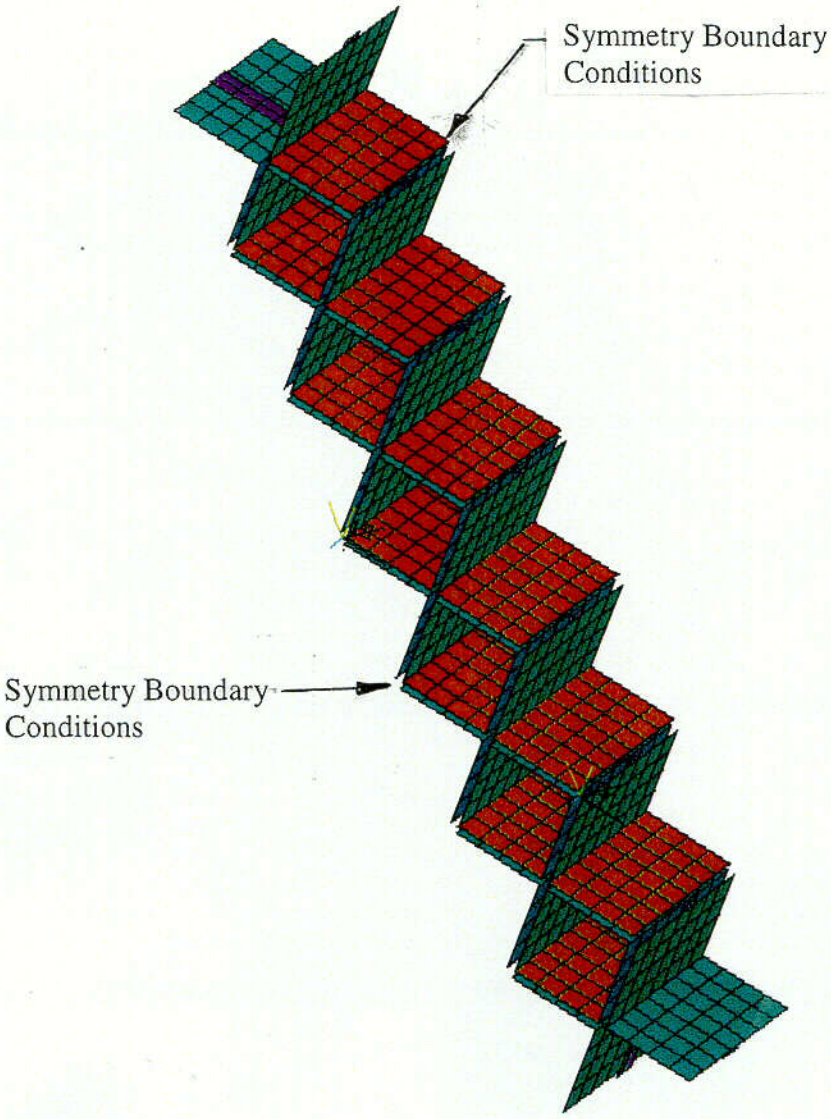

FIGURE 2.10.5-29B
BASKET MODEL FOR
SHEAR STRESS CALCULATION
(45° DROP)

REV. 0 4/99

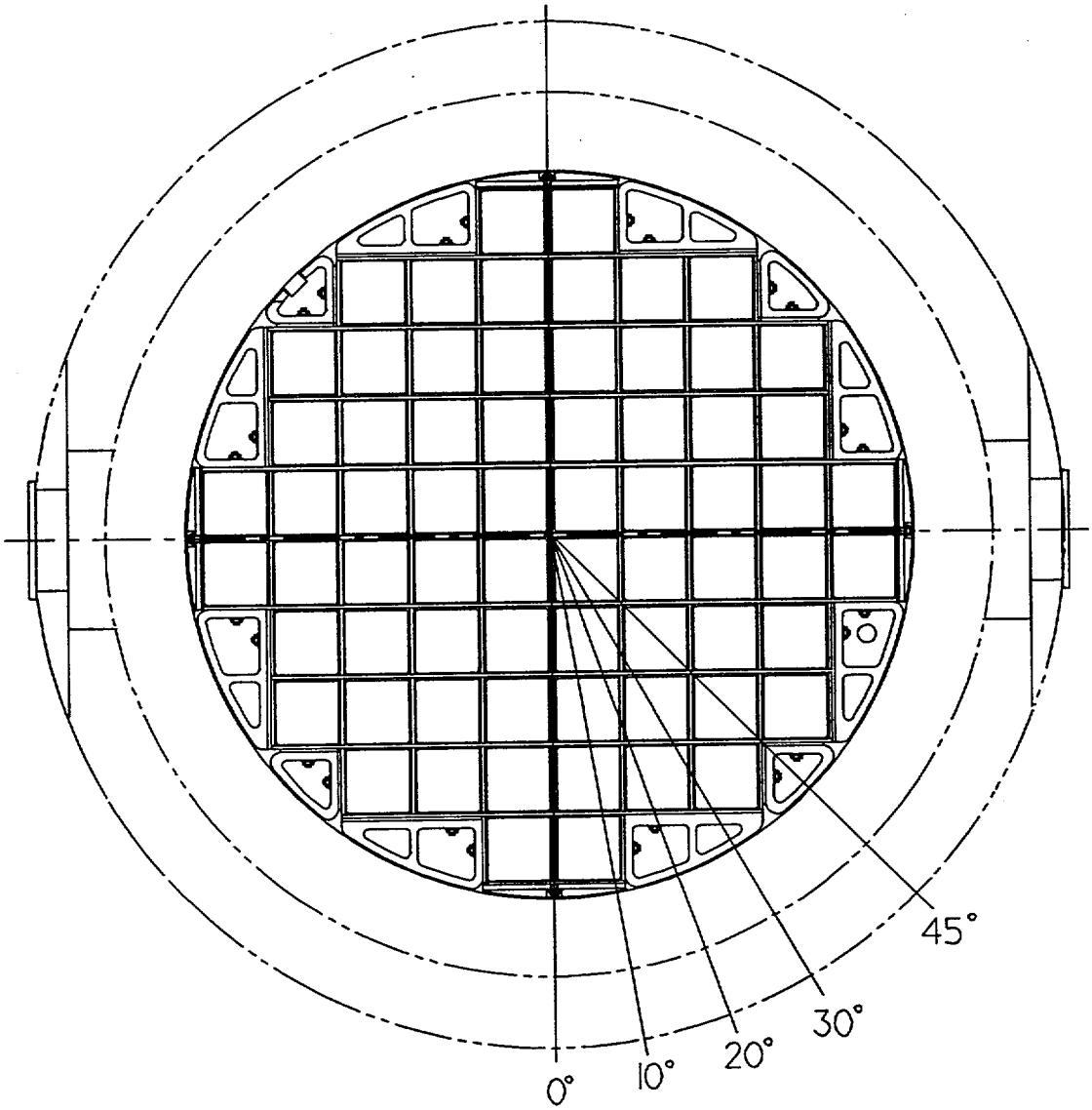

FIGURE 2.10.5-30
DROP ORIENTATION

REV. 0 4/99

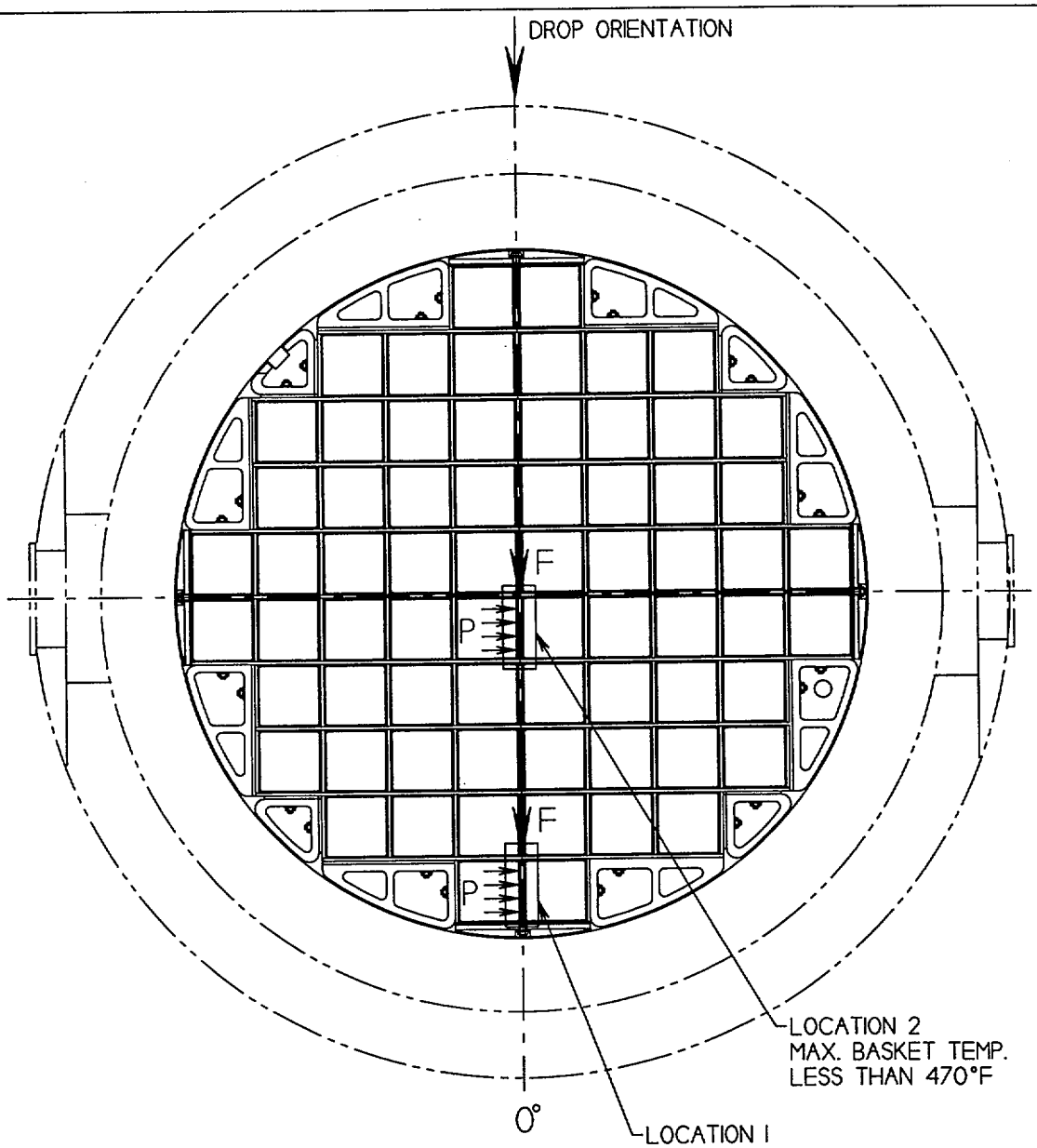

F- TOTAL WEIGHT ABOVE THE BOTTOM PANEL (SST AND POISON PLATES, FUEL ASSEMBLIES, AND RAILS)

P- PRESSURE FROM FUEL ASSEMBLY DUE TO DROP ORIENTATION OTHER THAN 0°

FIGURE 2.10.5-31
FINITE ELEMENT MODEL SIMULATION

FIGURE WITHHELD UNDER 10 CFR 2.390

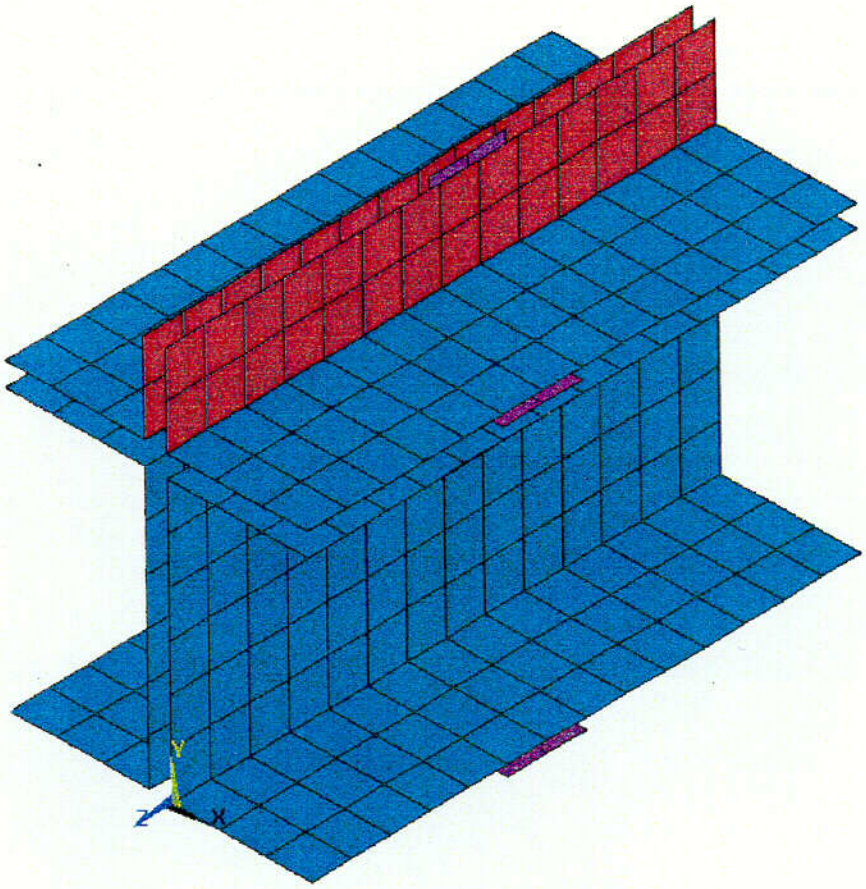

FIGURE 2.10.5-33
FINITE ELEMENT MODEL PLOT

C-18

F- TOTAL WEIGHT ABOVE
THE BOTTOM PANEL
(SST AND POISON PLATES.
FUEL ASSEMBLIES. AND RAILS)

P- PRESSURE FROM FUEL ASSEMBLY
DUE TO DROP ORIENTATION
OTHER THAN 0°

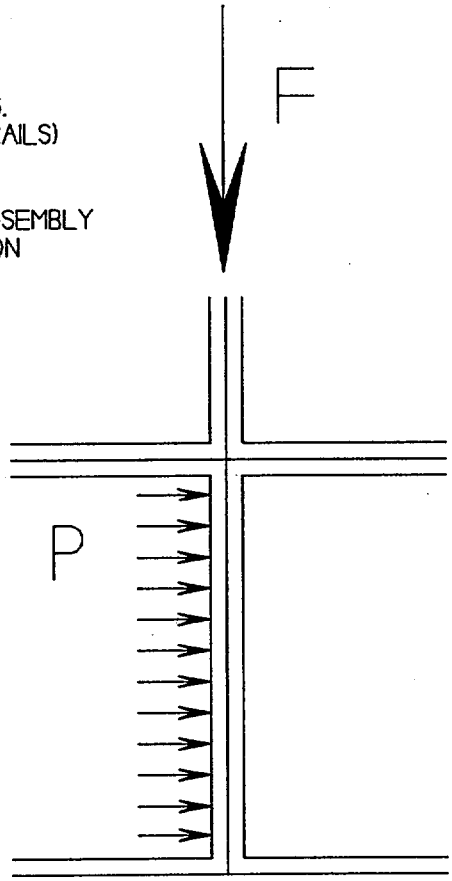

FIGURE 2.10.5-34
LOADING CONDITIONS

REV. 0 4/99

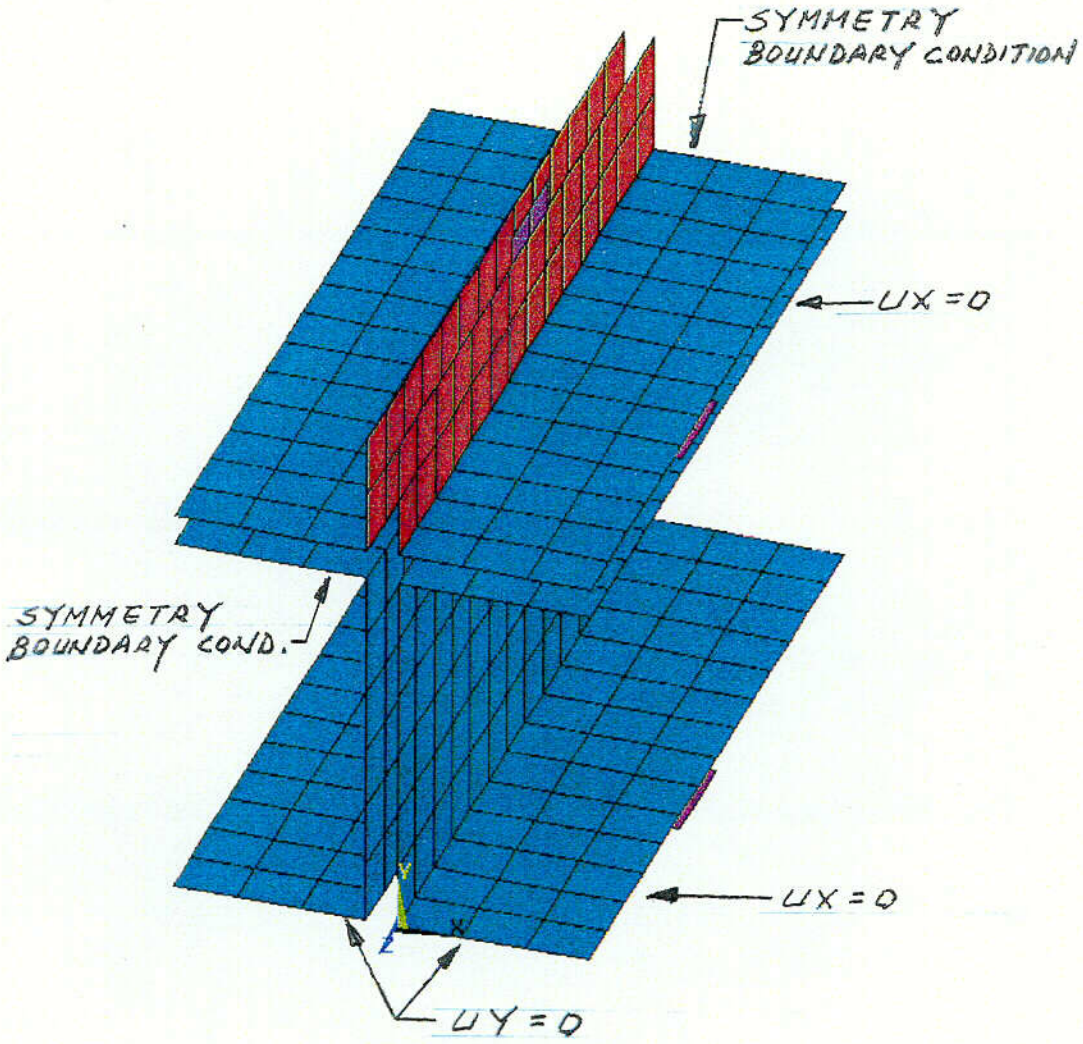

FIGURE 2.10.5-35
BOUNDARY CONDITIONS

Figure 2.10.5-36
0° Drop Buckling Analysis - ANSYS Computer Plot

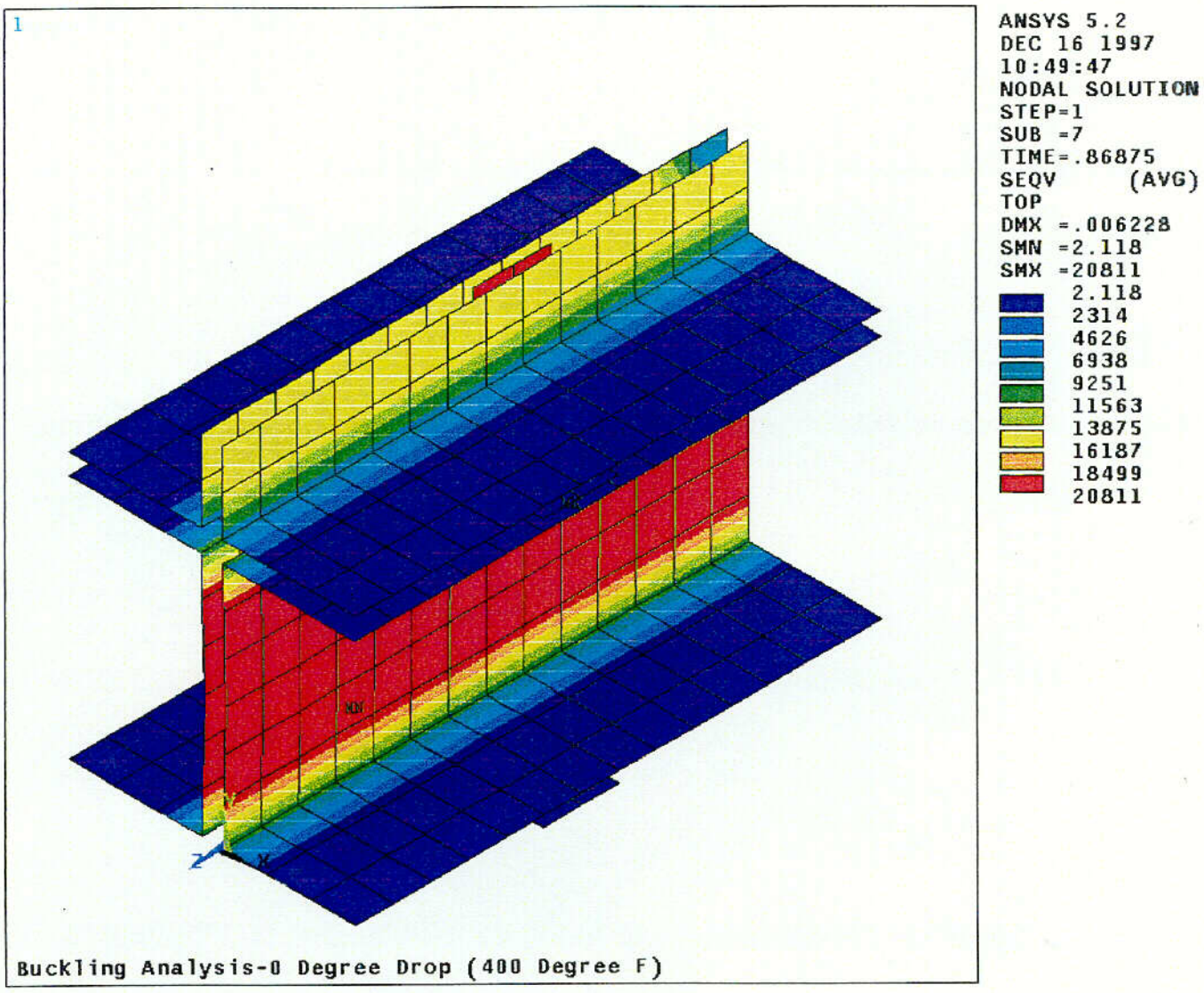

C-20

Figure 2.10.5-37
10° Drop Buckling Analysis - ANSYS Computer Plot

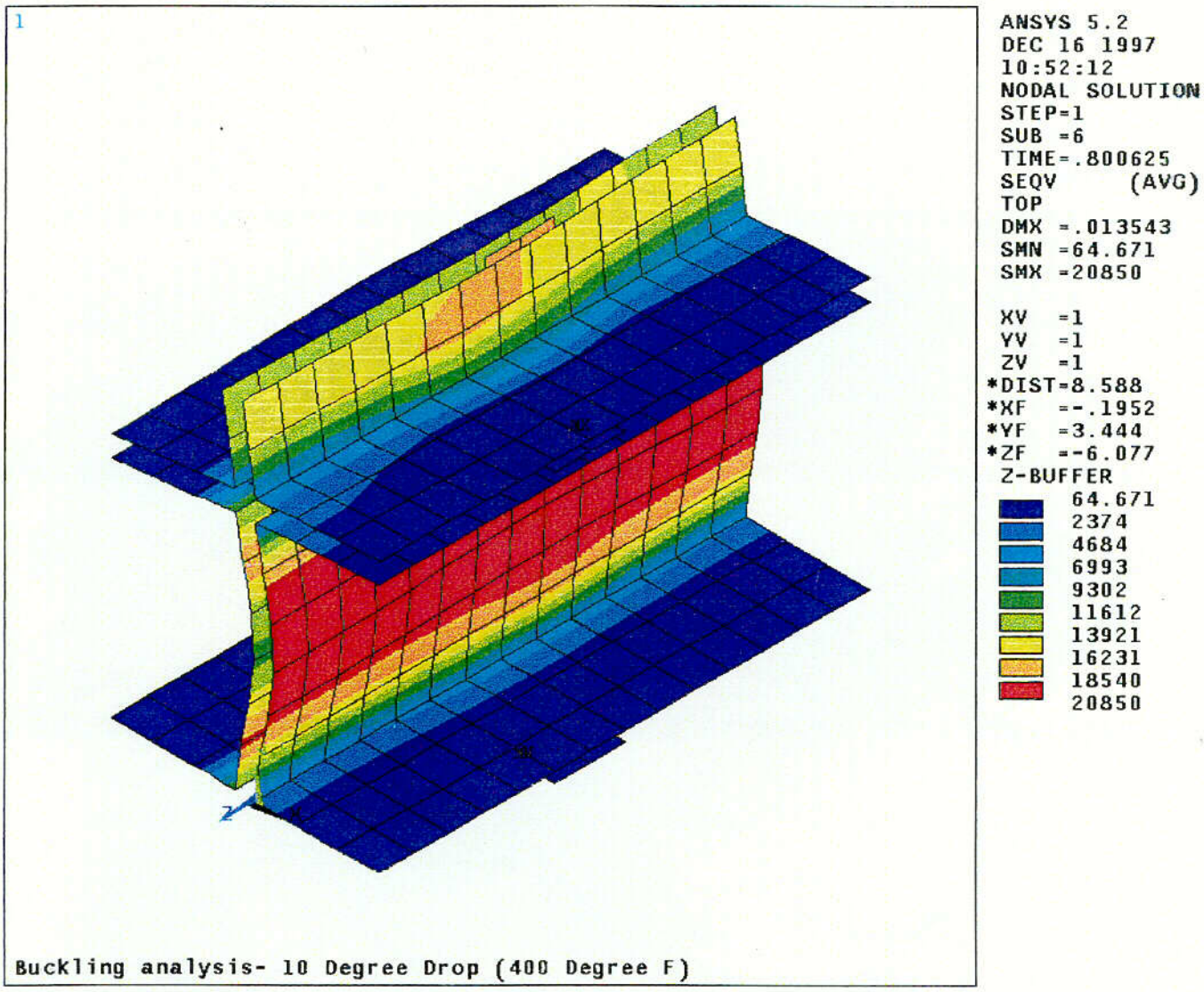

C-21

Figure 2.10.5-38
20° Drop Buckling Analysis - ANSYS Computer Plot

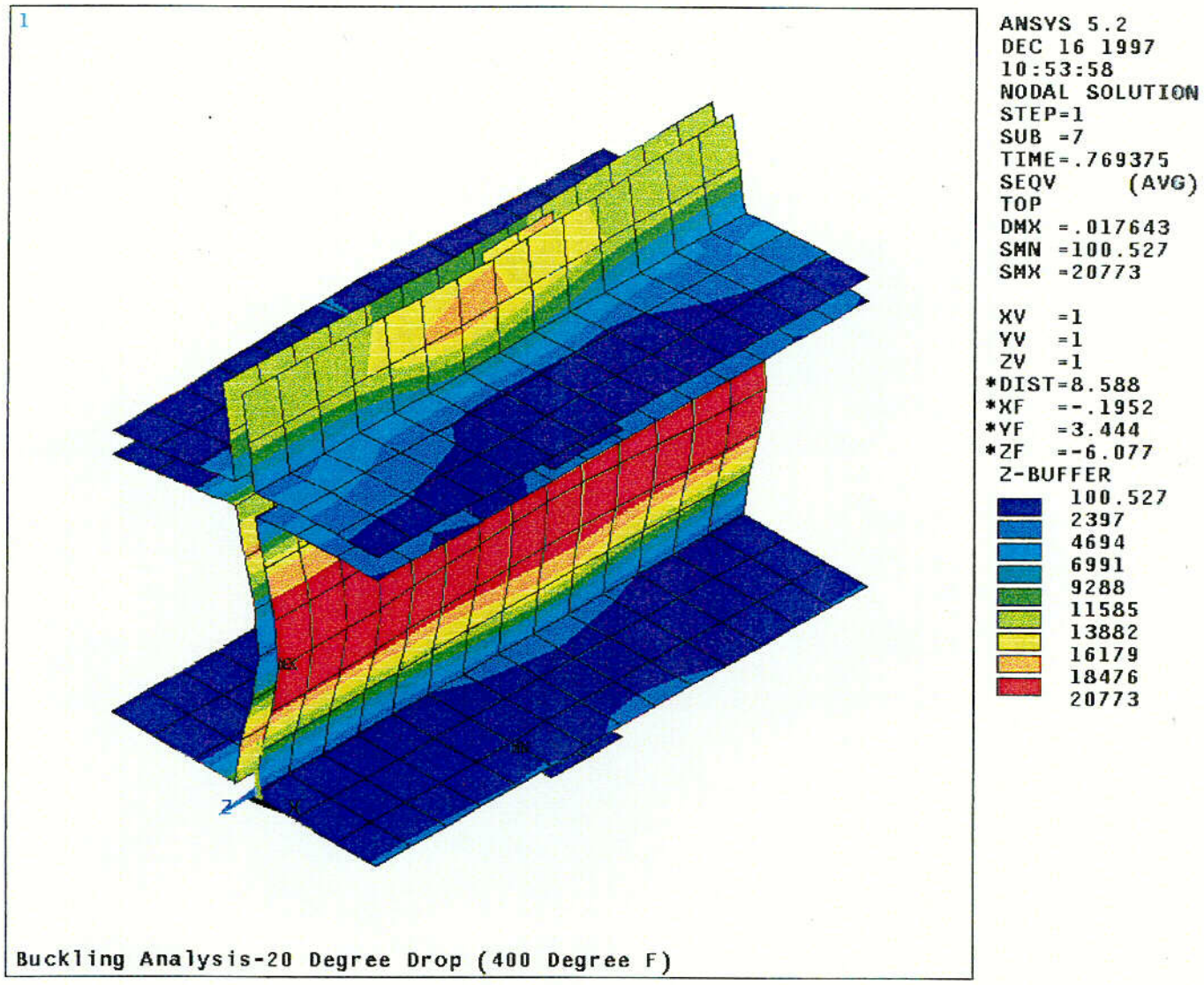

C-22

Figure 2.10.5-39
30° Drop Buckling Analysis - ANSYS Computer Plot

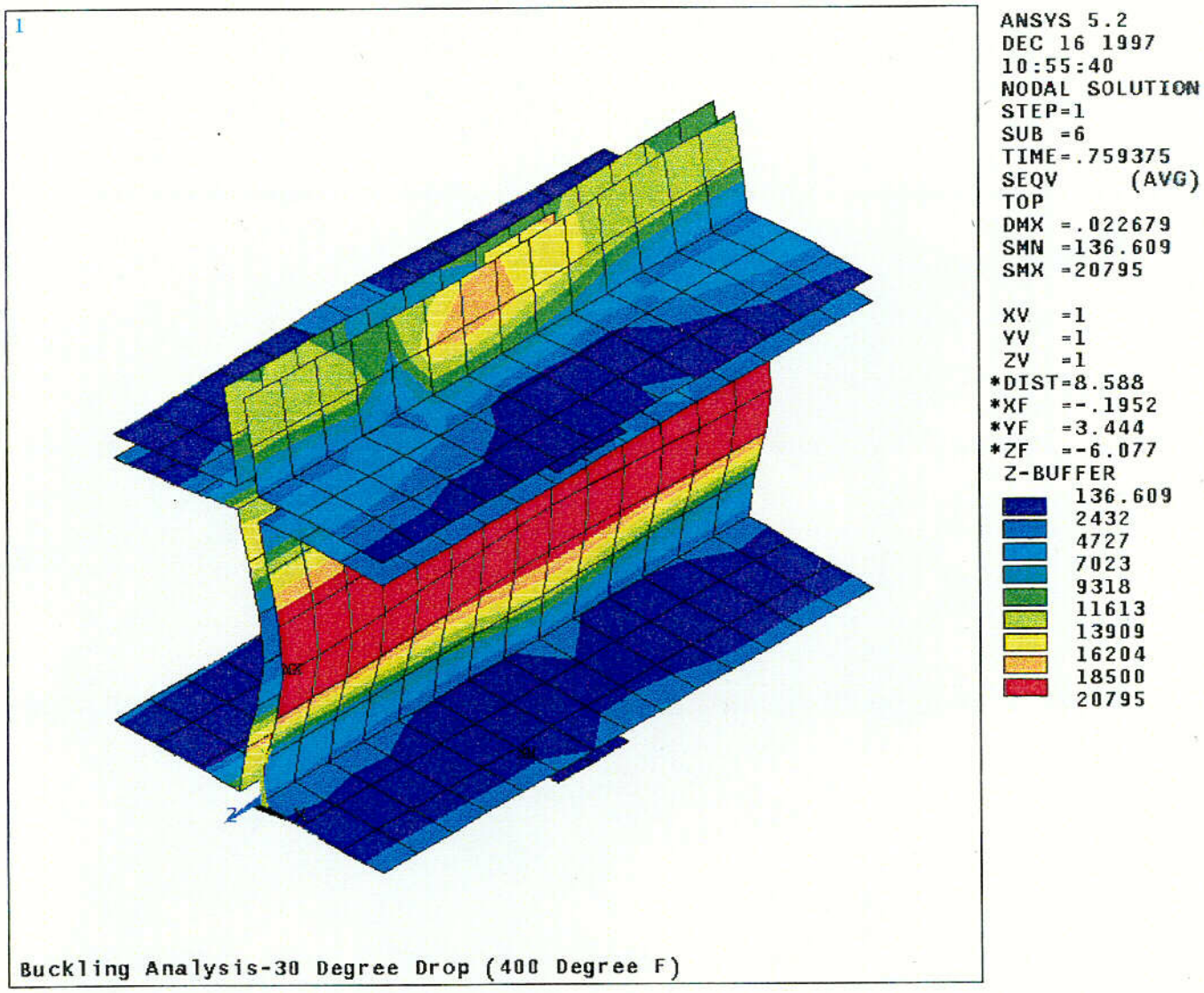

C-23

Figure 2.10.5-40
45° Drop Buckling Analysis - ANSYS Computer Plot

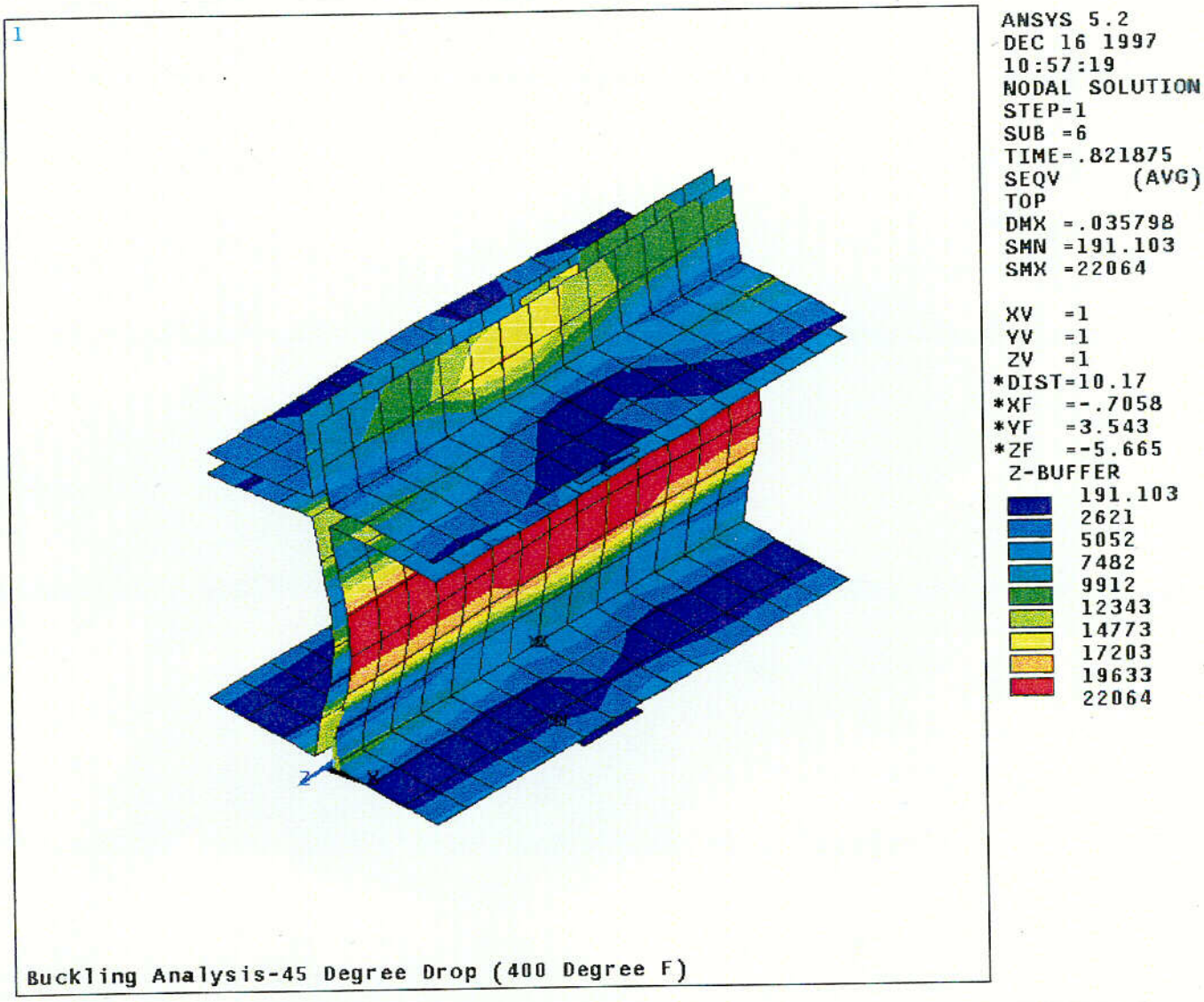

C-24

TN 68 TRANSPORT PACKAGING

APPENDIX 2.10.6

TABLE OF CONTENTS

LIST OF FIGURES

THIS PAGE IS INTENTIONALLY LEFT BLANK.

APPENDIX 2.10.6

DYNAMIC LOAD FACTOR FOR BASKET DROP ANALYSIS

2.10.6.1 Introduction

This appendix presents the modal analysis of the TN-68 fuel support basket. The TN-68 basket is analyzed for 30 foot end drop and side drop accidents in Appendix 2.10.5 using equivalent static methods. The equivalent static loads for the drop evaluations of the TN-68 basket are determined by multiplying the peak rigid body accelerations (analyzed in Appendix 2.10.8) by the corresponding dynamic load factor (DLF). The dynamic load factor is a function of the rise time of the applied load, the duration of the load, the shape of the load, and the natural period of the structure. The purpose of this analysis is to determine the fundamental frequencies of the basket which have the most significant effect on the response of the basket 30 foot side impact. Based on the fundamental frequencies of the basket structure, the dynamic amplification factor is determined from the results shown in Figure 2.10.6-15 which is taken from the NUREG/CR-3966[1]. The results give the dynamic load factors for a half-sine-wave as a function of the ratio of the impulse duration to the natural period of the structure. The half sine wave dynamic load factors are conservative relative to the triangular pulse.

2.10.6.2 Modal Analysis

Finite Element Model

The ANSYS[2] finite element model described in Appendix 2.10.5 is used to perform the modal analysis. The supporting rails are removed from the finite element model and boundary conditions are directly applied to the panels. It is reasonable to remove the supporting rails because the coupling of rail nodes to the panel nodes would have resulted in stiffer panels and higher frequency modes. The basket finite element model is shown on Figure 2.10.6-1.

Material Properties

Material properties based on a basket temperature of 500°F are used as described in Appendix 2.10.5. Weight densities are changed to mass densities ($\rho_m = \rho_w / 386.4$).

Boundary Conditions

Boundary conditions applied to the model are as follows: restraint of the bottom half of the perimeter in the direction parallel to the drop angle vector, and restraint the direction perpendicular to the drop angle vector on the remainder of the perimeter. These boundary conditions are chosen to eliminate modes of vibration that are incompatible with the orientation of the drop. For instance, side to side modes are not important for the 0° drop, because they are restrained by the rails and cask wall and, more importantly, because they have no modal weight in the drop direction, and therefore are not activated by the drop. For 30 and 45 degree drops, boundary conditions are modified by rotating the perimeter support nodes for the drop angle and then applying the appropriate displacement boundary conditions in the rotated coordinate system.

Also for 30 and 45 degree drops, the modal weight is associated with both horizontal and vertical panels of the basket. Typical boundary conditions for the 0° modal analysis are shown on Figure 2.10.6-2.

2.10.6.3 Results of the Modal Analysis

Modes and Frequencies From ANSYS Analysis

The first six mode frequencies resulting from the different drop orientation ANSYS modal analyses are tabulated below:

ANSYS Modal Analysis Results

Mode	Frequency (Hz.)		
	0°	30°	45°
1	204	195	181
2	225	253	232
3	237	258	272
4	242	264	281
5	246	266	282
6	247	268	292

Results From Hand Calculations

For the first mode shape of each drop, the deformed shape of the central basket panels resembles a simple-simple supported beam.

As an order of magnitude check, the frequency of the fundamental mode of vibration for the simple-simple supported beam is calculated below and compared to the frequency of the first mode of 0° ANSYS modal analysis result. Reference 3, page 369, case 6,"Single span, end supported, uniform load W", lists the following equation for the fundamental frequency:

$$f = 3.55 / (5WL^3/384EI)^{1/2}$$

Where:

$W = 5.1577$ lbs.
$L = 6.1875$ in.
$E = 25.8 \times 10^6$ psi
$I = 0.001462$ in.^{4}

Substituting the values given above,

F = 173 Hz

This value is reasonably close to the solution given by ANSYS for the basket. The actual support conditions for the basket are somewhere in between simple-simple and fixed-fixed supports. A fixed-fixed beam's fundamental frequency is approximately double that of a simple-simple supported beam. Therefore, we should expect the ANSYS solution to be somewhere between these values.

The first four (4) mode shapes of the 0, 30, and 45 degree modal analyses are plotted on Figures 2.10.6-3 through 2.10.6-14. Except for the first mode shapes of each drop orientation, the mode shapes are neither symmetric nor have significant modal deflection in the direction of the drop angle. Therefore, the frequencies of these modes with substantial modal weight in the direction of the drop - for angles 0°, 30°, and 45° are 204 Hz, 195 Hz, and 181 Hz, respectively.

2.10.6.4 Dynamic Load factor Calculations

The dynamic load factor is a function of the rise time of the applied load, the duration of the load, the shape of the load, and the natural period of the structure. ADOC computer program as described in Appendix 2.10.8 is used to predict the impact duration during the 30 foot end drop, side drop and 15° slap down drop with the maximum wood properties. Using the maximum wood properties to predict the impact duration is conservative since it results in less crush depth and shorter impact duration. The following table lists the results from the ADOC runs and also compares them with the test results of the TN-BRP[4] 1/3 scale impact limiter model.

Drop Orientations	Impact Duration (sec)	
	ADOC Runs (TN-68 Impact Limiters)	TN-BRP, 1/3 Scale Impact Limiter Testing (Convert to Full Scale)
End Drop	0.025	0.036
Side Drop	0.036	---
15° Slap Down	0.031	0.042

The TN-68 and TN-BRP have similar geometry. The test results from TN-BRP give slightly longer duration due to the TN-68 ADOC runs using the maximum wood properties. Therefore, it is conservative to use the impact duration of 0.025 sec for the TN-68 dynamic load factor calculations.

From Figure 2.10.6-15, the dynamic load factor is calculated as follows:

t = impact duration = 0.025
T = 1/f = 1/181 = 0.0055
t/T = 0.025/0.0055 = 4.5

Therefore, the dynamic load factor is approximately 1.1. This result is in agreement as described in Section 2.2.3 of NUREG/CR-3966.

2.10.6.5 References

1. NUREG/CR-3966, "Methods for Impact Analysis of Shipping Containers", 11/1987.

2. ANSYS Engineering Analysis System User's Manual, Rev. 5.2, Vol. 1 to 4, 1995.

3. Roark, R. "Formulas for Stress and Strain" Fourth Edition.

4. TN-BRP Safety Analysis Report for Transport, Rev. 4, March, 1991.

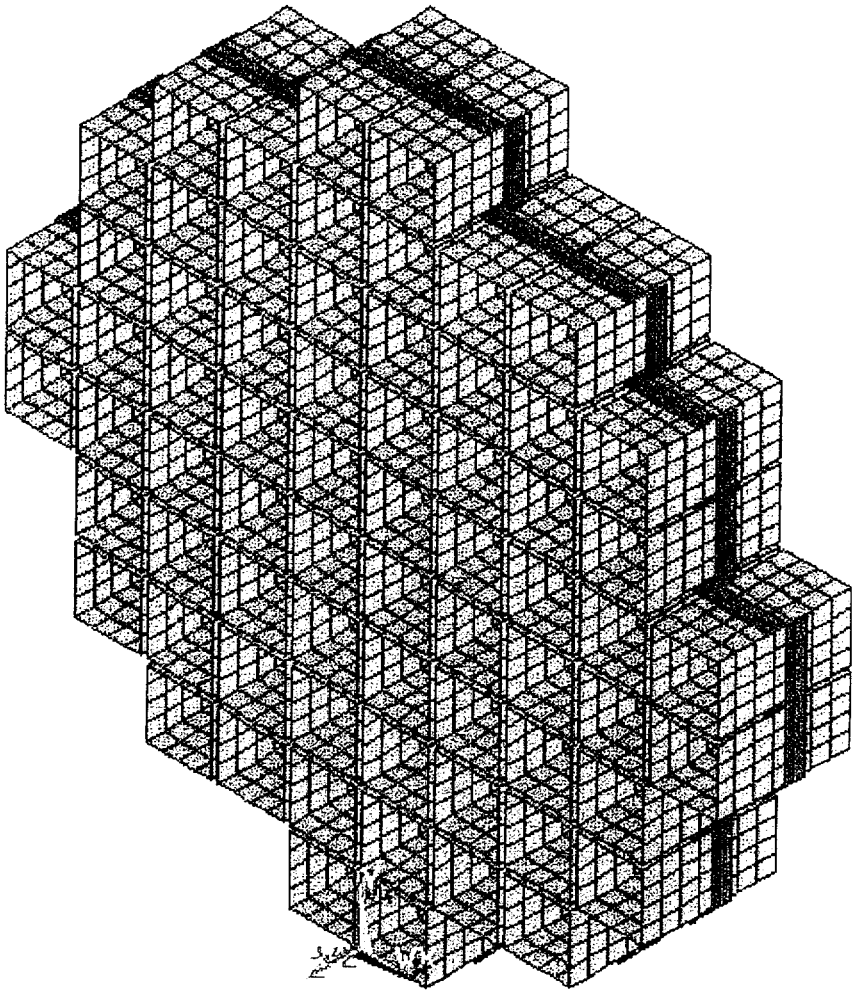

FIGURE 2.10.6-1
BASKET FINITE ELEMENT
MODEL
FOR MODAL ANALYSIS

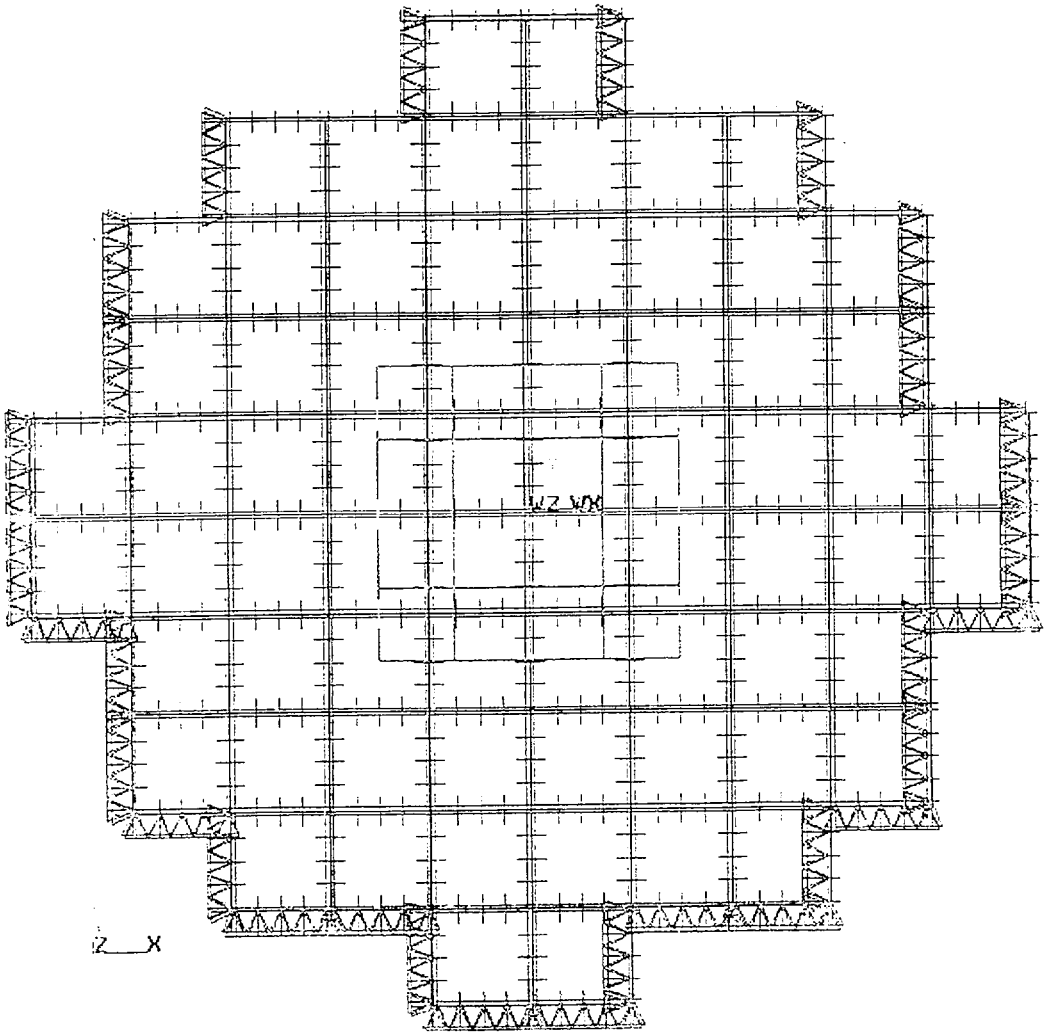

FIGURE 2.10.6-2
BOUNDARY CONDITION - 0°
MODAL ANALYSIS

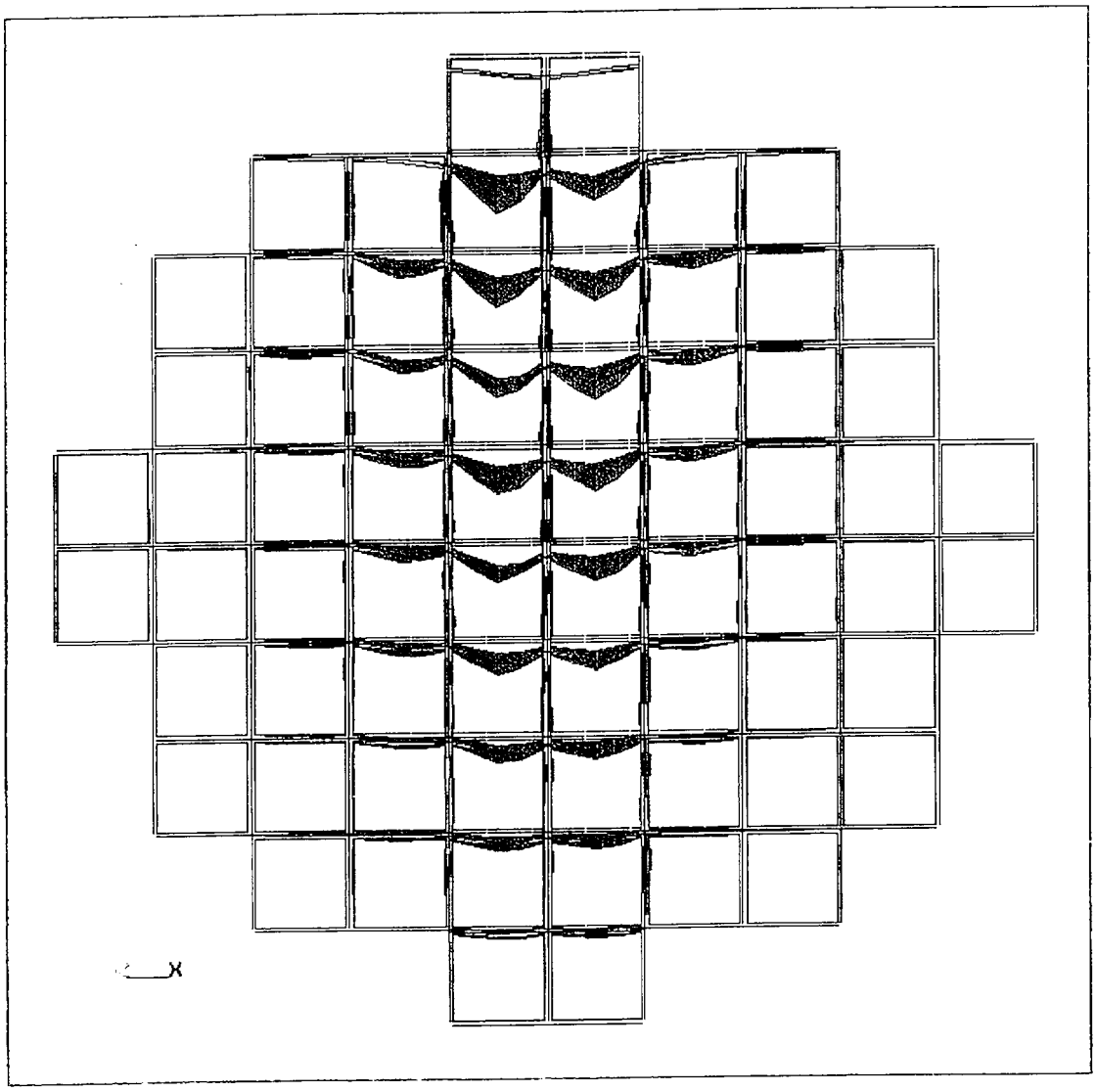

FIGURE 2.10.6-3
0° MODAL ANALYSIS - FIRST MODE (204 HZ)

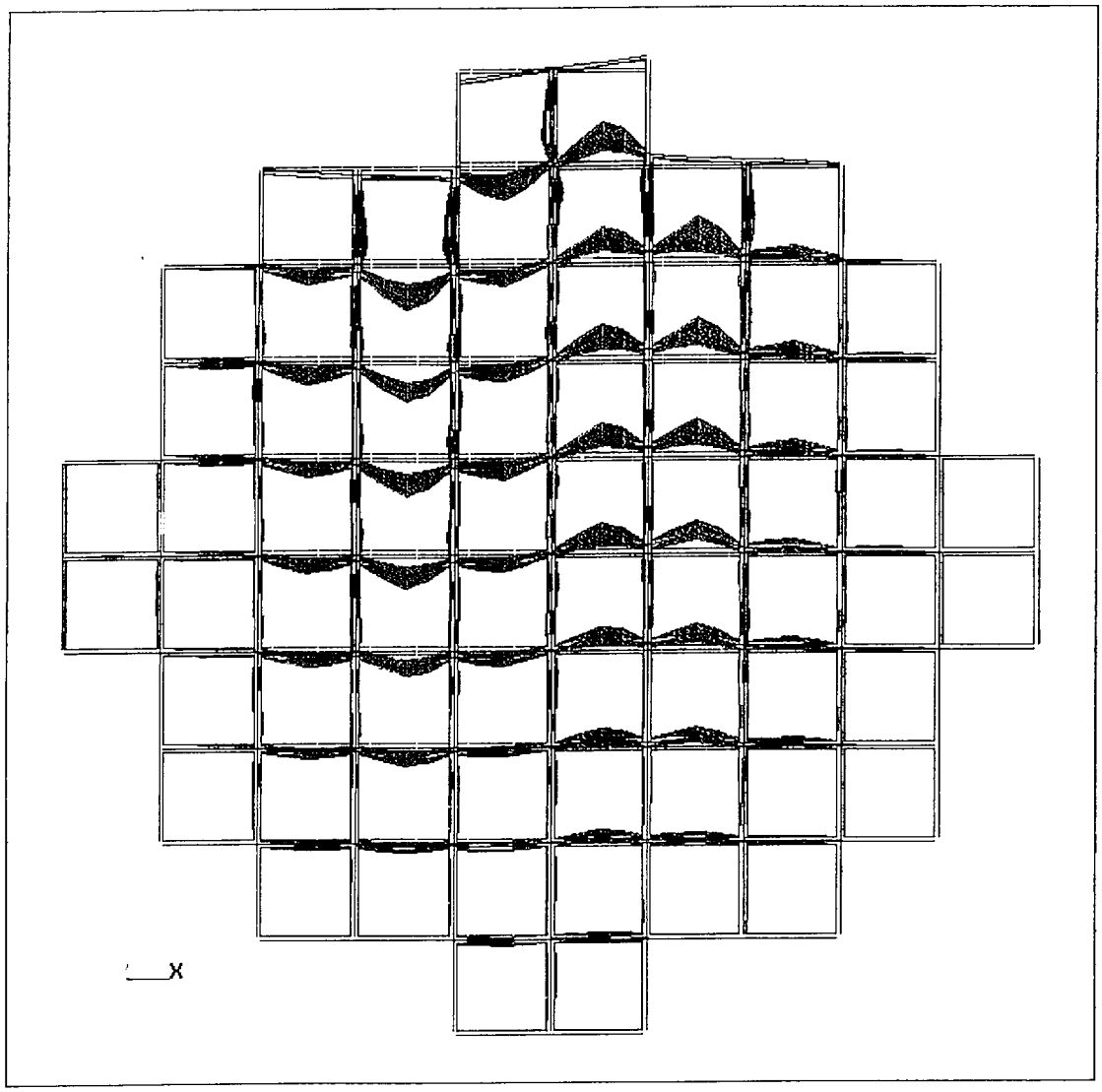

FIGURE 2.10.6-4
0° MODAL ANALYSIS -
SECOND MODE (225 HZ)

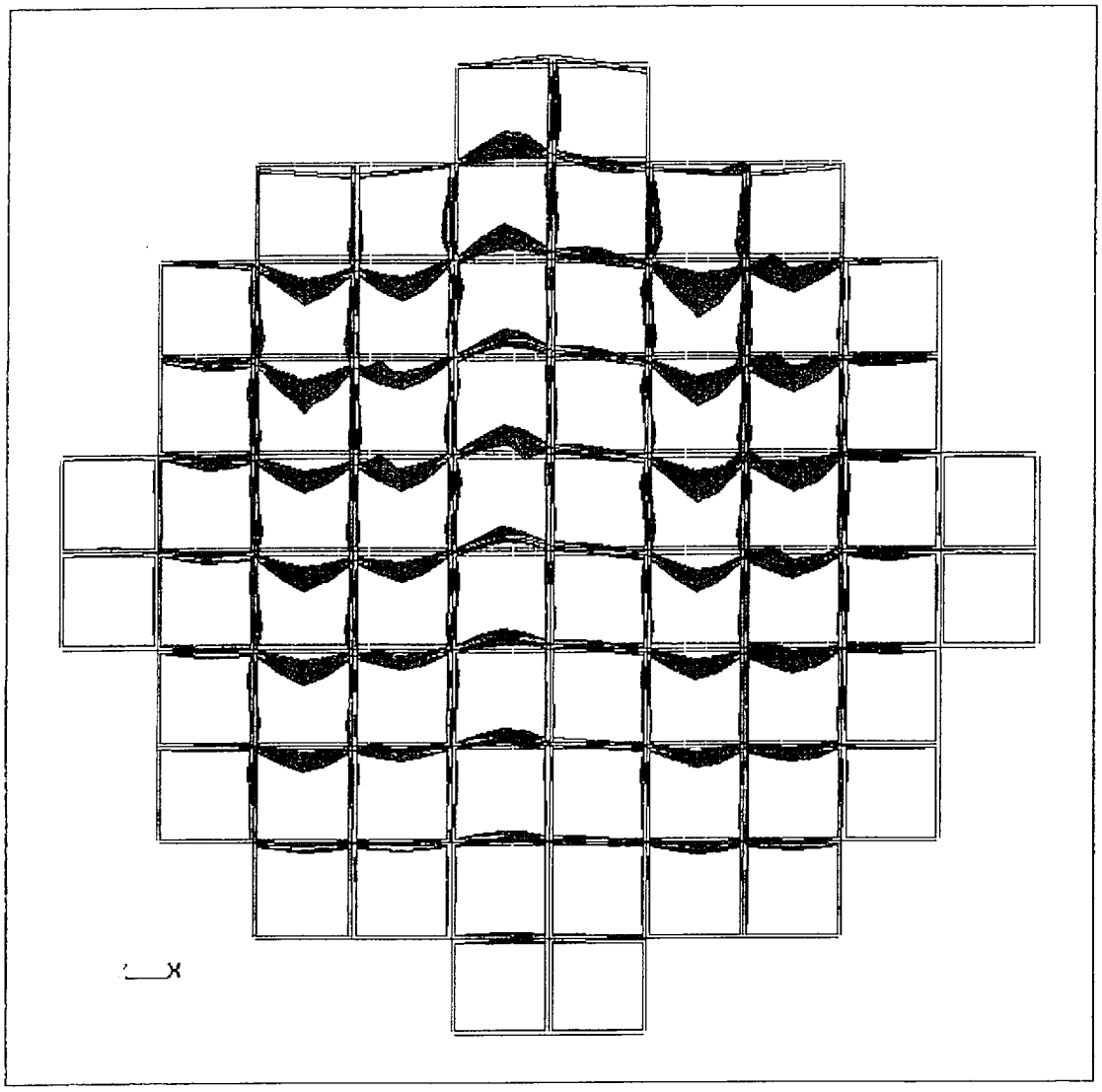

FIGURE 2.10.6-5
0° MODAL ANALYSIS - THIRD MODE (237 HZ)

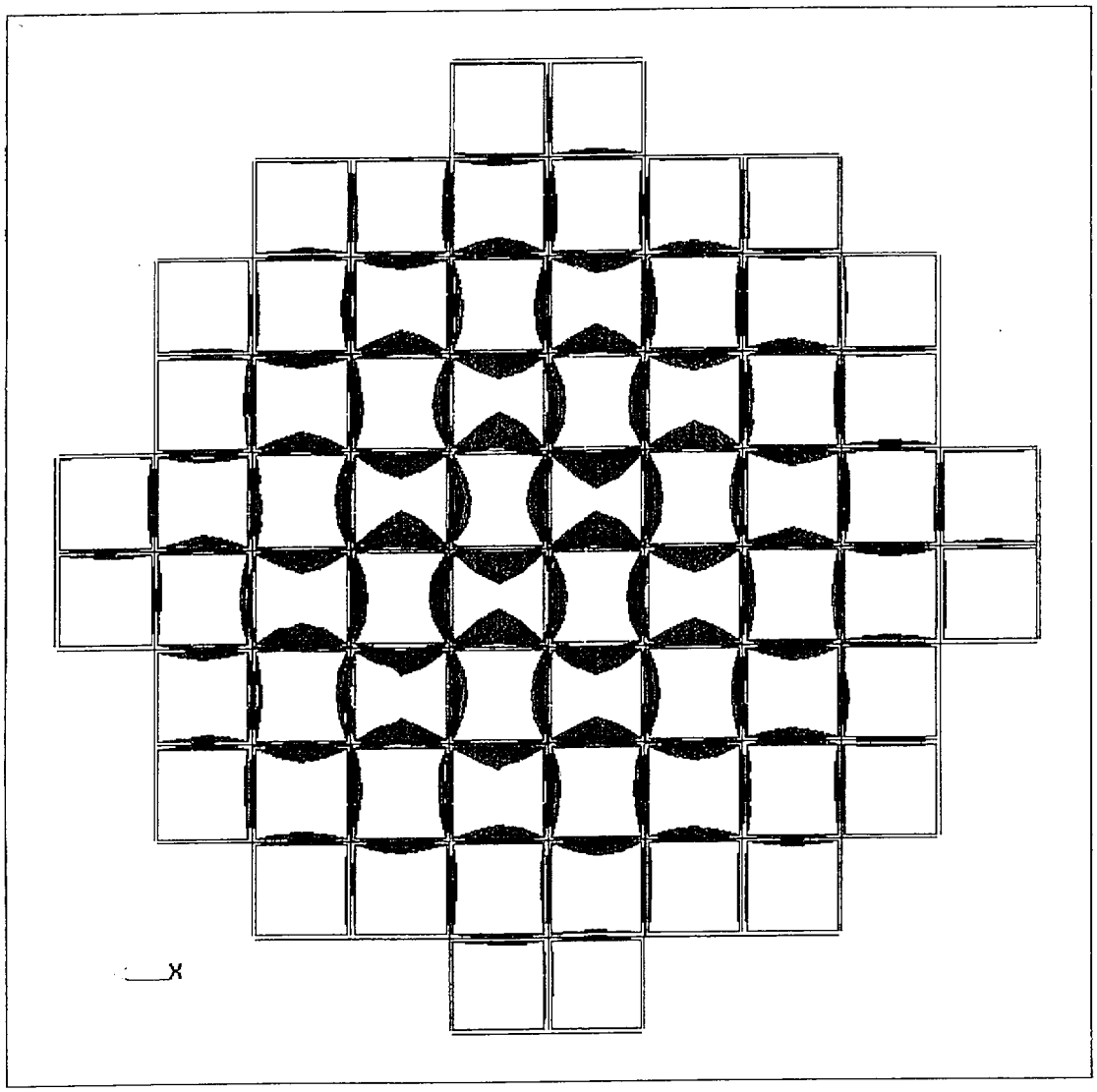

FIGURE 2.10.6-6
0° MODAL ANALYSIS -
FOURTH MODE (242 HZ)

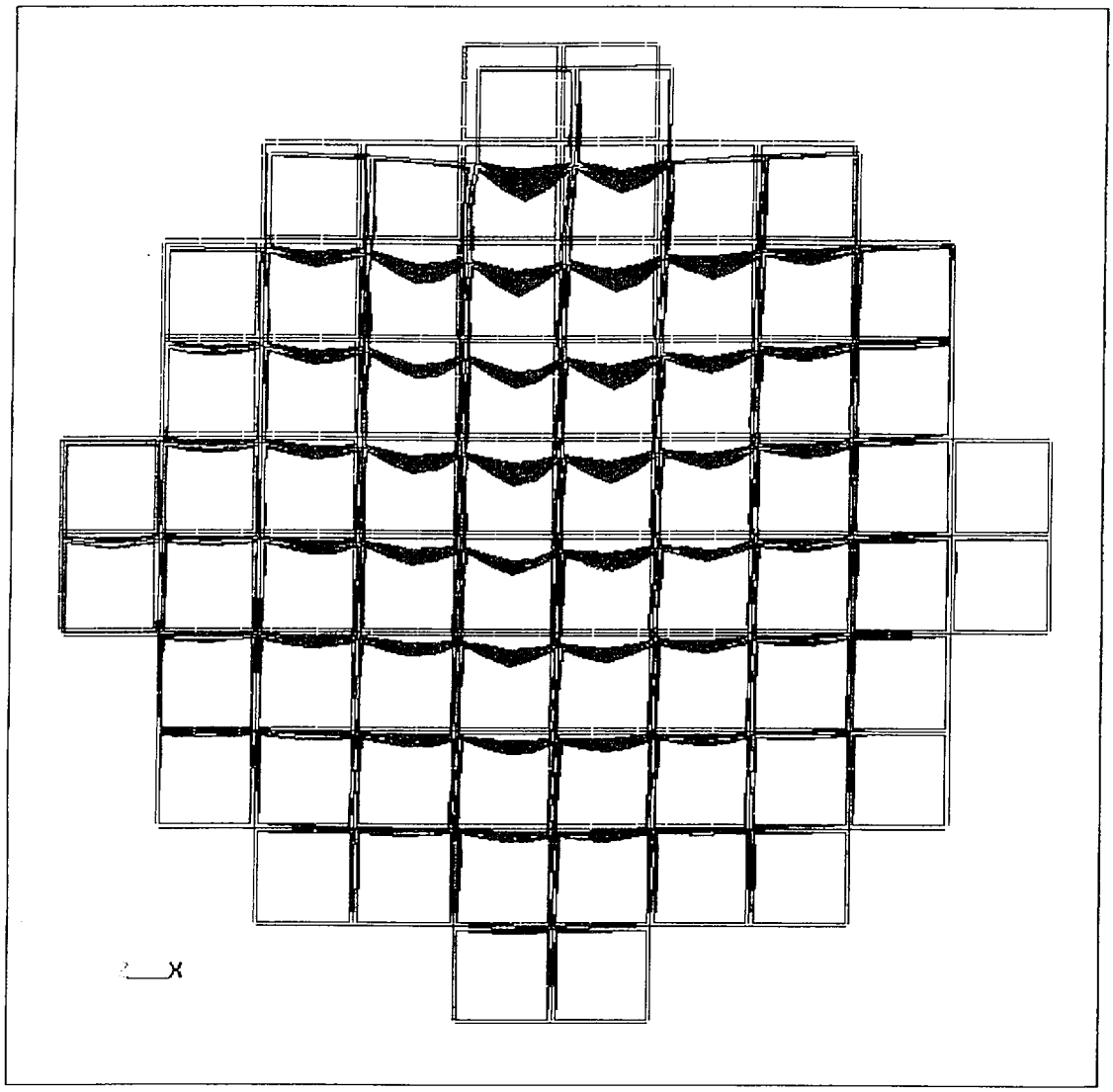

FIGURE 2.10.6-7
30° MODAL ANALYSIS - FIRST MODE (195 HZ)

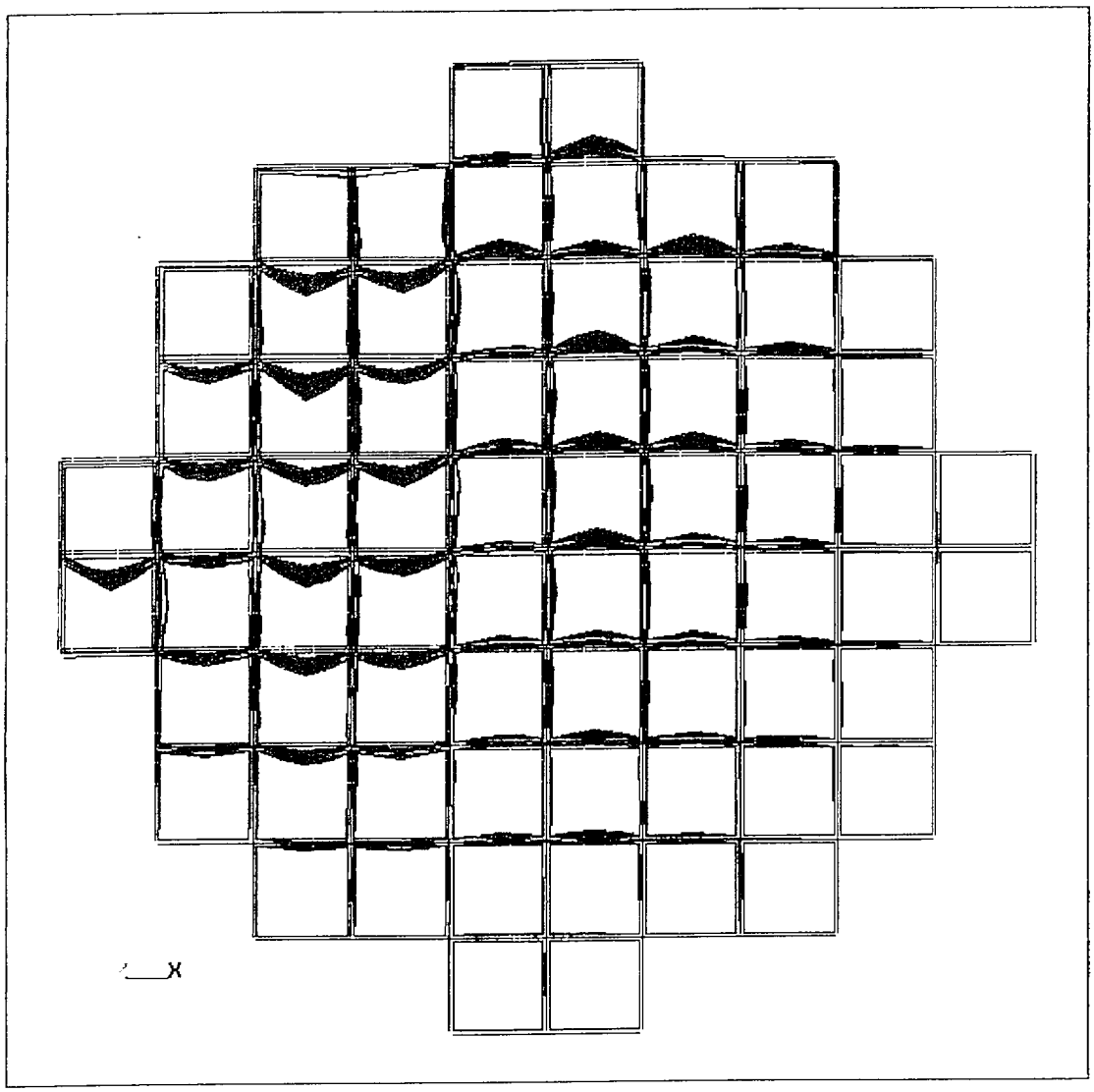

FIGURE 2.10.6-8
30° MODAL ANALYSIS -
SECOND MODE (253 HZ)

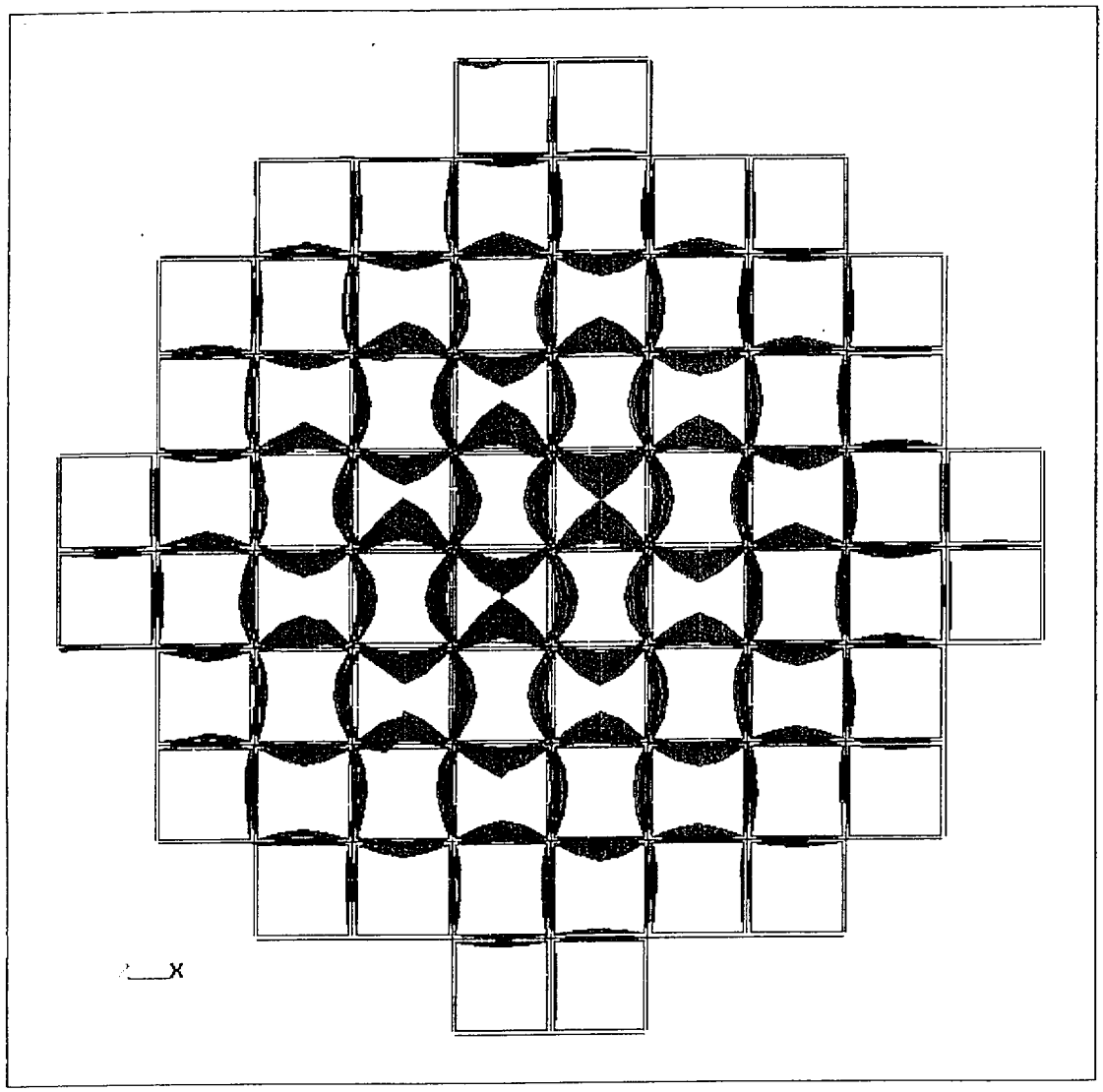

FIGURE 2.10.6-9
30° MODAL ANALYSIS - THIRD MODE (258 HZ)

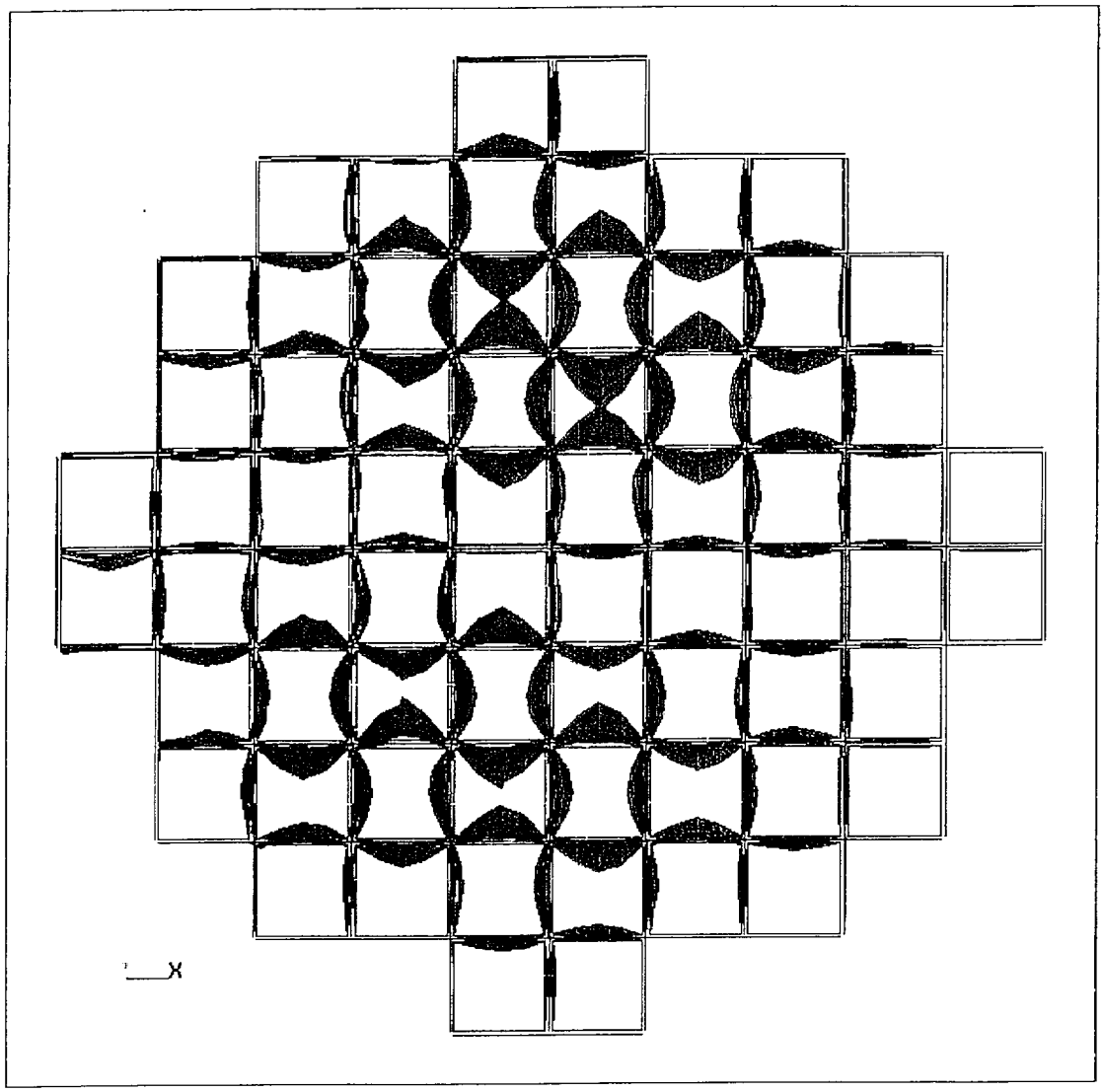

FIGURE 2.10.6-10
30° MODAL ANALYSIS -
FOURTH MODE (264 HZ)

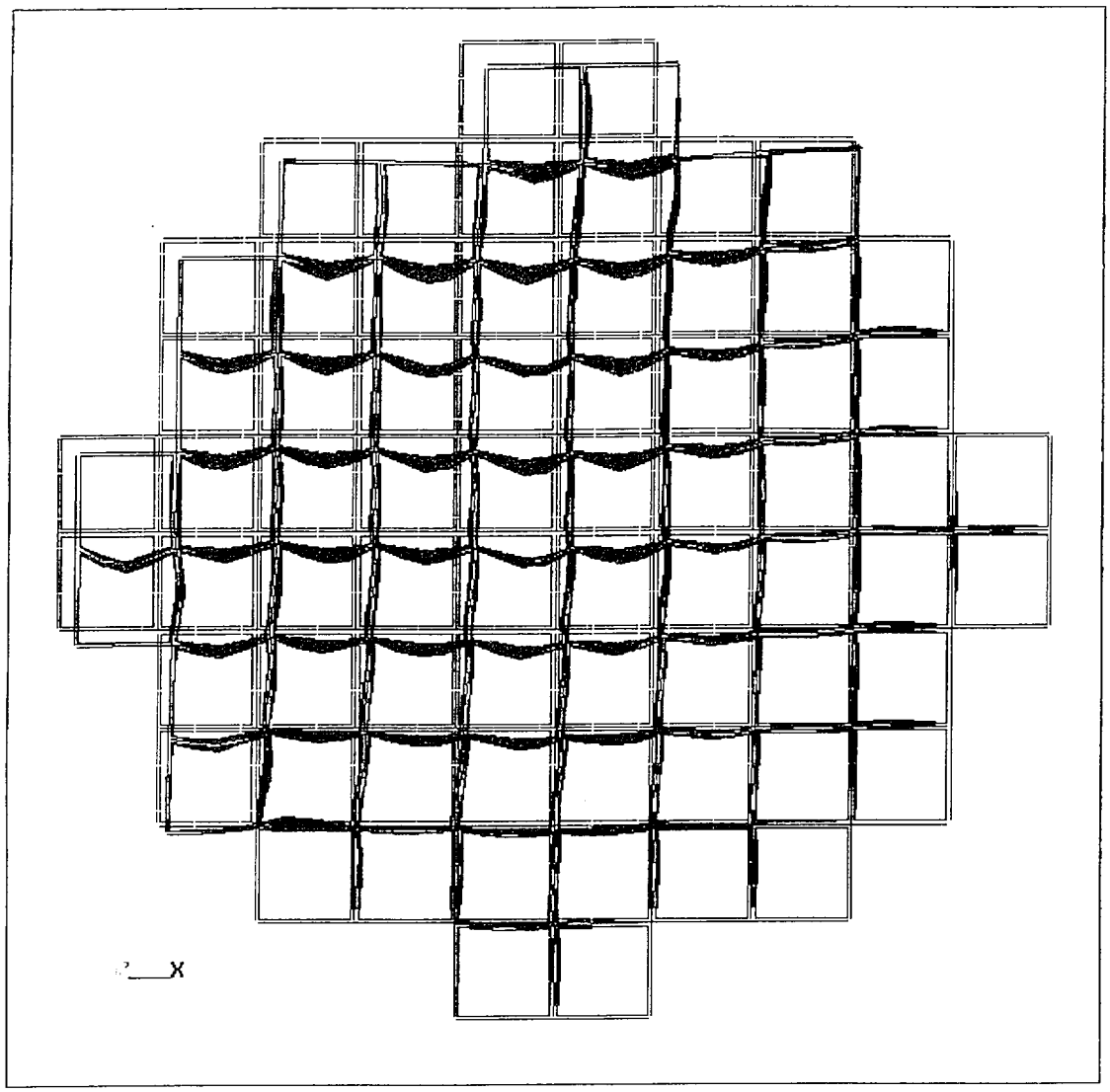

FIGURE 2.10.6-11
45° MODAL ANALYSIS - FIRST MODE (181 HZ)

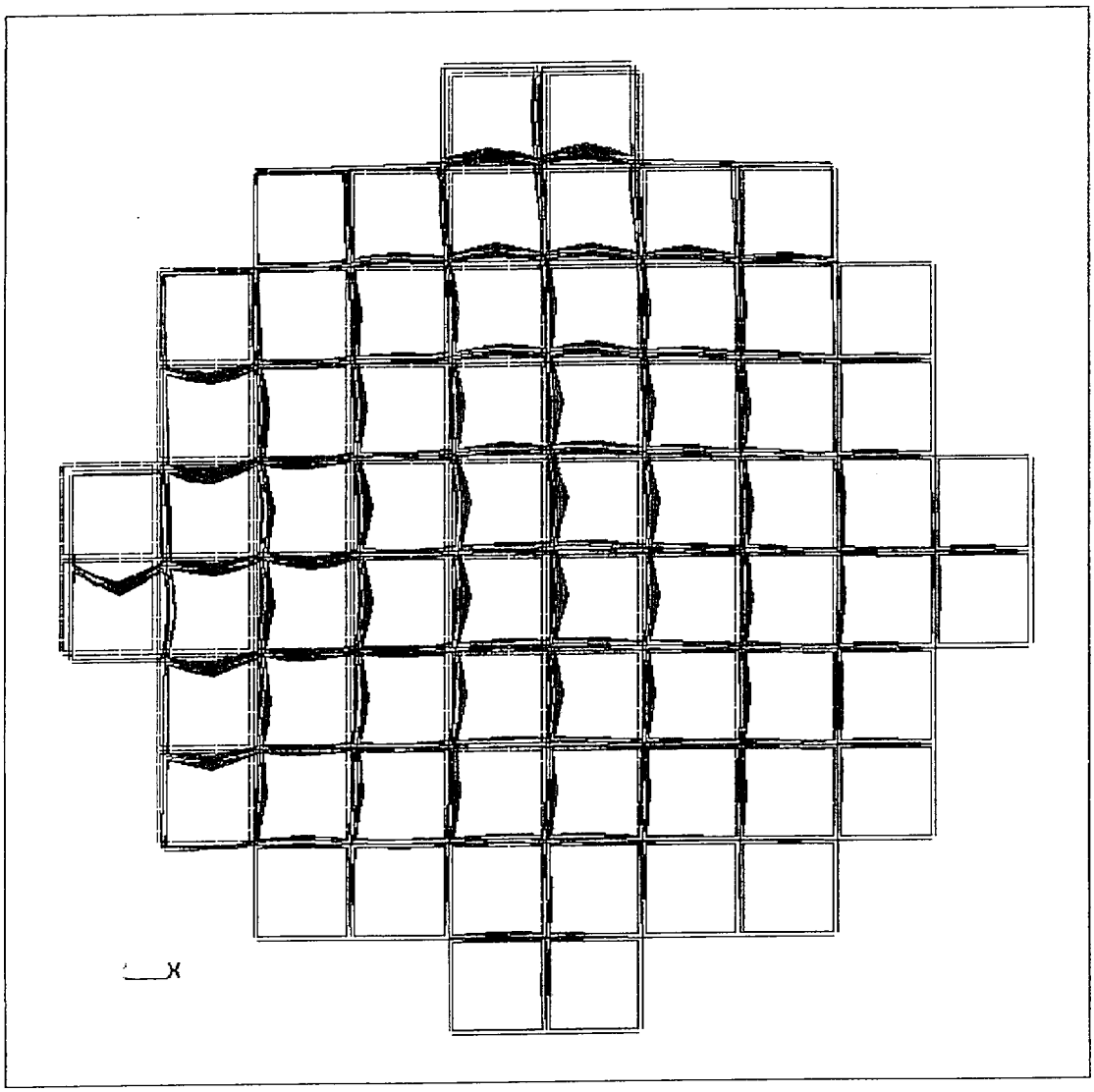

FIGURE 2.10.6-12
45° MODAL ANALYSIS -
SECOND MODE (232 HZ)

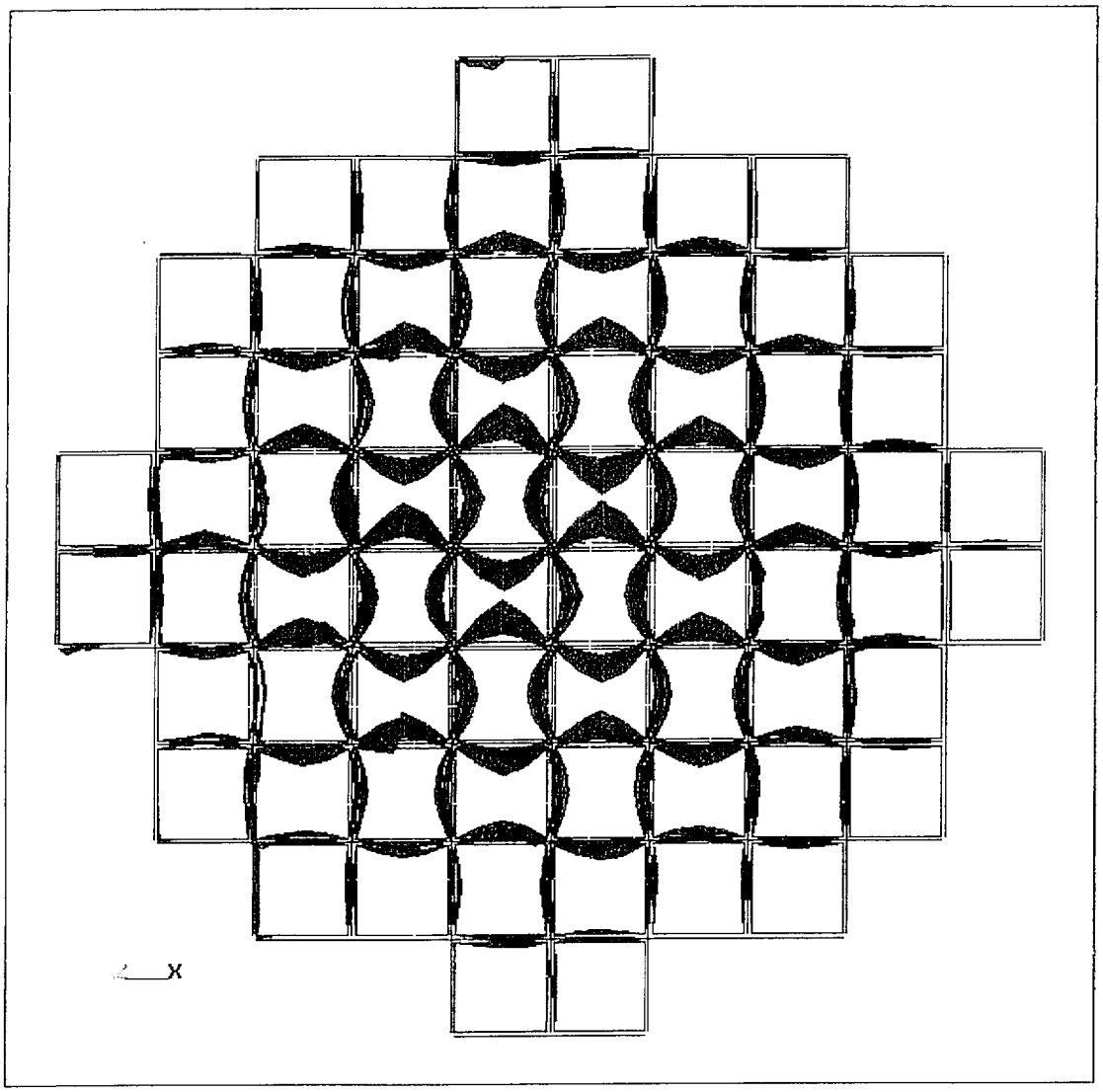

FIGURE 2.10.6-13
45° MODAL ANALYSIS - THIRD MODE (272 HZ)

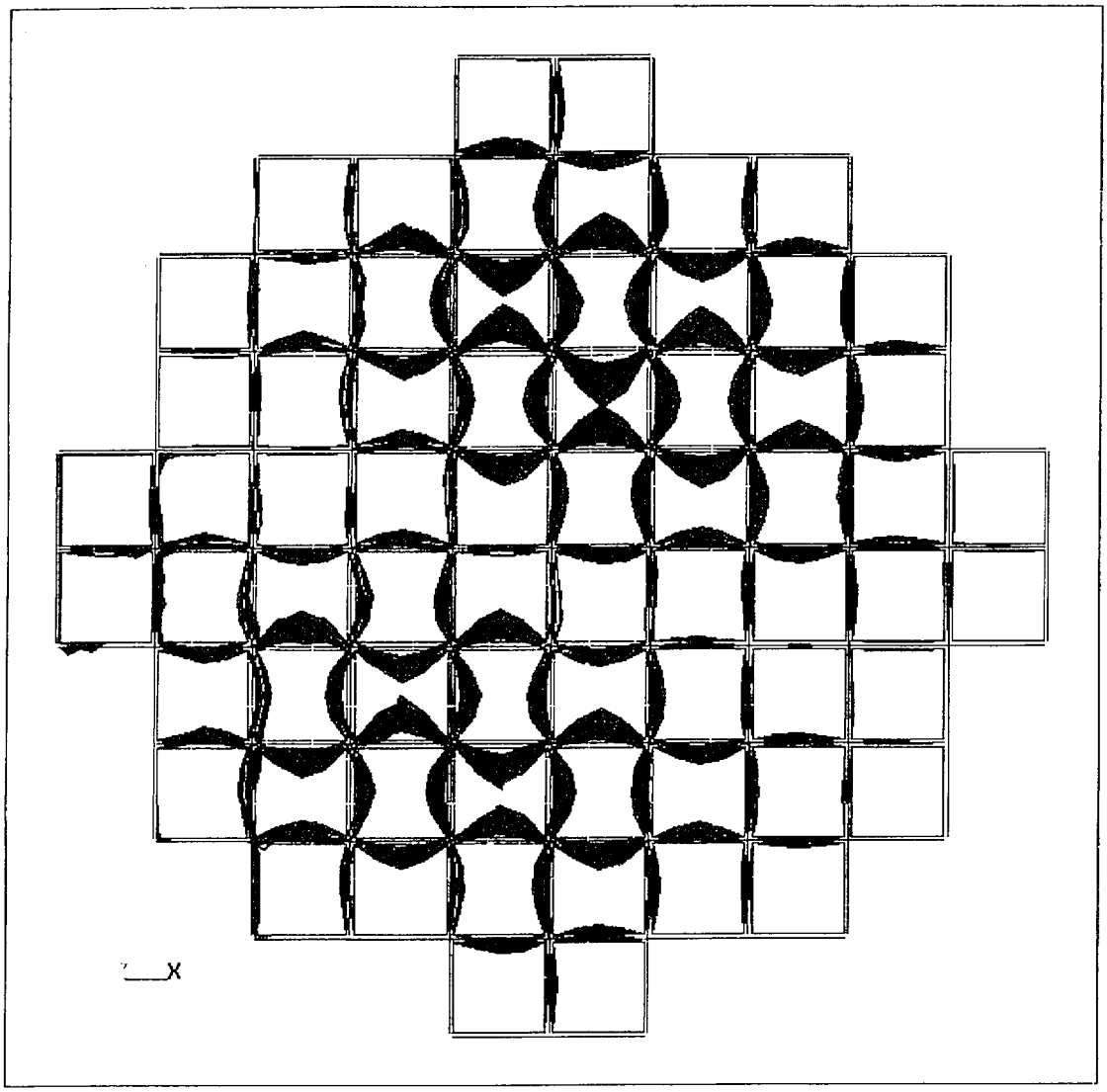

FIGURE 2.10.6-14
45° MODAL ANALYSIS -
FOURTH MODE (281 HZ)

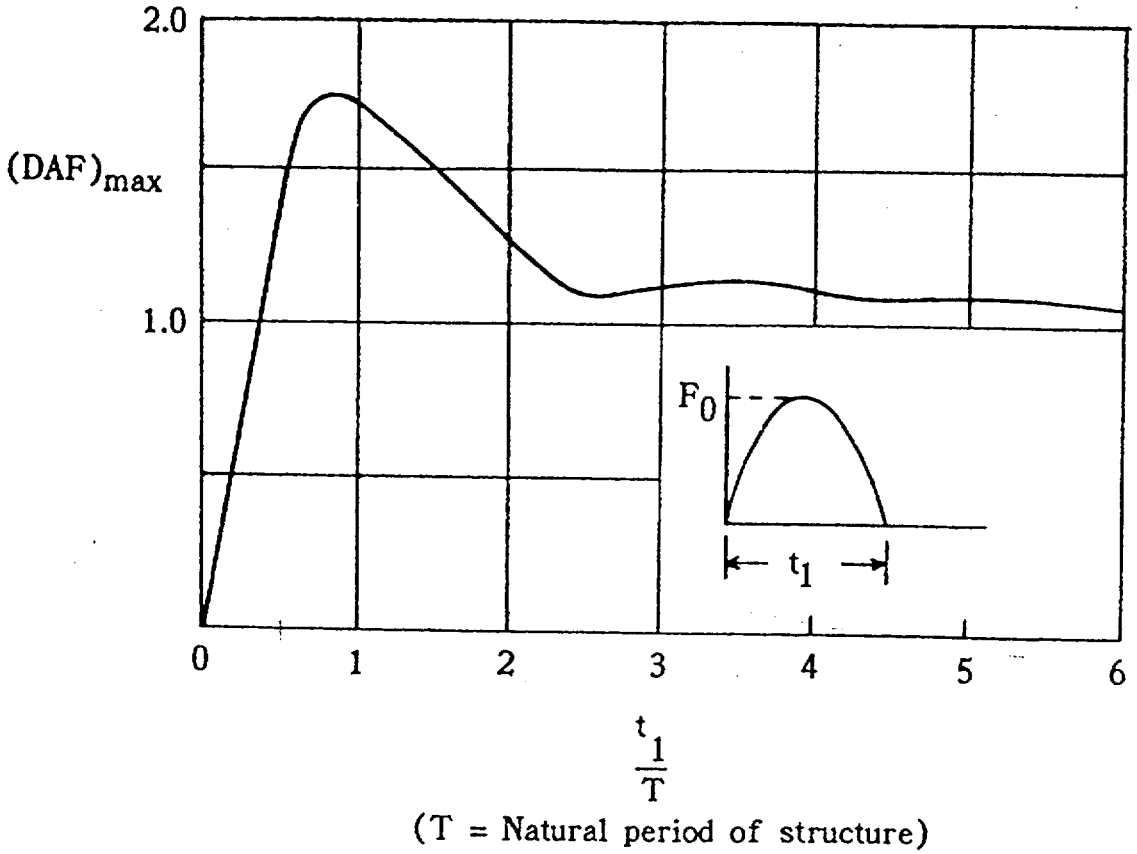

FIGURE 2.10.6-15
DYNAMIC LOAD FACTOR FOR A HALF-SINE WAVE
(From Fig. 2.15 of NUREG/CR-3966)

TN 68 TRANSPORT PACKAGING

APPENDIX 2.10.7

TABLE OF CONTENTS

LIST OF TABLES

LIST OF FIGURES

THIS PAGE IS INTENTIONALLY LEFT BLANK.

APPENDIX 2.10.7

EVALUATION OF FUEL ASSEMBLY UNDER ACCIDENT IMPACTS

2.10.7.1 Introduction

This appendix evaluates the effect of TN-68 cask impact (30 foot side drop or end drop) on the integrity of fuel rod cladding. The material properties of irradiated zircalloy cladding and the rod impact stress analysis approach are based on LLNL Report UCID-21246[1]. The fracture analysis of the fuel rod cladding is based on the ASME Code, Section XI, 1989[2]. The irradiated zircalloy fracture toughness data is obtained from ASTM Special Technical Publication 551[3]. Presented below are the analyses and results that are used to conclude that the fuel rod cladding will remain intact and retain the fuel pellets during all accident scenarios.

2.10.7.2 Material Properties

This section establishes the basis for assuming particular material properties. The value of some of the parameters used in the analysis are temperature dependent. The maximum temperature during the normal loading conditions is not expected to exceed 510°F (except fire accident). Consequently, material properties will be based upon this temperature, with the expectation that the ability of the zircalloy to absorb impact loads without rupture will increase as the temperature decreases with time.

Weight Density

The weight density of both Zircalloy-2 and Zircalloy-4 is very close to the weight density of Zirconium itself. From Reference 1,

$$\rho_{tube} = 0.234 \text{ lb/in}^3$$

Young's Modulus

The Young's modulus for typical Zircalloy cladding is illustrated in Table 5 of Reference 1. Thus, at 510°F,

$$E_{tube} = 11.7 \times 10^6 \text{ psi}$$

$$E_{fuel} = 13.7 \times 10^6 \text{ psi (conservatively assume a lower value)}$$

Yield Strength

The yield strength for typical Zircalloy cladding is illustrated in Table 5 of Reference 1. Thus, at 510°F,

$$S_{yield\text{-}tube} = 88{,}000 \text{ psi}$$

2.10.7.3 30 Foot Side Drop

The fuel rod side impact stresses are computed by idealizing fuel rods as continuous beams supported at each spacer grid. Continuous beam theory is used to determine the maximum bending moments and corresponding stresses in the cladding tube. The methodology used in performing the analysis is based on work done at Lawrence Livermore National Labs (Ref. 1). The fuel gas internal pressure is assumed to be present and the resulting axial tensile stress is added to the bending tensile stress due to 80G load (Appendix 2.10.8). The stresses for different General Electric fuel assemblies are computed in Table 2.10.7-1. It is seen that the 36,372 psi is the highest stress and occurs in GE9-8×8 and GE10-8×8 fuel assemblies. This stress is lower than the yield strength of zircalloy (88,000 psi). It is, therefore, concluded that the fuel tube will not fail and will withstand the side drop load without excessive plastic deformations. The grid supports (spacers) are expected to crush before 80G load is developed and the actual tube stresses will be much lower than the above noted stress.

2.10.7.4 Bottom End Drop

In case of an end drop, the inertial forces load the rod as a column having intermediate supports at each grid support (spacer). The tube limit load is that at which the fuel rod segments between the supports become unstable.

An elastic-plastic stress analysis was performed using the ANSYS Finite Element Program (Ref. 6). A three-dimensional finite element model of entire active tube length was constructed using plastic PIPE20 element for cladding tube and elastic PIPE16 element for fuel. The hinge supports were modeled at 7 grid support locations. The finite element model and support conditions for a typical tube model are shown in Figure 2.10.7-1. The tube and fuel nodes were coupled in X, Y and Z directions. The following material properties (at 510 °F) were input as a bilinear kinematic stress-strain curve for Zircalloy cladding tube. These properties are taken from Reference 1.

Yield Strength = 88,000 psi
Ultimate Strength = 98,000 psi
Modulus of elasticity = 11.7×10^6 psi
Elongation = 1.75%
Max. elastic strain = $88{,}000/11.7 \times 10^6 = 0.00752$ in/in
Tangent Modulus = $(98{,}000 - 88{,}000) / (.0175 - .00752) = 1.0 \times 10^6$ psi

For Fuel elements, Modulus of elasticity = 13.7×10^6 psi is conservatively used for analysis. The tube and fuel densities were modified to compensate for the extra tube length and the components which were not modeled.

In order to get the tube-buckling load, the large displacement option of ANSYS was used. The maximum inertia force of 200G was used. This load was applied gradually in a number of sub-steps. The analysis was continued to load sub-step till the tube model became unstable and did not converge. In each case, the lowest segment became unstable as it was supporting the entire tube and fuel weights. The last converged load sub-step was taken as the plastic instability load. The above analysis was repeated for one fuel rod of each fuel subassembly. All the input data and the resulting plastic instability loads are summarized in Table 2.10.7-2. 70% of ANSYS plastic instability load is used as the allowable buckling load (Reference 7, Para. F-1341.4).

Since the internal pressure produces tensile stresses in the cladding, it will reduce the compressive stresses caused by the end drop impact. The pressure is therefore conservatively neglected in this analysis. From the results in Table 2.10.7-2, it is seen that the lowest tube-buckling load of 95G occurs in GE5-8×8, GE8-8×8, GE9-8×8, GE10-8×8, and GE12-10×10 fuel assemblies. The actual end drop impact load is less than 80 G (Appendix 2.10.8). It is, therefore, concluded that the fuel cladding tubes will not be damaged during an end drop.

2.10.7.5 Brittle Fracture Evaluation

The following section demonstrates that the fracture toughness of the irradiated zircalloy cladding is sufficiently high to preclude brittle fracture failure during accident conditions.

The TN-68 cask is designed to store and transport intact fuel assemblies. Fuel assemblies known or suspected to have cladding defects greater than hairline cracks or pin holes shall not be loaded into TN-68 cask for storage and transport. The EPRI report, reference 5, provides a definition of pin holes or hairline cracks to include cracks of about 100μm (0.004") maximum width but whose length could be anywhere between 200-300 μm (.008" – 0.012") and up to several millimeters. For conservatism, the following surface flaw size is used for brittle fracture evaluation of the fuel rod cladding:

a= flaw depth = 150 μm = 0.006"
l = flaw length = 4 mm = 0.16"

Stress intensity factor K_I is calculated using the equation in ASME Code, Section XI, Appendix A, Article A-3000. The crack location and orientation are assumed to be that which is most detrimental to the rod cladding:

$$K_I = (\sigma_m M_m + \sigma_b M_b) \sqrt{\frac{\pi a}{Q}}$$

Where

σ_m, σ_b = membrane and bending stresses in psi

a = flaw depth

Q = flaw shape parameter as determined from Appendix A, Fig. A-3300-1

M_m = correction factor for membrane stress from Appendix A, Fig. A-3300-3

M_b = correction factor for bending stress from Appendix A, Fig. A-3300-5

It is seen from Tables 2.10.7-1 and 2.10.7-2, that the combined tensile stress in GE9-8 × 8 and GE10-8×8 fuel assemblies is the highest (36,372 psi). These fuel assemblies are, therefore, selected for fracture evaluations. It is conservatively assumed that all the stresses are membrane stresses.

t = cladding thickness = 0.030 inch
a = crack depth = 0.006 inch
l = crack length = 0.16 in
a/t = 0.2
a/l = 0.0375
zircalloy yield strength, S_y = 88,000 psi
$(\sigma_m + \sigma_b) / S_y = (36{,}372)/ 88{,}000 \approx 0.41$
$Q \approx 0.98$
$M_m = 1.35$

$$K_I = [(36{,}372 \times 1.35) \sqrt{\frac{\pi \times 0.006}{0.98}}]$$
$$= 6{,}810 \text{ psi } \sqrt{\text{in}} \approx 6.8 \text{ ksi } \sqrt{\text{in}}$$

The calculated Stress Intensity Factor for the flaw should satisfy the code faulted condition criteria (ASME Code Section XI, para. IWB-3612):

$$K_I < K_{ic} / \sqrt{2}$$

K_{ic} from Ref. 3 at 200° F (conservatively use lower temp.) = 30.0 ksi $\sqrt{\text{in}}$

Allowable fracture toughness = 30.0 / 1.414
= 21.2 ksi $\sqrt{\text{in}}$ > 6.8 ksi $\sqrt{\text{in}}$

Based on the above evaluations, it is concluded that the fracture toughness of the irradiated zircalloy cladding is sufficiently high to preclude a brittle fracture failure during accident conditions. Therefore, the fuel cladding tube will remain intact and retain the fuel pellets during accident conditions.

2.10.7.6 References

1. LLNL Report UCID-21246, Dynamic Impact Effects on Spent Fuel Assemblies, 10/1987.
2. ASME Boiler and Pressure Vessel Code, Section XI, 1989.
3. ASTM Special Technical Publication 551, Variation of Zircalloy Fracture Toughness in Irradiation, Walker and Kass, 8/1973.
4. PNL-6189, Recommended Temperature Limits for Dry Storage of Spent Light Water Reactor Zircalloy-Clad Fuel Rods in Inert Gas, May 1987.
5. EPRI report, 1994, Irradiation Damage to Fuel Assemblies.
6. ANSYS Engineering Analysis System User's Manual, Rev. 5.2.
7. ASME Code Section III, Division 1 Appendices, 1995.
8. Timoshenko, "Strength of Materials", Part II, 3rd Edition.
9. Roark, "Formulas for Stress and Strain", 4th Edition.

THIS PAGE IS INTENTIONALLY LEFT BLANK.

Table 2.10.7-1

Tipover/ Side Drop Impact Stress Calculations

Tube Arrays	7 x 7	8 x8	8 x 8	8 x 8	8 x 8	9 x 9	10 x 10
GE Designation	GE2, GE3	GE4	GE5	GE8	GE9, GE10	GE11, GE13	GE12
MTU/Fuel Assy.	0.1977	0.1880	0.1856	0.1825	0.1834	0.1766	0.1867
No. of fuel rods	49	63	62	60	60	74	92
Max. active fuel length, (in)	144	146	150	150	150	146	150
Fuel rod OD(1) (in)	0.559	0.489	0.479	0.479	0.479	0.436	0.400
S_y (psi)	88,000	88,000	88,000	88,000	88,000	88,000	88,000
No. of Spacers, n	7	7	7	7	7	8	8
L = length/n-1	24	24.3	25	25	25	20.9	21.4
Tube, E_1 (psi)	$11.7x10^6$	$11.7x10^6$	$11.7x10^6$	$11.7x10^6$	$11.7x10^6$	$11.7x10^6$	$11.7x10^6$
Tube, I_1 (in^4)	.00175	.001205	.001071	.001071	.001071	.000707	.000503
Fuel, I_2 (in^4)	.003044	.001602	.001513	.001513	.001513	.001067	.000754
TubeWt, (lb)	1.85	1.70	1.55	1.55	1.55	1.22	1.04
Fuel Wt, (lb)	10.09	7.46	7.49	7.61	7.64	5.97	5.07
Total Weight (lb)	11.94	9.16	9.04	9.16	9.19	7.19	6.11
W, (lb/in)	.0829	.0627	.0603	.0611	.0613	.0492	.0407
$M=.1058wl^2$,7supp $M=.1056wl^2$,8supp	5.053	3.920	3.987	4.038	4.053	2.269	1.970
$S_b = MC/I$ (1G) (psi)	294.6	341.4	369.5	374.2	375.7	278.8	313.4
S_b for 80G (psi)	23,568	27,312	29,561	29,936	30,056	22,304	25,072
Pressure, (psi)	1,311	1,256	1,674	1,702	1,688	1,608	1,614
$S_{press.}$ psi(2)	5,779	4,484	6,264	6,368	6,316	6,339	6,322
$S = S_b(77G) + S_{press.}$ (psi)	29,347	31,796	35,825	36,304	36,372	28,643	31,394

Notes:

(1) Includes 0.004 in. reduction in cladding OD to account for water side cladding corrosion (Ref.4).

(2) $S_{press.}$, axial stress = p x $D_{avg}/4t$

Table 2.10.7-2

Tube Buckling Loads Due to End drop Impact

Tube Arrays (No. of Tubes)	7 x 7 (49)	8 x8 (63)	8 x 8 (62)	8 x 8 (60)	8 x 8 (60)	9 x 9 (74)	10 x 10 (92)
GE Designation	GE2, GE3	GE4	GE5	GE8	GE9, GE10	GE11, GE13	GE12
Tube length, (in.)	158	158	158	158	158	158	158
Tube active length, (in)	144	146	150	150	150	146	150
No. of spacers	7	7	7	7	7	8	8
Length between spacers, L (in.)	24	24.3	25	25	25	20.9	21.4
Cladding tube OD, (in)	0.559	0.489	0.479	0.479	0.479	0.436	0.400
Tube area, A (in^2)	0.050	0.046	0.042	0.042.	0.042	0.033	0.028
Fuel area, ($in.^2$)	0.196	0.142	0.138	0.138	0.138	0.116	0.097
Tube weight = A x density x 158 (lb)	1.85	1.70	1.55	1.55	1.55	1.22	1.04
Fuel weight, (lb)	10.09	7.46	7.49	7.61	7.64	5.97	5.07
(Tube + Fuel) weight, (lb)	11.94	9.16	9.04	9.16	9.19	7.19	6.11
ANSYS Plastic Instability Load (G)	176	146	136	136	136	151	136
Axial Stress at Plastic Instability Load (psi)	8,542	7,114	6,830	6,921	6,944	7,287	6,648
Allowable Buckling G Load (70%)	123	102	95	95	95	109	95

Figure 2.10.7-1
Tube and Fuel Pellets Finite Element Model Simulation

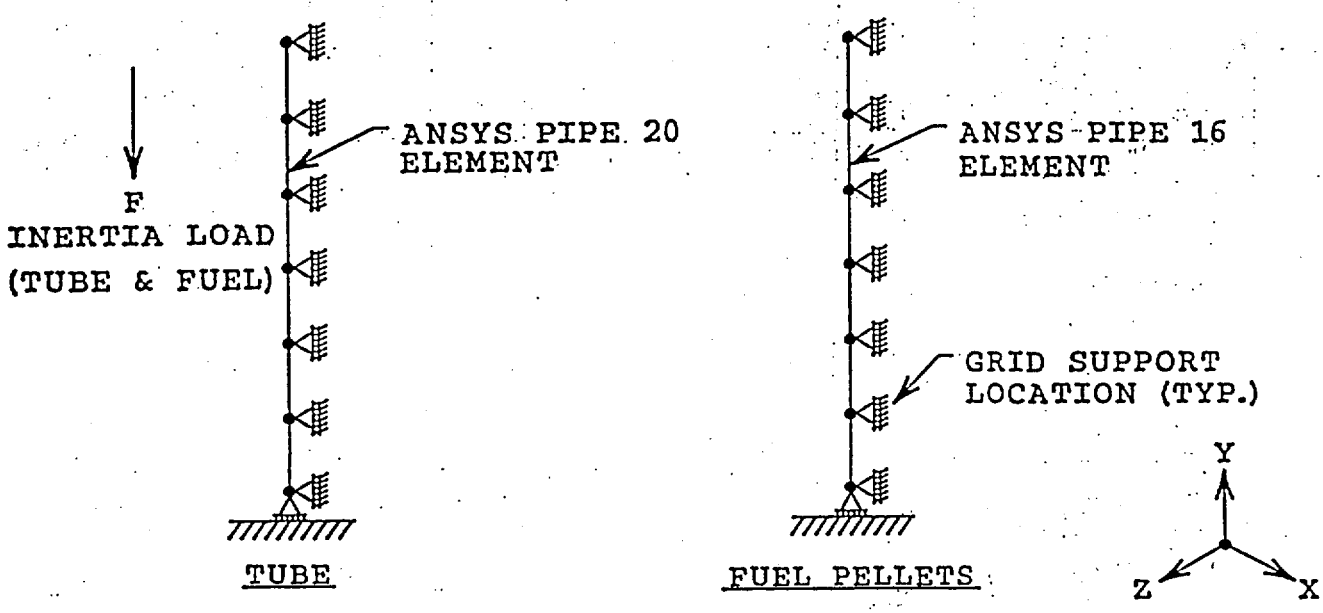

NOTE: THE TUBE AND FUEL PELLETS NODES ARE COINCIDENT BUT ARE SHOWN SEPARATELY FOR CLARITY. THESE NODES ARE COUPLED IN X, Y, & Z DIRECTIONS.

THIS PAGE IS INTENTIONALLY LEFT BLANK.

TN 68 TRANSPORT PACKAGING

APPENDIX 2.10.8

TABLE OF CONTENTS

LIST OF TABLES

LIST OF FIGURES

APPENDIX 2.10.8

STRUCTURAL ANALYSIS OF IMPACT LIMITERS

2.10.8.1 Introduction

This appendix presents the details of the structural analysis of the TN-68 impact limiters. The impact limiters are designed to absorb the kinetic energy resulting from the one (1) foot and thirty (30) foot normal and hypothetical accident free drop events specified by 10 CFR 71. Redwood and balsa wood are used as the primary energy absorption material(s) in the impact limiters. A sketch of the impact limiter is shown in Figure 2.10.8-1. A functional description of the impact limiters is given in Section 2.10.8.2. The impact limiter design criteria are described in Section 2.10.8.3.

A computer model of the TN-68 Packaging was developed to perform system dynamic analyses during impacts of 30 foot accident and 1 foot normal condition drops. The model was developed for use with the ADOC (Acceleration Due To Drop On Covers) computer code described in detail in Section 2.10.8.8 which determines the deformation of the impact limiters, the forces on the packaging and the packaging deceleration due to impact on an unyielding surface. Numerous cases were run to determine the effects of the wood properties and the initial drop angle. A description of the computer model, input data, analysis results and conclusions for the 30 foot accident condition and one foot normal condition free drops are given in Sections 2.10.8.4 and 2.10.8.5 respectively. The analysis of the impact limiter attachments is described in Section 2.10.8.6. A summary of results for all drop orientations is provided in Section 2.10.8.7. The forces and decelerations used in the cask body and basket structural analysis, presented in detail in Appendix 2.10.1 and Appendix 2.10.5, are given in Table 2.10.8-12 (loading values calculated in this appendix are increased for conservatism). Planned testing programs on the TN-68 wood filled limiters are discussed in Appendix 2.10.9. Test results to date indicate that ADOC predicts higher deceleration values, crush forces and crush depths than measured test results.

2.10.8.2 Design Description

The impact limiters absorb energy during impact events by crushing of balsa and redwood. The size, location and orientation of each wood block is selected to provide protection for the cask during all normal and hypothetical accident conditions of transport.

The top and bottom impact limiters are identical. Each has an outside diameter of 144 inches and a height of 48.00 inches. The inner and outer shells are Type A516 Grade 70 carbon steel joined by radial gussets of the same material. The gussets limit the stresses in the 0.25 in. thick steel outer cylinder and end plates due to pressure differentials caused by elevation and temperature changes during normal transport and provide wood confinement during impact. The metal structure positions, supports, confines and protects the wood energy absorption material. The metal structure does contribute to the energy absorbing capability of the impact limiter. However, the contribution to a side drop or oblique angles is negligible because contact starts at

a single point with the unyielding surface (target) and initiates buckling of a single gusset. After the drop event is complete, relatively few gussets are buckled.

The region of the impact limiter which is backed-up by the cask body is filled with balsa wood and redwood mostly oriented with the grain direction perpendicular to the end of the cylindrical cask (see Figure 2.10.8-1). The materials and grain orientations are selected to provide acceptably low deceleration to prevent excessively high stresses in the cask during impact after the thirty foot end drop. A 2.25 inch layer of balsa wood with the grain parallel to the end of the cylindrical cask is provided on the outer face of the impact limiter to minimize decelerations after a one foot end drop.

A 12.5 inch wide ring of redwood (consisting of 12 segments or blocks of wood) is located in the sides of the pie shaped compartments which surround the end of the cylindrical surface of the cask with the grain direction oriented radially. This ring of redwood absorbs most of the kinetic energy during a side drop. Redwood was selected for this portion of the impact limiter because of its high crush strength and hence the ability of a small amount of wood to absorb a large amount of energy in a relatively short crush distance.

The corners of the pie shaped compartments are filled with redwood. A 32.25 inch section of redwood is located next to the side redwood in the outer corner. The primary function of the redwood block is energy absorption during a 30 foot corner drop.

All wood blocks used in the impact limiters are composed of individual boards glued together with a Phenol Resorcinol Adhesive or equivalent. This adhesive is selected for its superior strength and moisture resistance. The wood blocks are assembled and glued together in accordance with an approved QA procedure. Minimum properties of the adhesive are listed in Table 2.10.8-1. Ranges of shear and tensile strengths of each type of wood are also listed. The adhesive is significantly stronger than any of the wood used in the limiter in terms of shear and tensile strength. Therefore the boards or blocks of wood will not fail along the glue joints.

The other mechanical properties of the wood used in the analysis are shown in Table 2.10.8-2. The crush strength properties used cover the range of expected values for the density and moisture content specified in the procurement specification. During procurement, wood samples are tested for density, moisture content and crush strength in accordance with an approved sampling plan.

If the density, moisture content, and crush strength are not within the specified range, the wood blocks from which samples are taken would be rejected.

During the end drop, all of the wood in the central part of the impact limiter that is directly "backed-up" by the cask body will crush. The wood in the corner and side of the limiter will tend to slide around the side of the cask since it is not supported or backed-up by the body and it will not crush or absorb energy as effectively as the wood that is backed-up. During the side or oblique drop the wood backed up by the cask will crush, while the wood beyond the end of the cask body will have a tendency to slide around the end of the cask. The analyses assume that the

effectiveness of the portion of the wood that is not backed-up is 20%. Effectiveness is defined as the actual crush force developed at the target by this material divided by the theoretical force required to deflect the material. The analysis also assumes a range of wood crush strengths. When determining maximum deceleration, the maximum crush strengths are used. When determining crush depth, the minimum wood crush strengths are used.

The impact limiters are attached to the cask using four attachment bolts each and attached to each other by thirteen tierods. The attachments have been sized to withstand the loads transmitted during a low angle drop slap down. This analysis is described in Section 2.10.8.6 of this Appendix.

2.10.8.3 Design Criteria

The outside dimensions of the impact limiter are sized to be within federal and state highway height and width restrictions. The balsa and redwood distribution and densities have been selected to limit the maximum cask body inertia loads due to the one foot normal condition drop and the thirty foot hypothetical accident drop so that the design criteria specified for the cask and basket (See Section 2.1) are met.

The welded carbon steel structure of the impact limiter is designed so that the wood is maintained in position and is confined during crushing of the impact limiters. The outer shell and gussets are designed to buckle and crush during impact. Local failure of the shell is allowed during impact limiter crushing. The welded carbon steel shell and its internal gussets are designed to withstand pressure differences and normal handling and transport loads with stresses limited to the material yield strength.

The impact limiters are designed to remain attached to the cask body during all normal and hypothetical accident conditions.

2.10.8.4 Analysis of 30 Foot Free Drop Accident Conditions

2.10.8.4.1 Approach

The kinetic energy due to the hypothetical 30 ft drop accident is absorbed by crushing of the impact limiters on the ends of the packaging. The limiters contain materials, i.e. balsa and redwood, which provide controlled deceleration of the packaging by crushing between the target surface and the cask body.

The applicable regulation, 10CFR71.73, requires that the packaging be oriented for the drop so that it strikes the target in a position for which maximum damage is expected. Dynamic impact analyses were performed for different packaging orientations using the ADOC computer code described in Section 2.10.8.8. This computer code has been validated by comparing its dynamic results with those from hand calculations for relatively simple problems, comparing its calculated force-deflection curves with those obtained from static crush tests, and by correlating dynamic results with actual measured cask behavior on other programs.

2.10.8.4.2 Assumptions and Boundary Conditions

The assumptions and boundary conditions are as follows:

1. The cask body is assumed to be rigid and absorbs no energy. This assumption is realistic since the design criteria of Section 2.1.2 limit metal deformations to small values. All of the impact energy is therefore assumed to be absorbed by the impact limiters.

2. The crushable material is one or several anisotropic materials. The different wood regions are modeled individually.

3. The crush strengths of the wood sections are obtained from the properties parallel to and perpendicular to the grain based on the orientation of the cask at impact.

4. Each wood region is modeled as a one dimensional elastic, perfectly plastic material up to a specific locking strain. After reaching the locking strain, the stress increases linearly with the additional strain. The wood properties (modulus of elasticity, average crush strength, locking modulus, and locking strain) are taken from force-deflection curves of sample blocks of wood. Typical force-deflection curves for balsa and redwood are shown in Figures 2.10.8-1A and 2.10.8-1B. Since the locking strain varies from sample to sample, conservatively low locking strains of 80% for balsa and 60% for redwood are used.

5. The crush properties of the wood are varied with the initial angle of impact and do not change during the drop event being evaluated.

6. The cask and impact limiters are axisymmetric bodies.

7. The crushing resistance of the impact limiter shell and gussets have a negligible effect on the crush strength of the limiter and, therefore, a negligible effect on the impact forces and inertia loads.

2.10.8.4.3 Packaging Dynamic Computer Model

Figure 2.10.8-2 illustrates the computer model used for all packaging orientations. Regions I, II, and III in the model are used to delineate regions where different impact limiter materials are used. It should be noted that the properties of the three regions have been designed by choosing wood types and orientations to accommodate the crush requirements of the drop orientations. The crushable materials of Regions I, II, and III are selected to control the decelerations resulting from end, corner, and side drop orientations, respectively. Table 2.10.8-2 tabulates the wood properties that were used to describe the wood stress-strain behavior in the analysis.

A portion of the impact limiter crushable material is backed up by the cask body as it crushes against the impact surface. The remaining material overhangs the cask body and is not backed up. Backed up regions project vertically from the target footprint to the cask body, while

unbacked regions do not project vertically to the cask. The effectiveness of the energy absorbing crushable material varies depending on whether it is "backed up" by the cask or is unsupported. Two cases are analyzed to bound impact limiter performance. In one case, the non-backed up material is assumed to be 20% effective and maximum wood crush strength is used (maximum of the possible range based on specified density). In the other case, the non-backed up material is also assumed to be 20% effective but the minimum wood strength is used. Evaluating impact limiter performance in this way results in a range of deceleration values, crush forces and crush depths. This, in combination with close control of wood properties during procurement, assures that the effects of wood property variations (including temperature effects) are bounded by the analyses.

2.10.8.4.4 Analysis Results Predicted by ADOC

The peak inertia loadings or cask body decelerations (in terms of *G'* s) versus initial angle of impact are presented in Tables 2.10.8-3 and 2.10.8-4 for the 30 foot drop. The 30 foot drop is measured from the impact surface to the bottom of the impact limiter; the center of gravity (CG) of the cask is much higher than 30 feet. The values of crush depth vs. impact force are shown in Tables 2.10.8-5 to 2.10.8-l0. Since the packaging CG is within a few inches of the packaging center and the impact limiters are identical, these tables are valid for impacts on either end.

Based on the crush depths for the side drop from Tables 2.10.8-5, the trunnions would not hit the impact surface. Using maximum wood properties, the clearance after the limiters crush would be approximately 8.11 inches. Using minimum wood properties, the clearance after the limiter crush would be 6.01 inches. It is expected that the crush depth would be somewhere between the two bounding cases.

2.10.8.5 Analysis for One Foot Drop Normal Condition

This section describes the analysis of the TN-68 for the one foot normal drop condition. The TN-68 is lifted vertically and is transported horizontally. End and side drop orientations are therefore considered to be credible normal drop events. Any other drop orientation will cause the cask to tip over onto its side, which is clearly an accident. The accident analyses in Section 2.10.8.4 bound any possible tipping accident. Therefore, the one foot drop analysis is performed for end and side drop orientations. A one foot, 60° corner drop is also analyzed to show that the normal condition side and end drops are critical with respect to acceleration and deformation.

The packaging kinetic energy is absorbed by crushing of the impact limiters. The dynamic system model of Section 2.10.8.4 was used to perform the side drop (0°) analysis using the ADOC computer program described in Section 2.10.8.9. The end drop analysis was performed assuming that the energy would be absorbed by the soft balsa wood (oriented in the weak direction) in the outer end of the limiter. This is an accurate way to determine G loads on an end drop since the G values can be calculated by the expression $F = Ma$ where F is the crush stress times the area and M is the package weight divided by the acceleration of gravity G.

The inertial load results of these one foot drop analyses are presented in Table 2.10.8-11. Again, two extreme cases are considered. The upper bound stiffness case assumes maximum wood crush strength and the lower bound stiffness case assumes minimum wood strength. Stress analyses in Section 2.10.1 are conservatively performed for the case(s) with maximum inertia loads resulting from upper bound stiffness cases.

2.10.8.6 Impact Limiter Attachment Analysis

The impact limiter attachments are designed to keep the impact limiters attached to the cask body during all normal and hypothetical accident conditions. The loading that has the highest potential for detaching the impact limiter is the slap down or secondary impact after a shallow angle 30 foot drop. During this impact, the crushing force on the portion of the impact limiter beyond the cask body (the non backed-up area) tends to pull the limiter away from the cask. The end and corner drops are not critical cases for the impact limiter attachments since the impact force tends to push the impact limiter onto the cask in these orientations.

For the tie rod evaluation, maximum wood crush strengths of 2010 psi for balsa and 6500 psi for redwood are assumed. The maximum wood properties produce the highest overturning moment on the limiter. Based on the dynamic analysis performed using the ADOC code, the most severe slap down impact occurs after a shallow angle oblique impact. The calculated peak contact forces at the end of the cask body subjected to secondary impact (slap down) for the orientations analyzed are as follows.

Drop Orientation	Impact Force (lb.×1000)
5°	6822
10°	6818
15°	6804
20°	6759
30°	5863

The 15° slap down impact will result in the most severe overturning moment, even though the 15° impact force is not the highest. This is because the crush depth for the 15° slap down impact results in a large moment arm. The peak impact force that is applied to the impact limiter is conservatively increased by roughly 50% to 10,133,000 lb for the structural analysis of the tie rods.

The maximum moment applied to the impact limiter attachments is conservatively determined ignoring the mass of the impact limiter which tends to reduce the attachment forces. The resultant of the external impact force on the limiter is offset 2.515 in. from the resultant of the cask reaction force. Therefore, the net moment applied to the limiter is $10.133 \times 10^6 \times 2.515$ or 2.548×10^7 in lb. There is also a frictional force that acts to pull the impact limiter away from the cask. Assuming a frictional coefficient of 0.12 between the cask and limiter and between the limiter and impact surface, the magnitude of this force is

$$F_f = \mu R = (0.12)(10.133\times10^6) = 1.216\times10^6 \text{ lbs.}$$

The crush depth on the side is 11.1 inches. The resultant moment due to friction is

$$M_f = (1.216\times10^6)(29.225\text{-}11.1) = 2.204\times10^7 \text{ in lbs.}$$

The total moment is therefore 4.752×10^7 in lbs. This moment is reacted by the thirteen impact limiter tie rods. A free body diagram of the impact limiter is shown in Figure 2.10.8-13. It is conservatively assumed that the impact limiter pivots about the edge of the cask. The tie rod forces vary linearly with distance from the pivot point, so that the maximum force, F_{max}, occurs in the tie rod farthest from the pivot point. The highest tie rod stress occurs when the package is oriented such that trunnion centerline is perpendicular to the impact surface (package rotated 90° from transport orientation). In this orientation, the tie rods react to the total moment, M, in the following way.

$$M = 2(103.78)F_{\max} + \frac{92.54^2}{103.78}F_{\max} + 2\frac{(71.51^2)}{103.78}F_{\max} + \frac{38.47^2}{103.78}F_{\max}$$
$$+\frac{42.78^2}{103.78}F_{\max} + \frac{47.09^2}{103.78}F_{\max} + 2\frac{(14.04^2)}{103.78}F_{\max} = 445.67F_{\max}$$

therefore

$$F_{\max} = \frac{4.752\times10^7}{445.67} = 106{,}632 \text{ lbs.}$$

The minimum tensile area of a 1½ inch diameter tie rod is located at the threads and is 1.490 in^2. Consequently, the maximum tie rod tensile stress is 106,632/1.490 = 71.6 ksi. This conservatively calculated stress is well below the minimum tie rod ultimate tensile strength of 125 ksi. The factor of safety against tie rod failure is 1.43. Therefore, the tie rod will not fail and will hold the impact limiter on the cask.

Previous drop tests reveal that during a 30 foot corner drop some of the impact limiter crushing occurs from the inside, where the cask contacts the impact limiter. This brings the impact limiters closer together, and can loosen some of the tierods. To prevent the top impact limiter from falling off the cask during secondary impact, eight 1½ – 8UN bolts (four per impact limiter) are employed. These bolts are attached to brackets welded to the outer shell of the cask and are threaded into each impact limiter.

If we conservatively assume a 5G axial inertial load during secondary impact, the tensile force applied to the four bolts is,

$$15{,}450\times5 = 77{,}250 \text{ lbs.}$$

The tensile force per bolt would then be,

$$77{,}250 / 4 = 19{,}313 \text{ lb/bolt.}$$

The tensile stress area for the 1½ – 8UN bolts is 1.4899 in^2. Therefore the tensile stress is

$$19{,}313 / 1.4899 = 12{,}962 \text{ psi.}$$

The impact limiter bolt material is SA540 Class 1 with allowable stress, $S_u = 165$ ksi., which is well above the calculated bolt stress.

2.10.8.7 Summary of ADOC Results Used for Structural Analysis

Cask Structural Analysis - G Load and Drop Orientation

In order to determine the cask stresses, the maximum G loads from ADOC runs are converted to forces and applied as quasistatic loadings on the cask body. A detailed ANSYS finite element model of the TN-68 cask is used to perform this analysis.

Only the loads corresponding to the most critical normal and accident condition free drop orientations are used in the cask body analysis in Section 2.10.1. For the 30 foot accident condition drops, *G* loads corresponding to four different angles are evaluated, and for the 1 foot normal condition drops, G loads corresponding to two different angles are evaluated. The orientations evaluated in Section 2.10.1 are as follows.

Drop Height (Normal / Accident)	Orientation Analyzed
30 Foot Accident Condition Drop	0° Side Drop
	15° Slap Down
	60° C.G. Over Corner Drop
	90° End Drop
1 Foot Normal Condition Drop	0° Side Drop
	90° End Drop

The *G* loads corresponding to these drop orientations are provided in Tables 2.10.8-3, 2.10.8-4, and 2.10.8-11.

The thirty foot side drop is evaluated because it produces the highest normal transverse *G* load. The 15°, thirty foot slap down is analyzed because it produces a high normal as well as rotational *G* load at the ends of the cask (second impact). Stresses in the cask and lid bolts are most sensitive to *G* loads applied in the 60° (CG over corner) direction. Consequently, the thirty foot CG over corner drop is evaluated. The highest axial *G* load occurs during a 90°, thirty foot end drop, and is therefore also evaluated.

For the normal condition one foot drops, the 0° side drop, and the 90° end drop are bounding, since they produce the highest normal *G* loads in the transverse and axial directions respectively. The G loads from other drop angles are small and generate insignificant rotational inertia G loads due to much lower impact velocity.

When the G loads are applied to the cask model in Section 2.10.1, the *G* loads predicted by ADOC are increased in order to bound all drop angles, and to create conservatism. The *G* loads predicted by ADOC as well as the increased *G* loads used in the cask body analysis are shown in Figure 2.10.8-12.

Basket Structural Analysis - G Load and Drop Orientation

The loading conditions considered in the evaluation of the fuel basket consist of inertial loads resulting from normal handling (1 foot drop) and hypothetical accident (30 foot) drops. The inertial loads of significance for the basket analysis are those that act transverse to the cask and basket structural longitudinal axes, so that the loading from the fuel assemblies is applied normal to the basket plates and is transferred to the cask wall by the basket. The side drop will result in the highest inertia load due to the fuel assemblies impacting the basket. For example, the transverse G load (normal) resulting from maximum wood properties, 0° side drop is 53 G's, and the maximum transverse G load (normal) resulting from 5° slap down second impact is about 26 G's. The rotational G loads from slap down impact have a very small effect on the basket because the cask stiffness is much greater than the basket stiffness and the basket is enveloped by the cask. Any rotational bending affect will be absorbed by the cask body. Therefore, the basket structure is analyzed for 1 foot and 30 foot side drops. For clarity, the basket structure is also analyzed for 1 foot and 30 foot end drops to shown a large margin of safety.

Table 2.10.8-13 lists the G loads used for the basket structural analysis, as well as the dynamic load factors calculated in Appendix 2.10.6.

2.10.8.8 Summary Description of ADOC Computer Code

One of the accident conditions which must be evaluated in the design of transport packagings to be used for the shipment of radioactive material is a free drop from a thirty-foot height onto an unyielding surface (10CFR71). The packaging must be dropped at an orientation that results in the most severe damage. Impact limiters are usually provided on the packaging to cushion the effects of such impact on the containment portion of the packaging. The limiters are usually hollow cylindrical cups which encase each end of the containment and are filled with an energy absorbing material such as wood or foam.

A computer code, ADOC (Acceleration due to Drop On Covers), has been written to determine the response of a packaging during impact. The analysis upon which this code is based is discussed in this section. The overall analysis of the packaging response is discussed in Section 2.10.8.8.1, and the methods used to compute the forces in the limiters as they crush are presented in Section 2.10.8.8.2.

2.10.8.8.1 General Formulation

The general formulation used to compute the response of the packaging as it impacts with a rigid target is discussed in this section. The assumptions upon which the analysis is based are first presented followed by a detailed development of the equations of motion used to calculate the packaging dynamic behavior. This is followed by a discussion of the numerical methods and the computer code used to implement the analysis. A significant part of the development is concerned with the prediction of forces developed in the impact limiters as the impact occurs. This aspect of the evaluation is discussed in Section 2.10.8.8.2.

Assumptions

The cask body is assumed to be rigid and axisymmetric. Therefore, all of the energy absorption occurs in the impact limiters which are also assumed to have an axisymmetric geometry. Several assumptions are made in calculating the forces which develop in the limiters as they crush. These are discussed in Section 2.10.8.8.2. Since the packaging is axisymmetric, its motion during impact will be planar. The vertical, horizontal, and rotational components of the motion of the packaging center of gravity (CG) are used to describe this planar motion.

Equations of Motion

A sketch of the packaging at the moment of impact is shown on Figure 2.10.8-3. The packaging is dropped from a height (H), measured from the lowest point on the packaging to the target. The packaging is oriented during the drop, and at impact, so that the centerline is at an angle (r) with respect to the horizontal. At the instant of impact, the packaging has a vertical velocity of

$$V_0 = \sqrt{2gH} \,. \tag{1}$$

Where G is the gravitational constant.

At some time, t, after first impact, the packaging has undergone vertical, u, horizontal, x, and rotational, ρ, displacements. The location of the packaging at this time is shown on Figure 2.10.8-4. One or both of the limiters have been crushed as shown. The resulting deformations (and strains) in the limiters result in forces which the limiters exert on the packaging, thereby decelerating it. These forces, and their points of application on the packaging, are shown on Figure 2.10.8-4 as F_{v1}, F_{v2}, and F_h. The method used to calculate these forces and the points of application are provided in Section 2.10.8.8.2, below.

The three equations of motion of the cask are

$$M\ddot{u} + F_{v1} + F_{v2} - W = 0, \tag{2}$$

$$M\ddot{x} - F_h = 0, \text{ and} \tag{3}$$

$$J\ddot{\rho} - F_{v1}x_{v1} + F_{v2}x_{v2} + F_h Y_h = 0. \tag{4}$$

Where, M is the mass of packaging, J is the polar moment of inertia of the packaging about its CG, W is the packaging weight, and $\ddot{}$ denotes acceleration. At impact ($t = 0$), all of the initial conditions are zero except that u = the vertical velocity.

Computer Solution

The computer code is written to compute the motion of the packaging during impact. The solution is obtained by numerically integrating the equations of motion (equations 2, 3, and 4) from the time of impact, $t = 0$, to a specified maximum time, t_{max}. The integrations are carried forward in time at a specified time increment, Δt. Parametric studies indicate that a time increment of 1 msec is sufficiently small so that further reduction of the time increment does not affect the results. Solutions are usually carried out to about 150 msec for the near horizontal drops and to about 50 msec for the near vertical drops. The significant motions of the packaging normally occur within these time periods.

A standard fourth order Runge Kutta numerical integration method is used to perform the numerical integrations. The following procedure is used to carry the solution from time t_i to time t_{i+1}. Note that at time t_i the displacements and velocities of the three degrees of freedom describing the motion of the CG of the packaging are known.

1. Calculate the deformation of each of the limiters based on the packaging geometry and the motion of the packaging's CG (see Section 2.10.8.8.2).

2. Calculate the forces which the limiters exert on the packaging body using the deformation of the limiters and their stress-strain characteristics (see Section 2.10.8.8.2).

3. Use Equations 2, 3, and 4 to calculate the accelerations during the time interval. Use the Runge Kutta equations to calculate the location and velocity of the cask CG at time t_{i+1}.

4. Go to step (1) to repeat the process until time t_{max}.

5. Generate the output.

Output from the code consists of:

- Problem title, packaging geometry, drop conditions, and integration data.
- Limiter geometric and material property data.
- History of packaging CG motion and amount of crushing in each of the limiters.
- Force history data.
- Plot of acceleration histories.
- Plot of maximum limiter deformations.

2.10.8.8.2 Forces in Limiters

The methods used to calculate the forces F_{v1}, F_{v2}, and F_h in the limiter at a given crush depth are discussed in this section. These calculations are used to perform steps (1) and (2) above. The limiter geometry and material specification is discussed first. The general methodology used to calculate the forces are then presented which is followed with a detailed development of the equations used to calculate the force-displacement relationships.

Limiter Geometry

A sketch of the model of a limiter is shown on Figure 2.10.8-5. Regions I, II and III are used to delineate regions where different materials are used. It should be noted that the properties of the three regions are designed to accommodate the crush requirements of the three significant drop orientations. The properties of regions I, II and III are selected to control the decelerations resulting from vertical, corner, and shallow drop orientations, respectively. The properties used to describe the stress-strain behavior of each of the three materials are discussed below. The dimensions A and B may vary for the limiters at each end of the packaging, but R_0 and R_i are taken to be the same for both limiters. The same material properties are used for each of the limiters.

General Approach

The ideal energy absorbing material is one that has a stress-strain curve that has a large strain region where the stress is constant. Such a material absorbs the maximum energy while

minimizing force (which determines the magnitude of the deceleration). Wood, foam, and honeycomb materials exhibit such behavior and are prime candidates for impact limiter crushable material. If the constant stress region of the stress-strain curve is of primary interest, the forces may be calculated as the crush stress times the area of the surface defined by the intersection of the target and the impact limiter. This approach assumes that the crush stress, which acts normal to the crush surface, is not influenced by stresses acting in directions parallel to the crush surface (i.e., the confining stresses). This assumption is made in the computer code. The crush stress used as input to the code is selected to represent that value which is consistent with the degree of confinement afforded by the impact limiter geometry for the drop orientation considered.

Therefore, the crushable material is modeled in the code with a one dimensional (oriented normal to the crush surface) stress-strain law. The properties of the stress-strain law are selected to represent the degree of confinement provided by stresses acting in the other two dimensions. The properties of the crushable material are not modified as the packaging rotates but are selected to represent the material properties for the initial crush direction of the material.

A portion of the "crushed" area of the limiter is often not backed up by the packaging body (*i.e.*, a projection of a point in this non backed up area normal to the target (impact surface) does not intersect the cask body). The user must specify the percentage of these forces which are to be included in the calculation. The confinement provided by the overall construction of the limiter will determine the extent to which these non backed up forces are actually effective. The computer code does not perform any computations which would allow the user to judge the adequacy of the selected percentage of non backed up forces which are counted.

The evaluation of the impact area and its centroid (required to locate the impact forces) is computationally complicated because of the many variations possible in the manner in which the target intersects the limiter. This problem is resolved by dividing the surface of the limiter into many small segments. The segment is located relative to the target at each computation. If the segment's original location is below the target, then it has crushed and it contributes a force equal to the stress times its area projected on the target. The location of this force is also known. The strain at the segment may also be evaluated so that the peak strains may be determined and stresses may be evaluated for strains which fall outside of the constant crush stress region of the stress-strain law.

The forces must be calculated at each time that the solution for the packaging response is computed. The problem, therefore, is to determine the forces acting on the limiters given the current location of the packaging center of gravity. The solution for the location of the packaging center of gravity is discussed in Section 2.10.8.8.1. The procedure used to perform these computations is as follows (each of the steps is detailed below).

1. Define the location of the target relative to the limiters from the current location of the packaging center of gravity relative to the target.

2. Divide the surface of the limiter into segments and calculate the strain in a one-dimensional element spanning the distance between the center of the segment and the packaging body.

3. Compute the stress in the element from the stress-strain relationship. Multiply the stress by the area of the element projected onto the target.

4. After all of the segments on the limiter are evaluated, sum the segment forces and moments of the forces to find the total force and moment acting on the packaging.

5. Calculate the horizontal force and moment of the horizontal force.

6. Use equations 2, 3, and 4 to extend the solution to the next time step. The new solution consists of the location of the packaging CG at the new time. The above steps are then repeated. This process is continued until the specified maximum time is reached.

Details of Force Computations

Details of each of the six steps outlined above are given in this section. Note that the location of the packaging CG is known at the beginning of this computational sequence.

Deformation of the Limiter

The first step in the computation is to evaluate the location of the limiters relative to the target given the location of the packaging CG relative to the target. The limiter position relative to the target is defined by the six variables, D_1 through D_6, as shown on Figure 2.10.8-6. The location of the cask at first contact is shown on Figure 2.10.8-6a with the subscript 0 added to the D's indicating initial values. The initial values of these parameters (when the lowest corner of the packaging first contacts) are found from the following geometric considerations.

$$\begin{aligned} D_{10} &= 2R_0 \cos\theta, \\ D_{20} &= 0, \\ D_{30} &= B_1 \sin\theta, \\ D_{40} &= D_{30} + D_{10} + L \sin\theta + B_2 \sin\theta, \\ D_{50} &= D_{40} - D_{10}, \\ D_{60} &= D_{30} + L \sin\theta, \end{aligned} \tag{5}$$

At a given time, t, the packaging CG has displaced vertically, u, horizontally, x, and has rotated, ρ, and reached the position shown in Figure 2.10.8-6b. Each of the six points have then fallen by an amount:

$$\Delta D = u + l\,[\sin\theta - \sin(\theta - \rho)] + r\,[\cos\theta - \cos(\theta - \rho)] \tag{6}$$

Where l is the axial distance CG to point (+CG to top), and r is the radial distance CG to point (+CG to impact).

Then the corner deformation, D_2, at time, $t+1$, becomes

$$D_{2(t+1)} = D_{2t} + \Delta D_2 .$$

Where

$$l_1 = l_2 = -yL^* - B_1,$$
$$l_3 = -yL^*$$
$$l_4 = l_5 = (l-y)L^* + B_2,$$
$$l_6 = (l-y)L^*,$$
$$r_1 = r_4 = -R_0, \text{ and}$$
$$r_2 = r_3 = r_5 = r_6 = R_0.$$

To facilitate the computation of strains in the limiter, the position of the limiter relative to the impact surface is classified as shown in Figure 2.10.8-7. There are three possible locations of the impact surface relative to the limiter. The task is therefore to define which of the three patterns apply, and to determine the parameters ϕ and Δ in terms of the variables D_1 through D_6, just determined.

These deformations are next related to the three types of crush patterns for the bottom limiter shown on Figure 2.10.8-7. Crush pattern I applies when

$$D_1 < 0; D_2 < 0; D_3 > 0. \tag{8}$$

Then,

$$\Delta = -\frac{D_2}{\cos\phi}, \text{ and} \tag{9}$$

$$\phi = \cos^{-1}\frac{D_3 - D_2}{B_1}.$$

Crush pattern II applies when

$$D_1 > 0; D_2 < 0; D_3 > 0. \tag{10}$$

Then,

$$\Delta = -\frac{D_2}{\cos\phi}, \text{ and} \tag{11}$$

$$\phi = \cos^{-1}\frac{D_3 - D_2}{B_1}.$$

Crush pattern III applies when:

$$D_1 > 0;\ D_2 < 0;\ D_3 < 0. \tag{12}$$

Then,

$$\Delta = \frac{D_2}{\sin\phi}, \text{ and} \tag{13}$$

$$\phi = \sin^{-1}\frac{D_1 - D_2}{2R_0}.$$

The same set of equations applies to the top limiter if D_1, D_2, D_3, and B_1 are replaced with D_4, D_5, D_6, and B_2 in equations (8) through (13).

Strains in Limiters

The next step in the computation is to calculate strains in the limiters given the deformation defined above. The limiters are first divided into segments as shown in Figure 2.10.8-8. The number of segments used for the bottom, *NB*, and the sides, *NS*, are input by the user. Locations on the surface of the limiters are described in terms of the (R, Z, β) coordinate systems shown on the figure. Strains in the segments along the sides of the limiters are calculated based on the location of the center of the segment (R_0, Z, β). The segments at the bottom are divided into two pieces: one for $R < R_i$ (i.e. in Region 1) and the second for $R > R_i$. A strain is calculated for each of these two pieces for each segment along the bottom surface.

The strains, ε, are calculated as the deformation of the point normal to the crush surface, δ, divided by the undeformed distance of the point from the surface of the limiter to the outer container (q), again measured normal to the crush surface. Therefore:

$$\varepsilon = \delta / q \tag{14}$$

Different equations govern each of these parameters for each of the three crush patterns as shown on Figure 2.10.8-7.

The geometry for crush pattern I is shown on Figure 2.10.8-9. Forces resulting from deformation of the side elements are neglected for this crush pattern. It may be shown that the deformation is

$$\delta = \Delta\cos\phi + (R\cos\beta - R_0)\sin\phi \tag{15}$$

The undeformed length of the element is taken measured to the plane of the packaging bottom so that

$$q = A_1 \cos\phi \tag{16}$$

The geometry for crush pattern II is shown on Figure 2.10.8-10. The deformation of the points on the bottom (a) and along the side (b) may be represented with the same equation

$$\delta = \Delta \cos\phi + (R \cos\beta - R_0) \sin\phi - Z/\cos\phi \tag{17}$$

The original length of the element depends on the intersection of the projection of the point on the impact surface with the outline of the limiter. Four points are identified as shown on Figure 2.10.8-10. The lengths are

$$\begin{aligned} q_1 &= \frac{A-Z}{\cos\phi}, \\ q_2 &= \frac{X}{\sin\phi}, \\ q_3 &= \frac{B-Z}{\cos\phi}, \text{ and} \\ q_4 &= \left[\left(R_0^2 - R^2 \sin^2\beta\right)^{1/2} + R\cos\beta\right]\sin\phi. \end{aligned} \tag{18}$$

Where $X = R \cos\beta + (R^2 \cos^2\beta - R^2 + R_1^2)^{1/2}$.

The deformation for crush pattern III is shown on Figure 2.10.8-11. Deformations of points on the bottom of the limiter are neglected for this crush pattern. The deformation is

$$\delta = \frac{\Delta - Z/\tan\phi - R_0(1-\cos\beta)}{\sin\phi}$$

The original length is measured to, R_i, so that

$$q = \frac{R_0 - R_i}{\sin\phi}. \tag{20}$$

Segment Stress

The stresses in the elements are calculated from the above strains. As mentioned above, three sets of stress-strain laws are input to the code, one for each of the regions defined in Figure 2.10.8-5.

The location of the center of the segment on the surface of the limiter is used to determine which of the three stress-strain laws is to be used. The model may be viewed as a set of one dimensional rods which run from the center of the segment, normal to the target, to another boundary of the limiter. The entire rod is given the properties which the limiter material has at the beginning point of the rod (i.e., the intersection with the target).

The stress-strain law used for the materials is shown on Figure 2.10.8-12. Each of the seven parameters shown on the figure is input to the code for each of the three regions of the limiter. The arrows on the figure indicate the load-unload paths used in the model. The step in the crush strength is built into the stress-strain law so that two crushable materials in series may be modeled. The two crush strengths should be specified as the actual crush strengths of the two materials. The first locking strain, ε_l, should be specified as the locking strain of the weaker material times the length of the weaker material divided by the total specimen length. The higher locking strain, ε_L, should be specified as the first locking strain plus the locking strain of the stronger material times its length and divided by the specimen length.

As stated above, the properties of the limiter material are not varied as the limiter crushes and the packaging rotates. Limiter materials such as wood exhibit anisotropic material properties. This must be accounted for when the properties are input to the code based on the anticipated direction of crushing. Most of the anisotropic wood data is based on tests performed in the elastic range. The following relationship has been used to represent wood properties for a loading which is applied at an angle (a) with respect to the wood grain:

$$P = \frac{P_1 \cos^4 \alpha + P_2 \sin^4 \alpha}{\cos^4 \alpha + \sin^4 \alpha} \tag{21}$$

Where P is the property of interest at angle α, and P_1 and P_2 are properties parallel and perpendicular to grain.

Evaluation of Forces

The stresses determined above are multiplied by the area of the segment projected onto the crush surface. The areas of the sidewall segments are (see Figure 2.10.8-8):

$$A_s = \frac{2R_0 B \cos(6 - \rho)}{(NB)(NS)\tan\beta}. \tag{22}$$

The area of the bottom segments is divided into two parts, one in region I and the other in region II. These areas are

$$A_b = \frac{4R_0 L_b \sin(6 \ - \rho)}{NB} \tag{23}$$

Where, $L_b = (R_i^2 - R_c^2)^{1/2}$ for region 1, and $L_b = (R_0^2 - R_c^2)^{1/2} - (R_i^2 - R_c^2)^{1/2}$ for region II.

These forces are summed for all of the elements to determine the total force acting on the packaging. The forces are also multiplied by their moment arms about the packaging CG to calculate the total moment acting on the packaging. The point on the segment is first projected, normal to the target, to evaluate whether or not it intersects the packaging body. If the projection does not intersect the packaging body, only a percentage of the force is included in the summation. The user specifies the percentage to be used.

Horizontal Force

A horizontal force develops at the limiter/target interface. This force is only considered for the bottom limiter (i.e., the first to impact) since the packaging is always close to horizontal when the top impact limiter is in contact.

The horizontal force, F_h, is first calculated as that required to restrain horizontal motion of the tip of the limiter.

The horizontal acceleration, $\ddot{\Delta}_H$, at the tip of the bottom limiter (point 2 on Figure 2.10.8-6) may be related to the CG motion of the packaging by

$$\ddot{\Delta}_H = \ddot{x} - \ddot{\rho}\left[\left(\gamma L^* + B_1\right)\cos\phi + R_0 \sin\phi\right] \tag{24}$$

Where $\phi = \frac{\pi}{2} - \theta + \rho$.

Equating Δ_H to zero would result in no acceleration of the tip in the horizontal direction and provides the solution for x in terms of ρ.

Substituting this solution for x into Equation (3) results in an expression for the horizontal force, F_h, required to restrict horizontal acceleration of the tip, in terms of the rotational acceleration, ρ. Finally, equation 4 is used to eliminate ρ with the following result.

$$F_h = \frac{M_v W\left[\left(\gamma L^* + B_1\right)\cos\phi + R_0 \sin\phi\right]}{J_g + W\left[\left(\gamma L^* + B_1\right)\cos\phi + R_0 \sin\phi\right]^2} \tag{25}$$

Where M_v is the moment due to vertical forces, which is equal to $F_{v1}x_{v1} - F_{v2}x_{v2}$, and W is the packaging weight.

This force is restricted to

$$F_h < \mu F_{v1} \tag{26}$$

Where μ is the coefficient of friction specified by user.

2.10.8.9 References

(1) Federal Specification MMM-A-188b.

(2) Dreisback, J.F., Balsa Wood and Its Properties, Columbia Graphs, Columbia, CT 1952.

(3) Marks Standard Handbook for Mechanical Engineers, Eighth Edition, pg. 6-124.

TABLE 2.10.8 -1

Mechanical Properties of Wood and Wood Adhesive

Minimum Properties of Adhesive	
Shear Strength by Compression Loading	2,800 lb in^{-2} (1)
Shear Strength by Tension Loading	340 lb in^{-2} (1)
Properties of Heavy Balsa (10-12 lb ft^{-3})	
Shear Strength Parallel to Grain	315-385 psi max. (2)
Tensile Strength Perpendicular to Grain	140-160 psi (2)
Properties of Redwood	
Shear Strength Parallel to Grain	940 psi (3)
Tensile Strength Perpendicular to Grain	240 psi (3)

TABLE 2.10.8-2

Typical Wood Material Properties

Property	High Density Balsa	Redwood
Density	10-12 lb ft^{-3}	18.7-27.5 lb ft^{-3}
Parallel to Grain		
Crush Stress	1560-2010 psi	5000-6500 psi
Locking Strain	0.8	0.6
Unloading Modulus	32,000 psi	1,247,000 psi
Locking Modulus	10 × (max. crush stress)	10 × (max. crush stress)
Perpendicular to Grain		
Crush Stress	300-420 psi	750-975 psi
Locking Strain	0.8	0.6
Unloading Modulus	32,000 psi	1,247,000 psi
Locking Modulus	10 × (max. crush stress)	10 × (max. crush stress)

TABLE 2.10.8-3

First Impact Maximum Inertia *G* Load versus Initial Angle of Impact
For 30 Foot Drop,
Using Maximum Wood Crush Stress Properties

Impact Angle, 30 Foot Drop	Maximum *G* Load During First Impact (Bottom), Maximum Wood Properties			
	Axial	Transverse		
	CG	Top	Bottom	CG
0°	4	52	G_{nor} =53	51
5°	7	11*	G_{nor} =36 G_{rot} = 26	36
10°	8	8*	G_{nor} = 21 G_{rot} = 28	21
15°	12	10*	G_{nor} = 26 G_{rot} = 34	26
20°	17	11*	G_{nor} = 30 G_{rot} = 39	30
30°	23	5*	G_{nor} = 28 G_{rot} = 32	28
40°	21	2	36	18
45°	27	3	34	19
50°	27	7	24	15
60°	33	9	17	13
70°	54	9	17	13
80°	62	5	10	7
90°	66	2	0	1

* Maximum acceleration occurred during second impact.

TABLE 2.10.8-3A

Second Impact Maximum Inertia *G* Load versus Initial Angle of Impact
For 30 Foot Drop,
Using Maximum Wood Crush Stress Properties

Impact Angle, 30 Foot Drop	Maximum *G* Load During Second Impact (Top), Maximum Wood Properties					
	Axial	Transverse				
	CG	Top			Bottom	CG
		Normal	Rotational	Impact Force (lb.×1000)		
5°	0	25.5	47.0	6822	19	26
10°	0	25.5	46.9	6818	19	25
15°	0	25.4	46.8	6804	19	25
20°	1	25.2	45.8	6759	18	25
30°	5	21.3	36.6	5863	14	21

TABLE 2.10.8-4

First Impact Maximum Inertia *G* Load versus Initial Angle of Impact
For 30 Foot Drop,
Using Minimum Wood Crush Stress Properties

Impact Angle, 30 Foot Drop	Maximum *G* Load During First Impact (Bottom), Minimum Wood Properties			
	Axial	Transverse		
	CG	Top	Bottom	CG
0°	4	41	G_{nor} =39	39
5°	6	29*	G_{nor} = 33 G_{rot} = 14	33
10°	7	8*	G_{nor} = 19 G_{rot} = 25	19
15°	12	11*	G_{nor} = 26 G_{rot} = 34	26
20°	16	11*	G_{nor} = 28 G_{rot} = 37	28
30°	23	5*	G_{nor} = 29 G_{rot} = 32	29
40°	20	3	34	16
45°	23	2	30	16
50°	24	14	5	23
60°	30	7	15	11
70°	51	8	16	12
80°	60	6	10	8
90°	50	2	0	1

* Maximum acceleration occurred during second impact

TABLE 2.10.8-4A

Second Impact Maximum Inertia *G* Load versus Initial Angle of Impact
For 30 Foot Drop,
Using Minimum Wood Crush Stress Properties

Impact Angle, 30 Foot Drop	Maximum *G* Load During Second Impact (Top), Minimum Wood Properties					
	Axial	Transverse				
	CG	Top			Bottom	CG
		Normal	Rotational	Impact Force (lb.×1000)		
5°	0	25.1	47.5	6717	20	25
10°	0	20.1	37.3	5445	15	20
15°	1	20.3	37.5	5484	15	20
20°	1	20.2	36.4	5471	14	20
30°	6	20.1	36.3	5623	14	20

TABLE 2.10.8-5

Depth of Crush versus Crush Force. Impact Angle 0°

Maximum wood properties		Minimum wood Properties	
Displacement (in.)	Force (Kips)	Displacement (in.)	Force (Kips)
0	0	0	0
5.24	4458	5.25	3430
7.54	4458	7.64	2987
9.54	4458	9.79	2987
11.22	6187	11.69	5249
12.47	6822		

TABLE 2.10.8-6

Depth of Crush versus Crush Force. Impact Angle 15°

First Impact			
Maximum wood properties		Minimum wood Properties	
Displacement (in.)	Force (Kips)	Displacement (in.)	Force (Kips)
0	0	0	0
13.28	2719	13.29	2095
15.79	3405	15.83	2623
18.02	3723	18.18	2947
19.97	4748	20.30	3670
21.56	5273	22.14	4834
22.71	6315	23.61	5645
Second Impact			
Maximum wood properties		Minimum wood Properties	
Displacement (in.)	Force (Kips)	Displacement (in.)	Force (Kips)
0	0	0	0
7.48	4445	7.76	3419
10.58	4446	11.12	3561
13.02	6803	13.94	5202
		16.11	5234

TABLE 2.10.8-7

Depth of Crush versus Crush Force. Impact Angle 45°

First Impact			
Maximum wood properties		Minimum wood Properties	
Displacement (in.)	Force (Kips)	Displacement (in.)	Force (Kips)
0	0	0	0
5.29	856	5.29	658
10.51	2479	10.54	1906
15.40	4835	15.541	3725
19.60	5862	20.01	4664
22.77	7372	23.67	6273
24.63	8462	26.28	7177
		27.64	7330

TABLE 2.10.8-8

Depth of Crush versus Crush Force. Impact Angle 60°

First Impact			
Maximum wood properties		Minimum wood Properties	
Displacement (in.)	Force (Kips)	Displacement (in.)	Force (Kips)
0	0	0	0
5.29	526	5.29	405
10.53	1865	10.55	1425
15.48	4238	15.60	3258
19.85	7067	20.21	5444
23.31	8201	24.11	6922
25.62	9353	27.07	7795
		28.94	8299

TABLE 2.10.8-9

Depth of Crush versus Crush Force. Impact Angle 80°

First Impact			
Maximum wood properties		Minimum wood Properties	
Displacement (in.)	Force (Kips)	Displacement (in.)	Force (Kips)
0	0	0	0
2.64	152	2.64	117
5.29	563	5.29	431
7.91	2390	7.92	1824
10.44	4972	10.64	3793
12.77	7922	12.90	6042
14.82	11254	15.09	8678
16.47	13522	16.98	11132
17.66	15573	18.49	13724
18.31	16222	19.66	14083
		20.12	15745

TABLE 2.10.8-10

Depth of Crush versus Crush Force. Impact Angle 90°

First Impact			
Maximum wood properties		Minimum wood Properties	
Displacement (in.)	Force (Kips)	Displacement (in.)	Force (Kips)
0	0	0	0
0.53	3323	0.53	2374
1.05	17203	1.05	13146
2.54	17203	2.56	13146
4.55	17203	4.72	13146
6.17	17203	6.43	13146
6.76	17203	7.68	13146
6.97	17203	8.58	13146

TABLE 2.10.8-11

Maximum Inertial *G* Load During One Foot Drop

Impact Angle, 1 foot Drop	Maximum *G* Load During First Impact, Maximum Wood Properties			
	Axial	Transverse		
	CG	Top	Bottom	CG
90°	12	0	0	0
0°	1	32	30	31
60°	5	2	2	2

Impact Angle, 1 foot Drop	Maximum *G* Load During First Impact, Minimum Wood Properties			
	Axial	Transverse		
	CG	Top	Bottom	CG
90°	8	0	0	0
0°	1	24	23	24
60°	3	1	2	2

TABLE 2.10.8-12

Loading Used in Cask Body Analysis, Appendix 2.10.1
Versus
Maximum G Load Predicted by ADOC Program

Accident Conditions (30 Foot Drops)		
Drop Orientation	Maximum *G* Load, from ADOC	Input Loading Used in FEA** (Section 2.10.1)
90° End Drop	66 G Axial	80 G Axial
0° Side Drop	53 G Transverse	80 G Transverse
60° CG over Corner Drop	33 G Axial	69 G Axial
	17 G Transverse	40 G Transverse
		80 G Resultant Vertical
15° Slap Down (Second Impact)	25.4 G Normal	42.22 G Normal
	46.8 G Rotational	77.78 G Rotational
	6.804×10^6 lb. Impact Force	10.79×10^6 lb. Impact Force

Normal Conditions (1 Foot Drops)		
Drop Orientation	Maximum G Load from ADOC	Input Loading Used in FEA** (Section 2.10.1)
90° End Drop	12 G Axial	15 G Axial
0° Side Drop	32 G Transverse	35 G Transverse

** Conservatively Using Higher G loads

TABLE 2.10.8-13

Loading Used in Basket Structural Analysis, Appendix 2.10.5
Versus
Maximum G Load Predicted by ADOC Program

Accident Conditions (30 Foot Drops)		
Drop Orientation	Maximum G Load, from ADOC	Input G Load Used in Basket Structural Analysis, Including Dynamic Load Factor
90° End Drop	66 G Axial	80 G Axial (Conservatively Using Higher G load)
0° Side Drop	53 G Transverse	80 G Transverse (Conservatively Using Higher G load)

Normal Conditions (1 Foot Drops)		
Drop Orientation	Maximum G Load from ADOC	Input G Load Used in Basket Structural Analysis, Including Dynamic Load Factor
90° End Drop	12 G Axial	15 G Axial
0° Side Drop	32 G Transverse	35 G Transverse

THIS PAGE IS INTENTIONALLY LEFT BLANK.

FIGURE WITHHELD UNDER 10 CFR 2.390

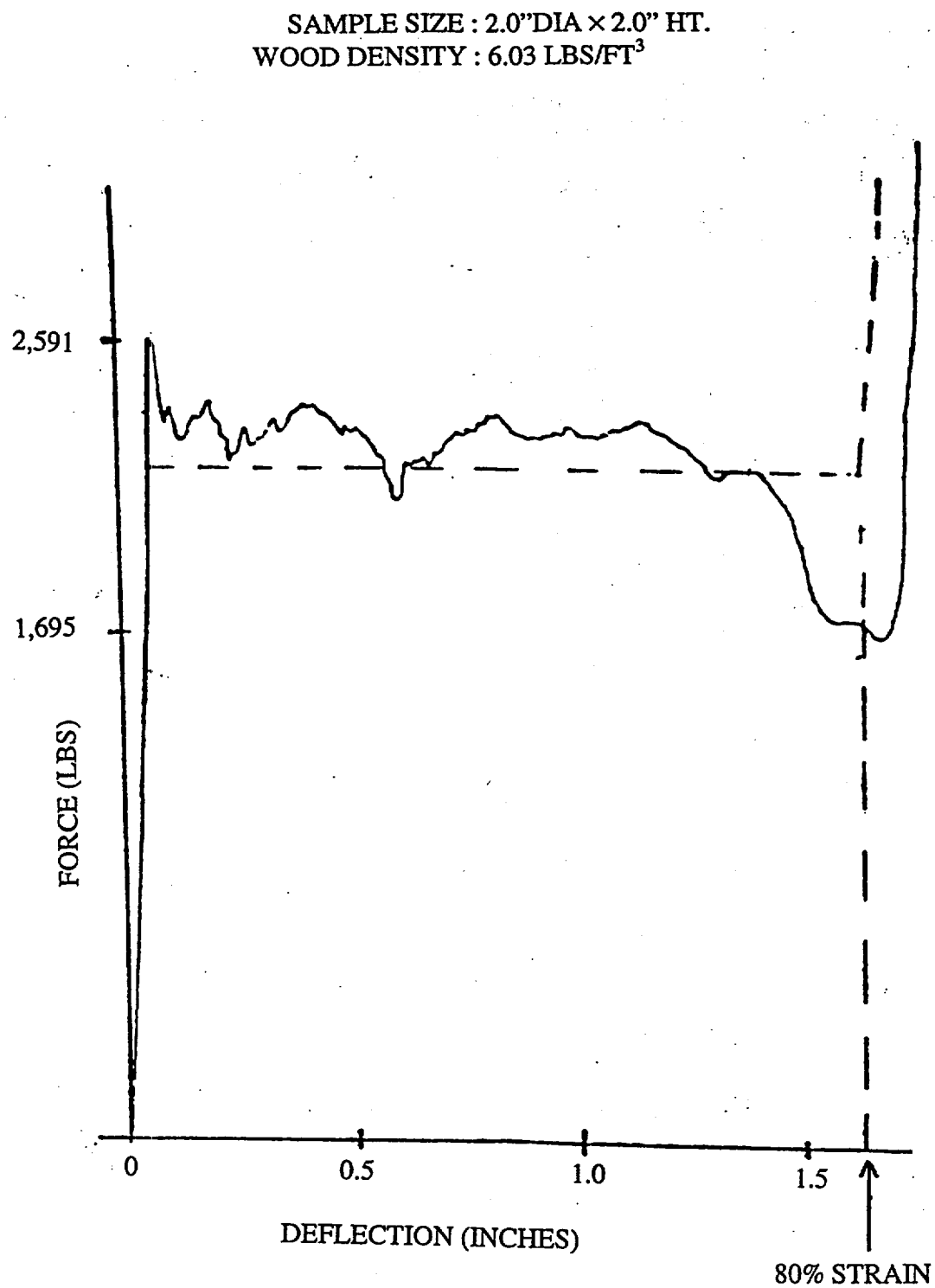

FIGURE 2.10.8-1A
SAMPLE FORCE - DEFLECTION CURVE FOR BALSA

REV. 0 4/99

NOTE : NOMINAL SAMPLE 1.625"DIA × 1.625" HT.

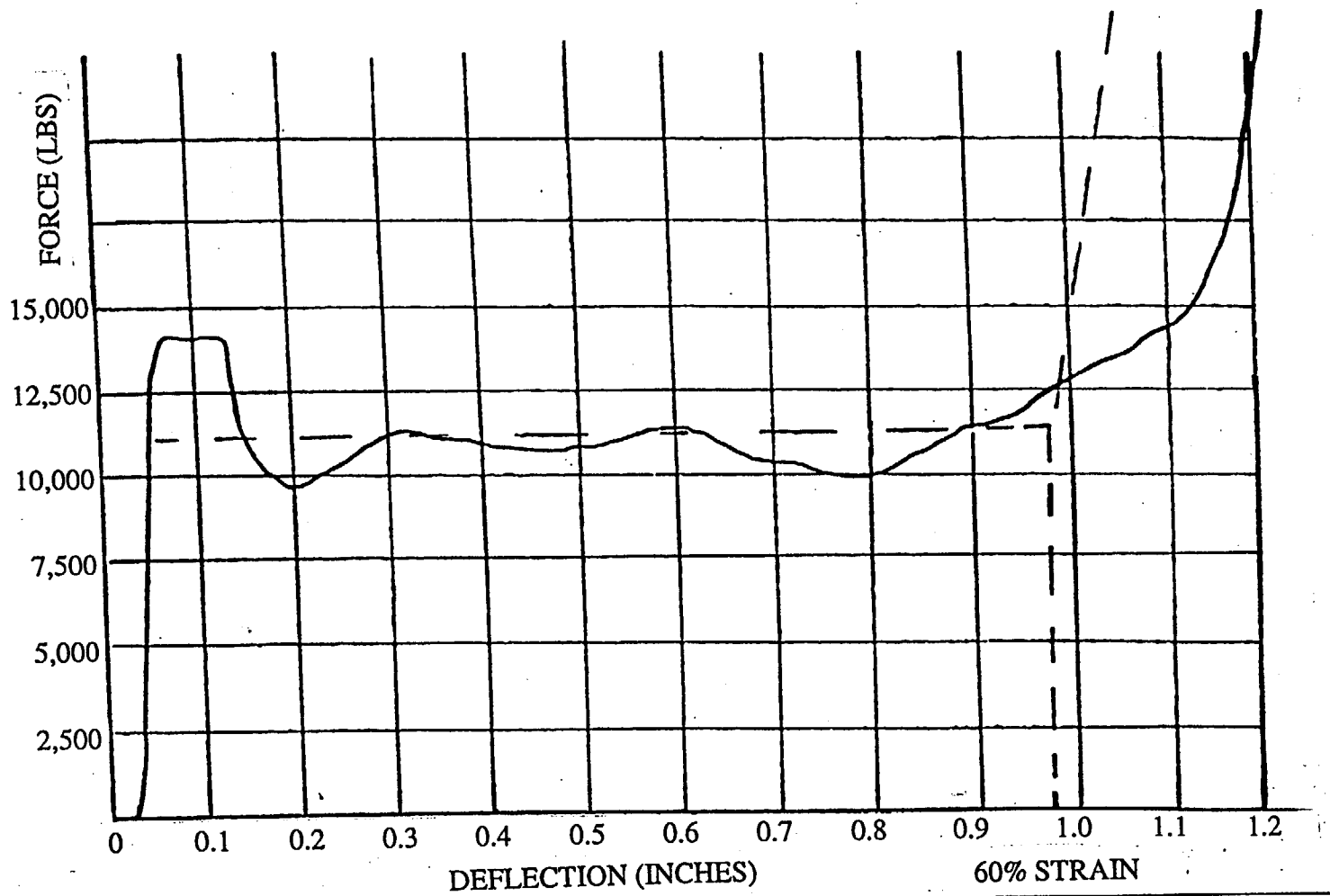

FIGURE 2.10.8-IB
SAMPLE FORCE - DEFLECTION CURVE FOR REDWOOD

REV. 0 4/99

FIGURE WITHHELD UNDER 10 CFR 2.390

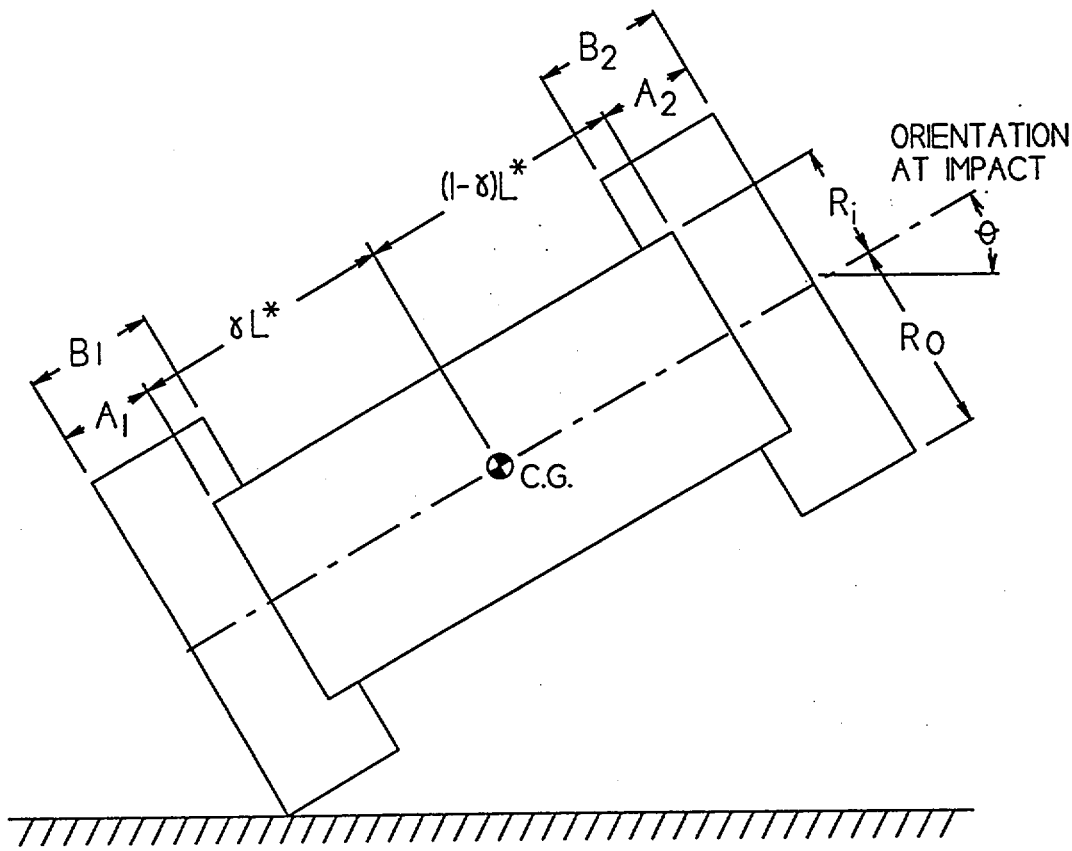

FIGURE 2.10.8-3
GEOMETRY OF PACKAGING

REV. 0 4/99

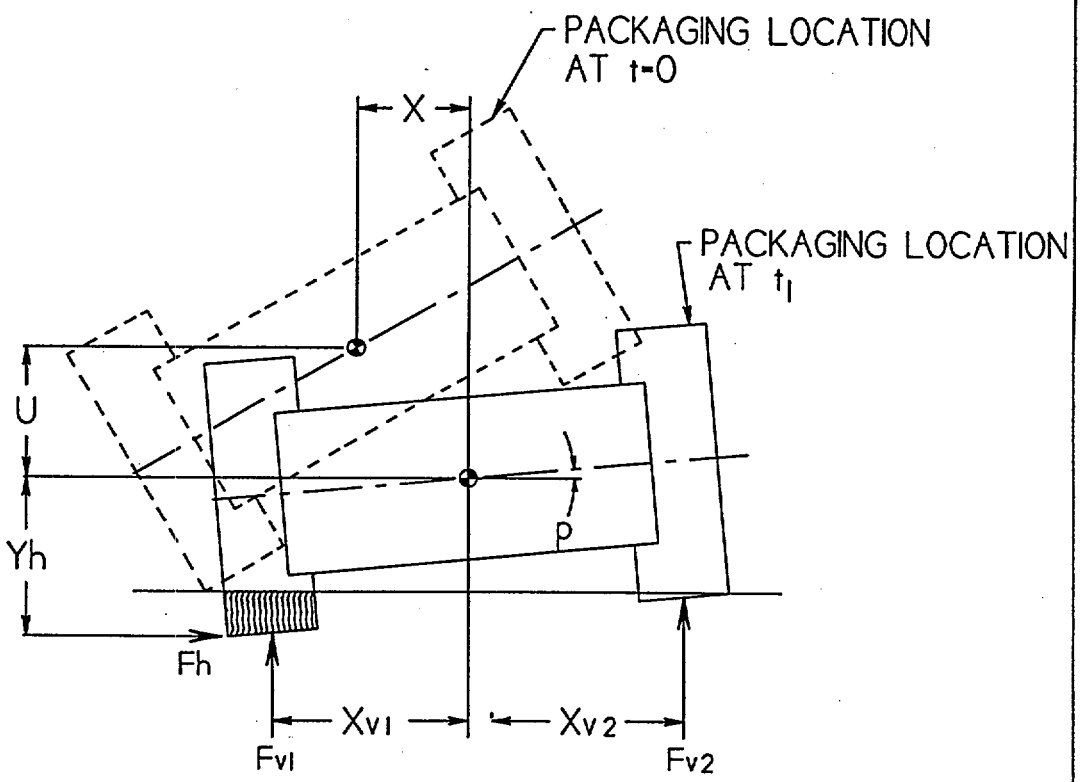

FIGURE 2.10.8-4
PACKAGING LOCATION AT TIME (t)

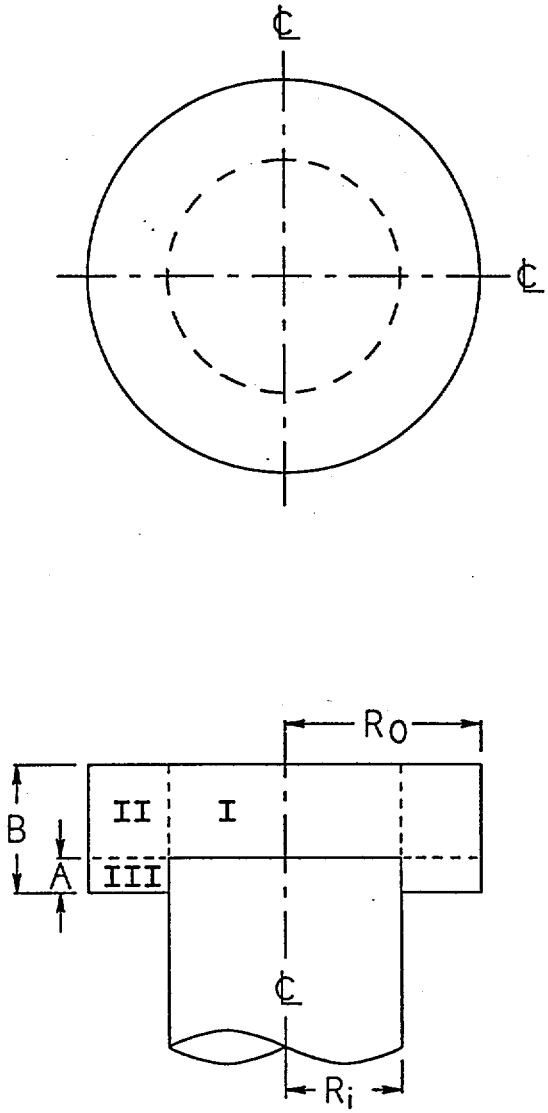

FIGURE 2.10.8-5
GEOMETRY OF LIMITER

REV. 0 4/99

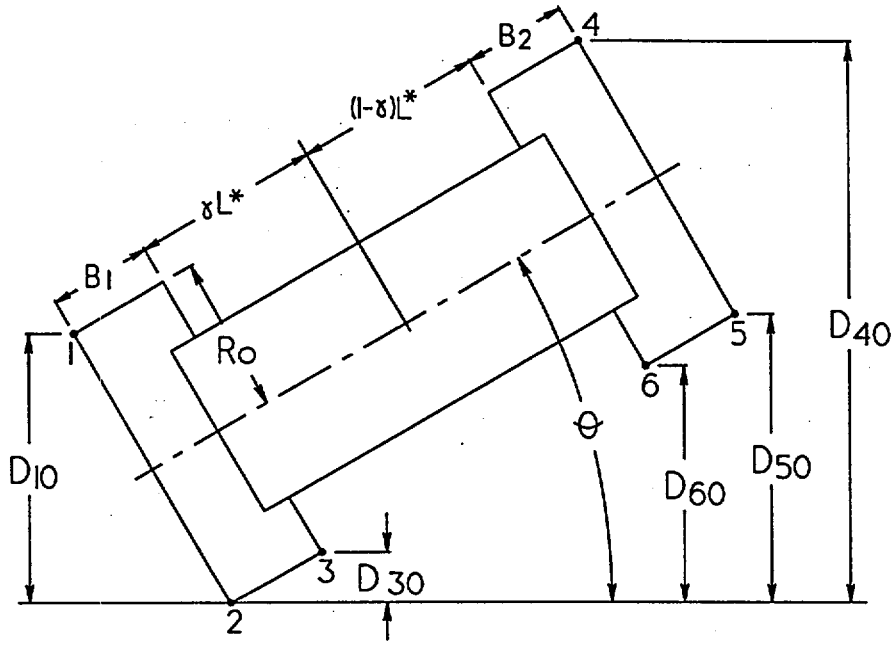

a) IMPACT LIMITER PARAMETERS AT FIRST IMPACT

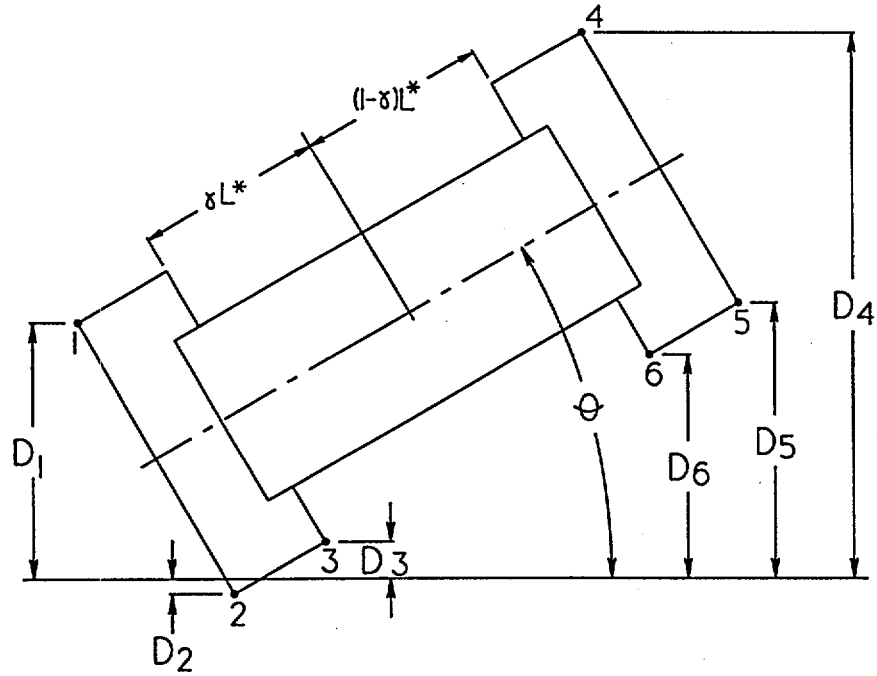

b) IMPACT LIMITER PARAMETER - GENERAL

FIGURE 2.10.8-6
DEFINITION OF LIMITER DEFORMATION

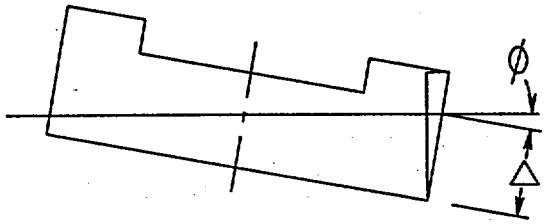

a) CRUSH PATTERN I

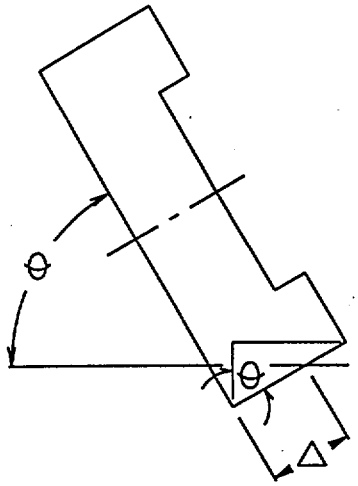

b) CRUSH PATTERN II

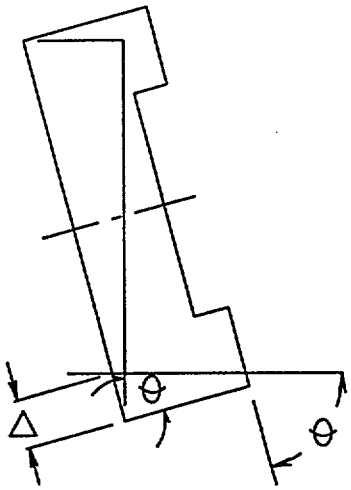

c) CRUSH PATTERN III

FIGURE 2.10.8-7
CRUSH PATTERN IN LIMITER

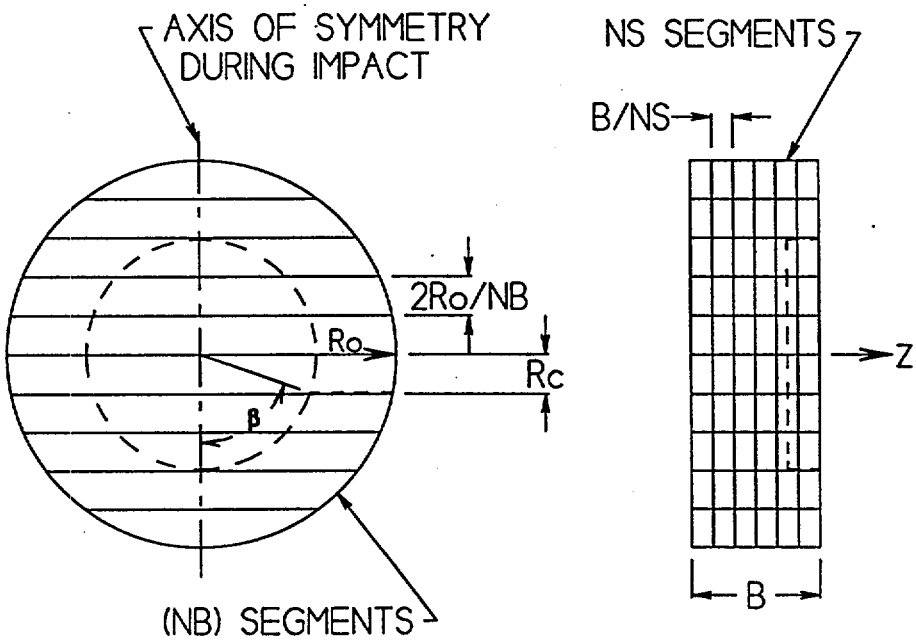

FIGURE 2.10.8-8
SEGMENTED LIMITER

REV. 0 4/99

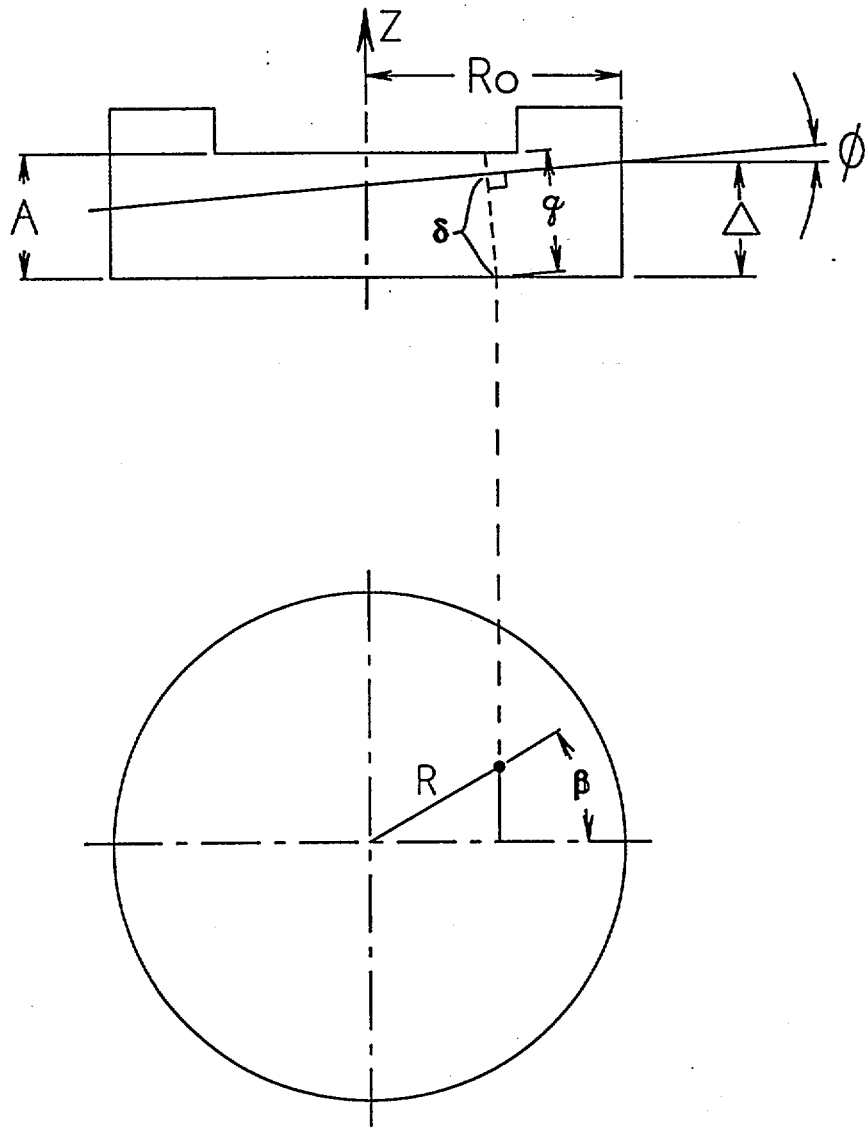

FIGURE 2.10.8-9
STRAIN COMPUTATION FOR CRUSH PATTERN I

REV. 0 4/99

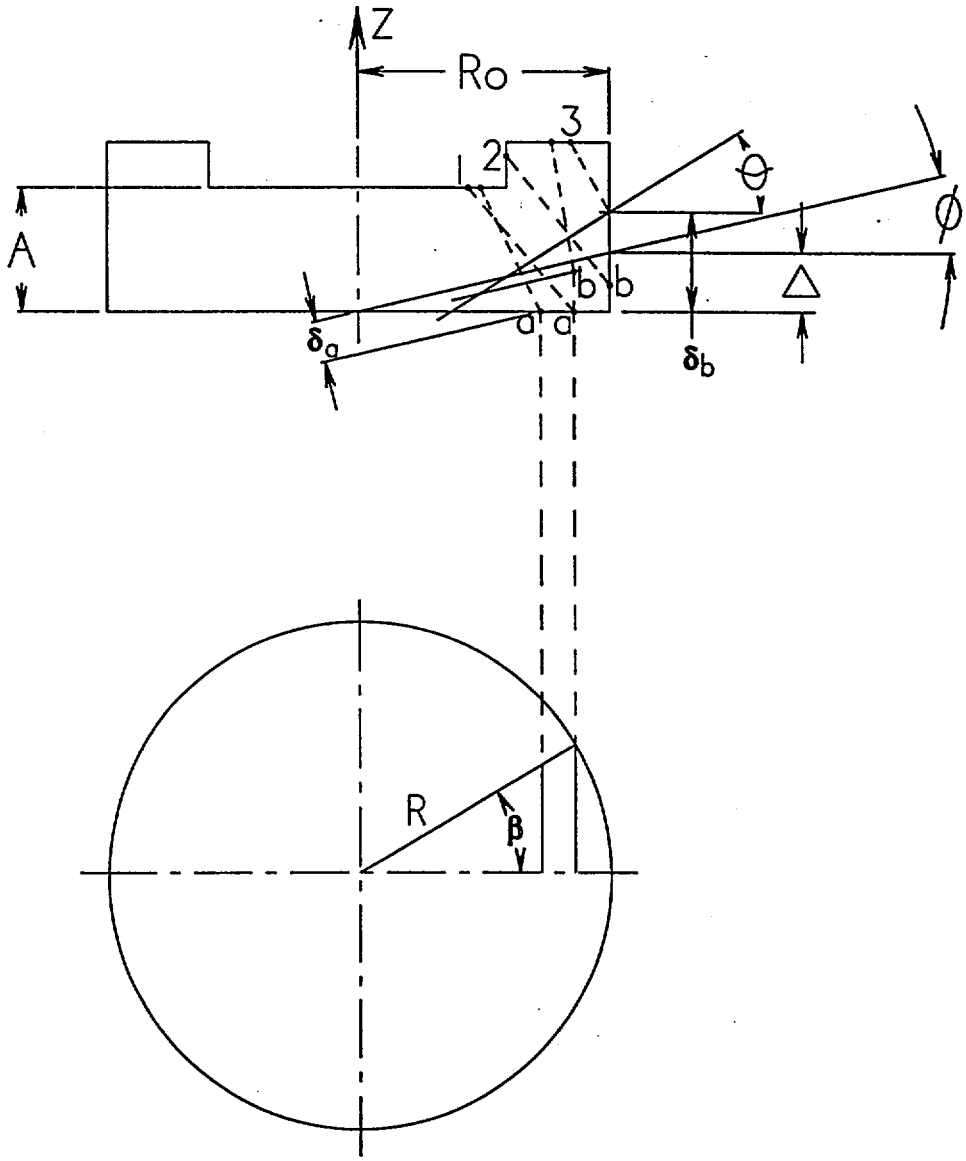

FIGURE 2.10.8-10
STRAIN COMPUTATION FOR CRUSH PATTERN II

REV. 0 4/99

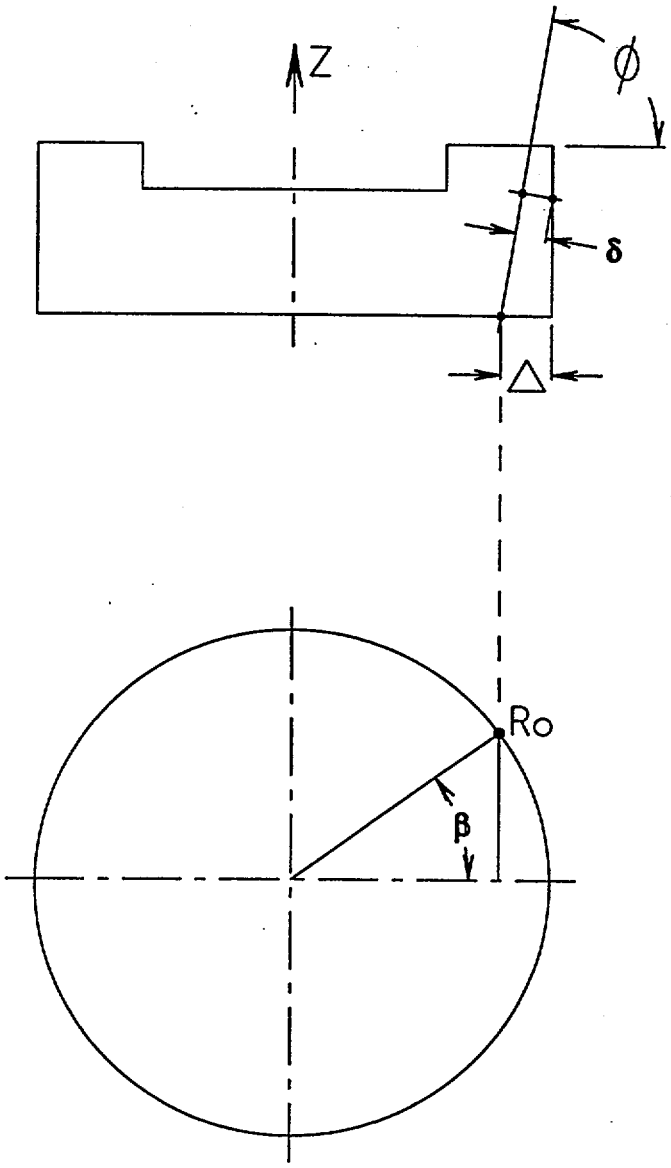

FIGURE 2.10.8-11
STRAIN COMPUTATION FOR CRUSH PATTERN III

REV. 0 4/99

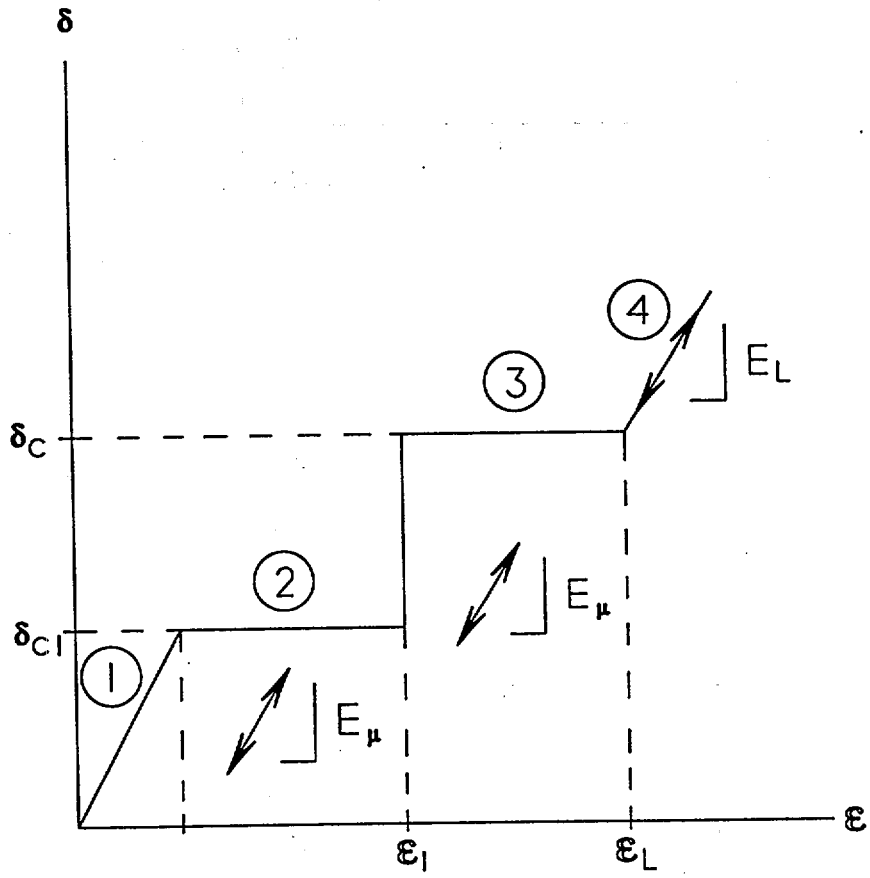

FIGURE 2.10.8-12
WOOD STRESS - STRAIN CURVE

REV. 0 4/99

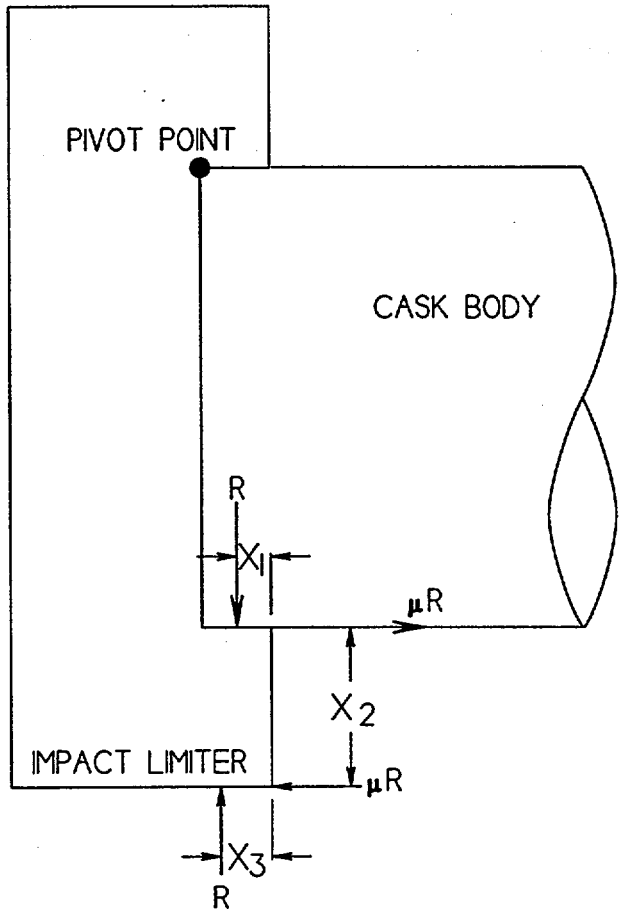

WHERE:

R = 10,132,800 LBS.
μ = 0.12
X_1 = 12.75/2 = 6.375 IN.
X_2 = (144-85.55)/2 - 11.1 = 18.125 IN.
X_3 = 8.890 IN.

FIGURE 2.10.8-13
FREE BODY DIAGRAM OF IMPACT LIMITER DURING 15° SHALLOW DROP SLAPDOWN

THIS PAGE IS INTENTIONALLY LEFT BLANK.

TN 68 TRANSPORT PACKAGING

APPENDIX 2.10.9

TABLE OF CONTENTS

LIST OF FIGURES

THIS PAGE IS INTENTIONALLY LEFT BLANK.

APPENDIX 2.10.9

IMPACT LIMITER TESTING

2.10.9.1 Introduction

A series of dynamic tests will be performed on one-third scale models of the TN-68 impact limiters. The tests will be performed to evaluate the effect of the 30-foot free drop hypothetical accident defined in 10 CFR 71.73(c)(1)[1]. The test results will be used to verify the analyses performed for the TN-68 cask and basket. The objectives of the test program are to:

- Demonstrate that the inertia G values and forces calculated in Appendix 2.10.8 and used in the structural analyses of the TN-68 cask and basket are acceptable.
- Verify the adequacy of the impact limiter tie rods and bolts.
- Demonstrate the adequacy of the impact limiter enclosure.

The one-third scale impact limiters are identified as A, B, C and D and will be tested in the following sequence:

Test Number	Drop Orientation		Impact Limiter(s) Used
1	15° Slap Down	First Impact	A
		Second Impact	B
2	0° Side Drop		A and B Both Rotated 180°
3	90° End Drop		C
4	60° CG over Corner Drop		D

The impact limiters for the 15° slap down orientation are chosen to be performed because the 15° orientation puts the highest stresses on the tie rods and attachment bolts.

The impact limiter for the 90° end drop orientation is also chosen to be performed because the 90° orientation drop case is expected to cause the highest deceleration.

The 0° side drop and the 60° CG over corner drop will be performed because these two drops are expected to cause the highest deformations in the impact limiters. This is especially important during the side drop, since it will provide a reasonable estimate of the likelihood of the trunnions impacting the target.

2.10.9.2 Scaling Relationships

The TN-68 and impact limiter models are constructed with a geometric scale factor of $1/\lambda = 1/3$. Consequently, the following scale factors apply.

Length:

$$L_p = \lambda L_m$$

Surface area:

$$A_p = \lambda^2 A_m$$

Moment of inertia:

$$I_p = \lambda^4 I_m$$

Section modulus:

$$S_p = \lambda^3 S_m$$

Weight:

$$W_p = \lambda^3 W_m$$

Energy absorbed during drop (from same height h):

$$E_p = W_p h = \lambda^3 W_m h = \lambda^3 E_m$$

Velocity at beginning of impact:

$$V_p = \sqrt{2gh} = V_m$$

where λ is the scale factor, the subscript p refers to the full size, and the subscript m refers to the model.

During impact, the impact limiter materials will deform or crush. Since the model and full size impact limiters are made of the same materials, they deform under the same stress,

$$S_p = S_m.$$

Therefore we have the following relationships.

Force during impact:

$$F_p = S_p A_p = S_m \lambda^2 A_m = \lambda^2 F_m$$

Deformation:

$$D_p = E_p / F_p = \lambda^3 E_m / \lambda^2 F_m = \lambda D_m$$

Impact duration:

$$T_p = D_p / V_p = \lambda D_m / V_m = \lambda T_m$$

Impact deceleration:

$$a_p = V_p / T_p = V_m / \lambda T_m = 1/\lambda a_m$$

2.10.9.3 Dynamic Testing

Test Model Description

The test model for the dynamic tests consists of a solid carbon steel test body with an impact limiter on each end. The test model, shown in Figure 2.10.9-1, is constructed to be as close as possible to one-third of the full size packaging.

The model test body provides the proper one-third scale weight, CG location, and dimensions. The test body is 66.25 inches long with a gamma shield outside diameter of 28.17 inches, and an outer shell outside diameter of 32.67 inches. The reduced diameter portion, located in the axial center of the dummy is not important dimensionally, but is required to provide the proper overall weight and CG location. Important test model and full size packaging dimensions are shown below.

Test Model vs. Full Size Packaging

Component	Test Model (in)	Full Size Packaging (in)
Body Length (with spacer)	66.25	198.75
Length Including Impact Limiters	89.08	267.25
Gamma Shield Diameter	32.67	98.00
Outer Shell Diameter	28.17	84.50

The outer shell of the TN-68 package is simulated by welding a hollow ¼ inch carbon steel shell to the dummy body. The geometry of the outer shell model is shown in Figure 2.10.9-1. The outer shell model is broken up into two separate pieces because of the central reduced diameter section of the dummy body. Modeling the outer shell is important because it will reveal any influence the outer shell has on the performance of the bottom impact limiter, as well as providing an accurate simulation of the structure that the impact limiter bolt brackets are welded to.

The scale model impact limiters are a one-third scale model of the full size impact limiters. The carbon steel impact limiter structure is the same as that described in Appendix 2.10.8, i.e. steel shells closed off by flat plates and reinforced by twelve (12) radial gussets. The model and full scale configurations are almost identical, except that all linear dimensions in the model are one-third of those in the full scale impact limiter. The balsa and redwood used in the model are consistent with that specified for fabrication of the full scale impact limiters. The model contains the same number of wood blocks as the full size impact limiters. The wood blocks are made up of a number of smaller pieces of wood glued together with phenol resorcinol adhesive, using the same procedure to be used on the full size impact limiters.

The attachment bolts, bolt brackets, tie rods, and tie rod brackets are made of the same material specified for the full size limiters, but their dimensions are scaled down by a factor of one-third.

The fusible plugs and impact limiter support angles are not included in the models. They do not affect the compression properties of the impact limiter. The lifting lugs are made larger than one-third scale to facilitate lifting. The model impact limiters are fitted with two steel plugs each, for leak testing.

Test Description

Accelerometers will be mounted to brackets around the exterior of the test body at 0°, 90°, 180°, and 270° orientations at the approximate center of gravity location and adjacent to each impact limiter. The locations of the accelerometers are shown in Figure 2.10.9-2.

The test setup for the side drop is shown in Figure 2.10.9-4. For the side drop test, the accelerometers will be oriented to measure accelerations in the radial direction.

The test setup for the end drop is shown in Figure 2.10.9-5. It is important to note that the package will be oriented with the cask bottom facing down so that impact will occur on the bottom end of the package. This is conservatively done because the increased surface area created by the outer shell may increase axial G loads. For the end drop test, the accelerometers will be oriented to measure accelerations in the drop (axial) direction.

The test setups for the CG over corner and 15° slap down drops are shown in Figures 2.10.9-6 and 2.10.9-3 respectively. For both slap down and corner drop, the accelerometers will be oriented to measure accelerations in both axial and radial directions.

The dynamic drop test will be performed at an approved test facility, and will be performed in accordance with approved written procedures.

An inclinometer will be placed on the test body to measure the initial angle (± 1°) of its longitudinal axis with respect to the target (i.e., impact surface). The impact surface will be an essentially unyielding horizontal surface. A steel tape will be used to measure the initial height of the lowest surface of the test model above the target. The height will be set at 30 feet +1.0, – 0.0 inches.

Data will be collected by accelerometers capable of measuring data at a minimum frequency response of 10,000 Hz per channel. The lowest natural vibration frequencies of the test body, which are excited during the test, are much lower than this. These body vibrations involve small displacements (low stresses) at high frequencies, which excite the accelerometers and tend to mask the low frequency rigid body acceleration. This low frequency acceleration is masked, because both low frequency rigid body and high frequency natural vibration accelerations superimpose and the net acceleration is recorded. Filtering the data is necessary to remove these high frequency accelerations. A cutoff filter will be used to eliminate data above a specified cutoff frequency. The cutoff frequency used to filter the data will be set at a value slightly below the significant natural frequency of the test body.

In addition to the acceleration data previously discussed, the following data will be measured and recorded after each drop test.

- Observation of crush on the impact limiters, tie rods, and attachment bolts.

- Dimensional measurements of the impact limiters and their contour lines, establishing the deformed shape.

The dynamic test will consist of the following sequence of events.

1. Impact limiters A and B attached to the test model via tie rods and attachment bolts.

2. 30 foot 15° slap down, initially crushing impact limiter A on 0° side, then crushing impact limiter B on 0° side.

3. Check impact limiter tie rods and bolts for damage or looseness, and replace or tighten as necessary.

4. 30 foot 0° side drop, crushing impact limiters A and B on 180° side simultaneously.

5. Impact limiters A and B removed from the test body.

6. Impact limiters C and D attached to the test model via tie rods and attachment bolts.

7. 30 foot 90° end drop crushing impact limiter C.

8. Check impact limiter tie rods and bolts for damage or looseness, and replace or tighten as necessary.

9. 30 foot 60° CG over corner drop crushing impact limiter D.

10. Impact limiters C and D removed from the test body.

Test Results

The test results will be provided once the dynamic tests are complete.

2.10.9.4 Conclusions

The dynamic impact limiter test, once completed, will provide accurate data confirming that the TN-68 impact limiters provide acceptable accelerations during all hypothetical 30 foot accident drops. The dynamic test will also confirm that the impact limiter tie rods and bolts are strong enough to keep the impact limiter on the cask during an accident drop.

2.10.9.5 Photographs

Photographs depicting the dynamic tests will be included in this section.

2.10.9.6 Reference

1. 10CFR Part 71, Packaging and Transportation of Radioactive Material.

THIS PAGE IS INTENTIONALLY LEFT BLANK.

FIGURE WITHHELD UNDER 10 CFR 2.390

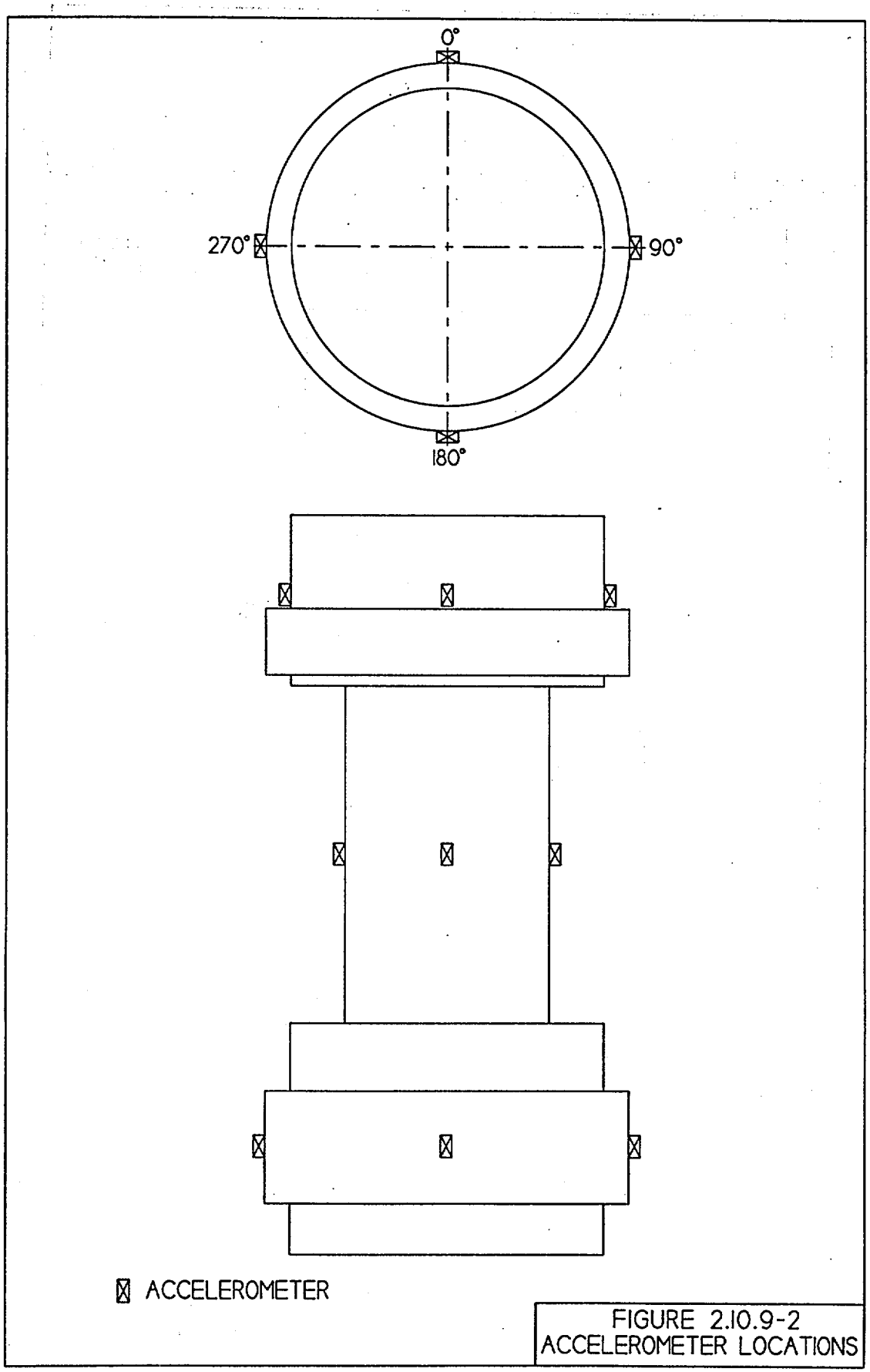

FIGURE 2.10.9-2
ACCELEROMETER LOCATIONS

REV. 0 4/99

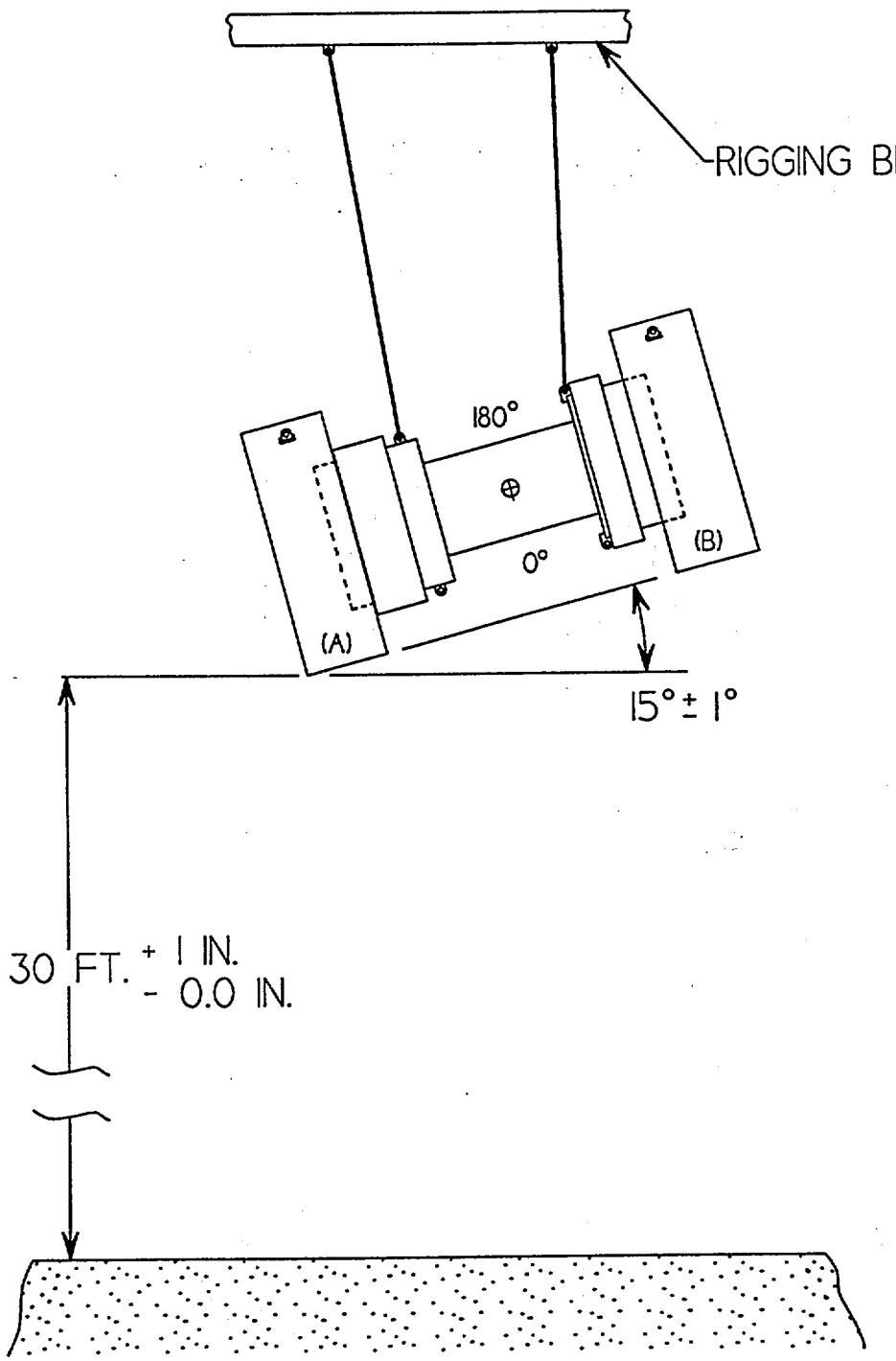

FIGURE 2.10.9-3
TN-68 SCALE MODEL
15° SLAPDOWN TEST SETUP

REV. 0 4/99

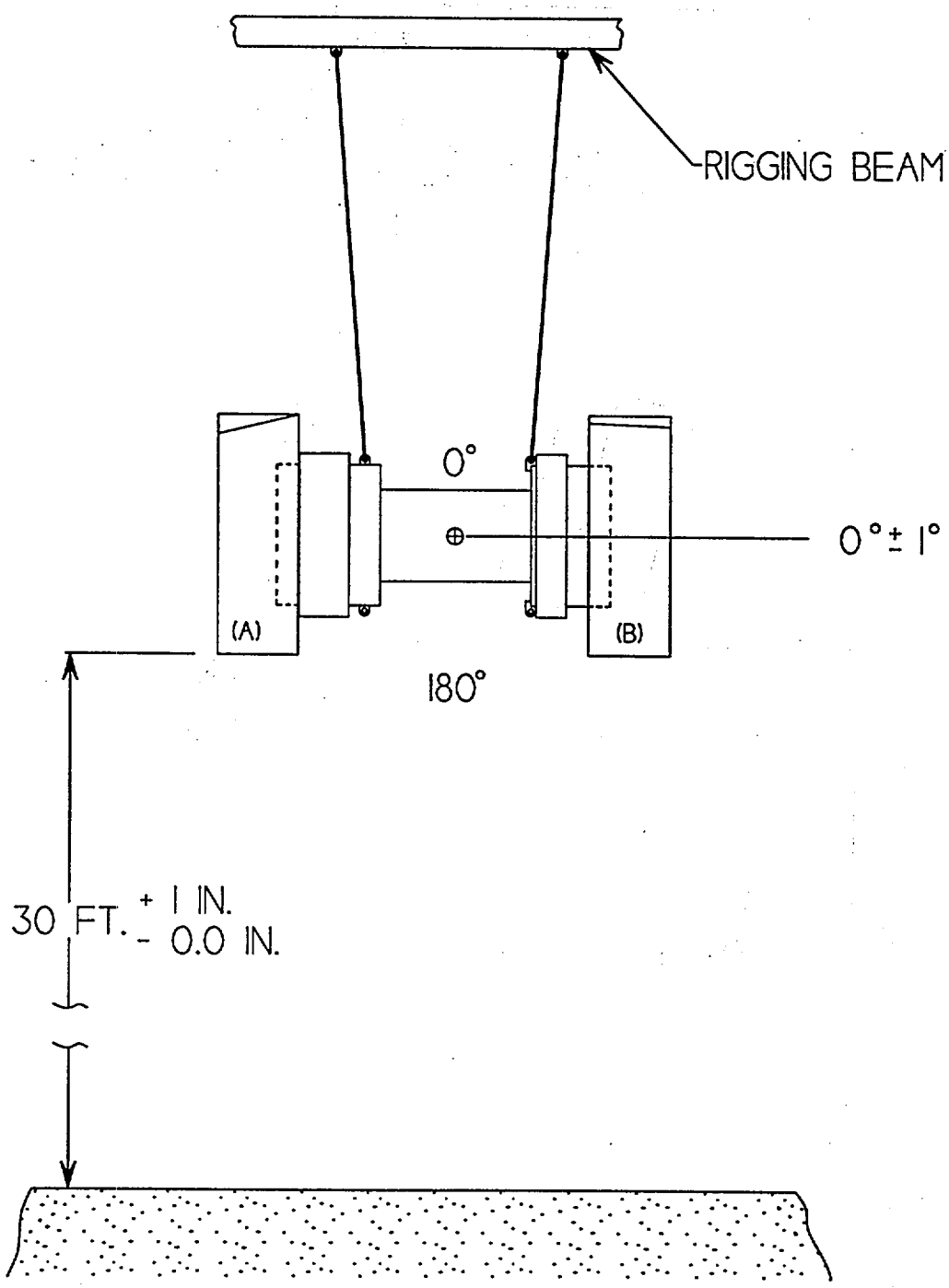

FIGURE 2.10.9-4
TN-68 SCALE MODEL
0° SIDE DROP TEST SETUP

REV. 0 4/99

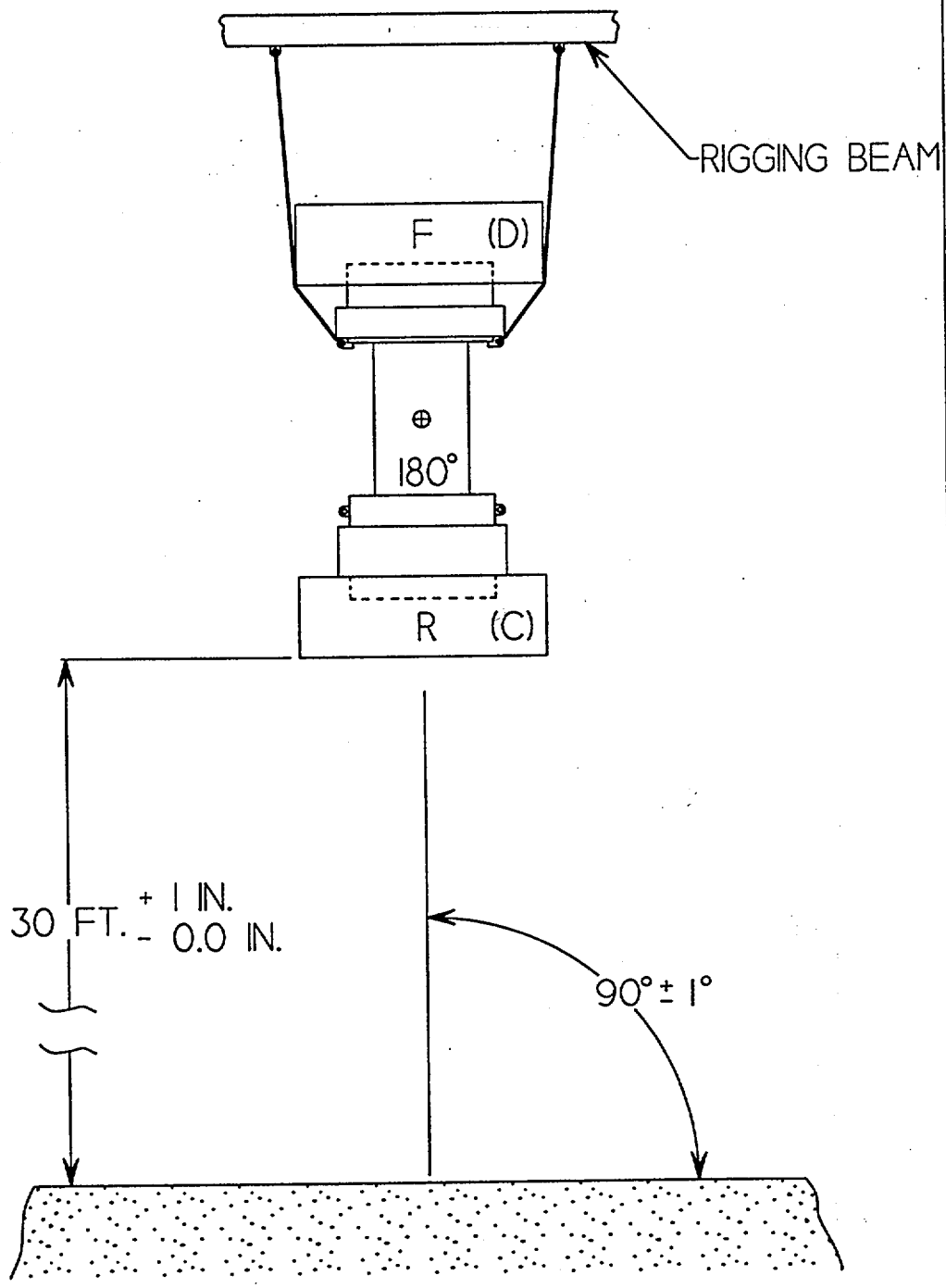

FIGURE 2.10.9-5
TN-68 SCALE MODEL
90° END DROP TEST SETUP

REV. 0 4/99

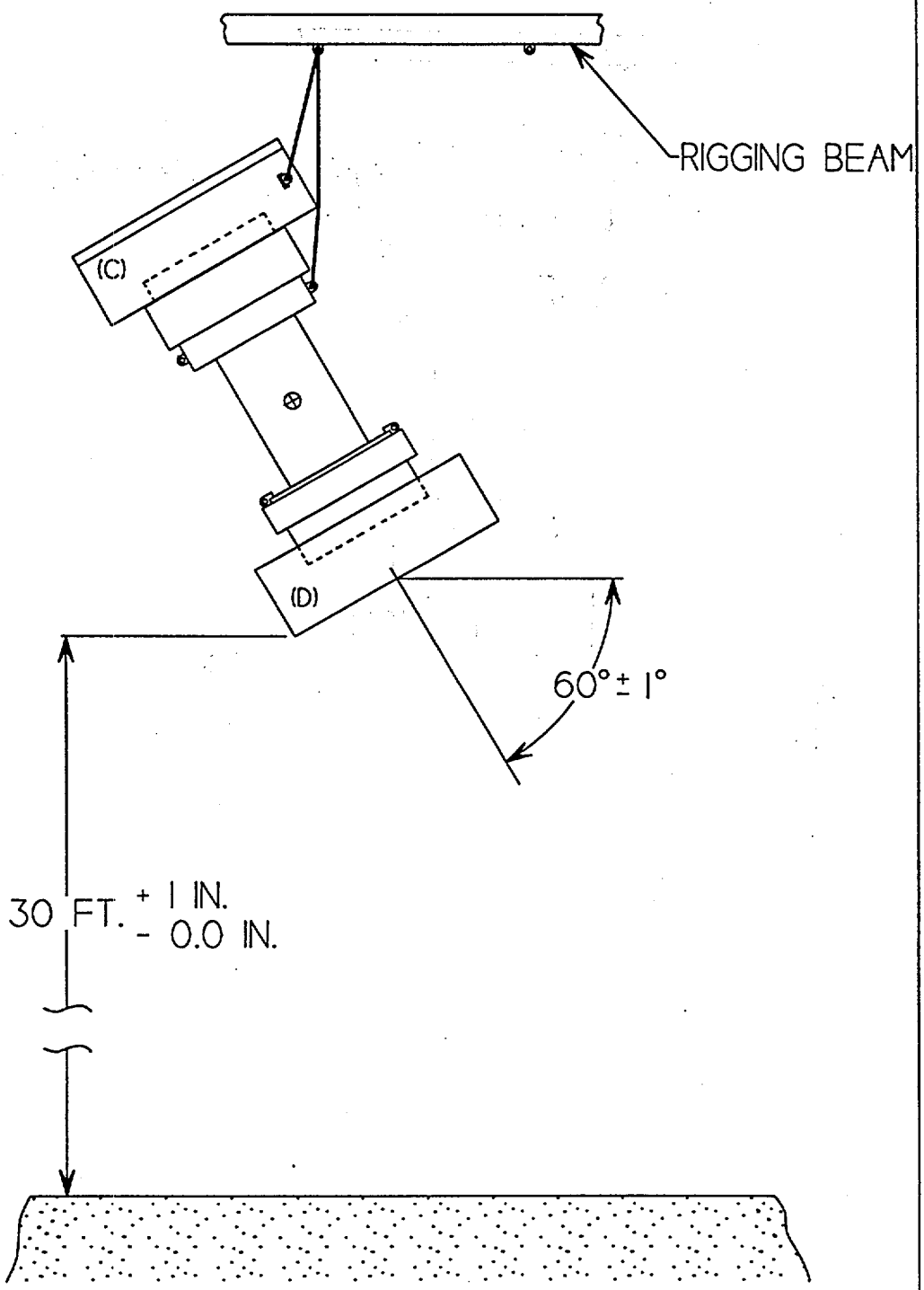

FIGURE 2.10.9-6
TN-68 SCALE MODEL
60° CG OVER CORNER DROP TEST SETUP

REV. 0 4/99